Department of Mechanical Engineering

Experimental Investigation of Surface Radiation and Mixed Convection Heat Transfer in Duct Flows

Rajamohan Ganesan

This thesis is presented for the degree of
Doctor of Philosophy
of
Curtin University

November 2012

DECLARATION

To the best of my knowledge and belief this thesis contains no material previously published by any other person except where due acknowledgement has been made. This thesis contains no material which has been accepted for the award of any other degree or diploma in any university.

Signature: 

Date: 31 / 10 /2012

ABSTRACT

Mixed convection heat transfer in horizontal and vertical ducts with flow through the duct plays an important role in the design and operation of several industrial equipment involving heat transfer and fluid flow phenomena. The estimation of heat transfer requires consideration of both free and forced convective heat exchange mechanisms, in addition to surface radiation among the internal walls of the duct. Free convection leads to the onset and growth of secondary flows, which interact with the forced convection heat transfer rate, and thereby affecting the overall heat removal rates from a duct. Surface radiation in the presence of mixed convection is found to affect both free and forced convection heat transfer rates. Therefore, the combination of the convection (free and forced) and radiation heat transfer modes present an interesting situation. Due to the emissivity of the walls of the duct, surface radiation from the walls of the duct will affect the overall heat transfer phenomena. The present study therefore focuses on the interaction of surface radiation on the free and forced convective heat transfer phenomena occurring in airflow through a duct. Three configurations: mixed convection heat transfer in thermally developing flow in horizontal ducts (CS1), hydrodynamically developed thermally developing flow in horizontal ducts (CS2) and thermally developing flow in vertical ducts (CS3), are analyzed. Experiments are performed to study the mixed convection heat transfer in horizontal and vertical ducts with two differentially heated isothermal hot and cold walls and two adiabatic walls. Radiative heat transfer is estimated using a numerical scheme, with the help of experimentally obtained temperatures.

The experimental work involved fabrication, assembly and instrumentation of test sections on horizontal and vertical ducts of suitable sizes. The major parameters considered in this work include wall emissivity, Reynolds number, thermal and geometric parameters and aspect ratios. To cover the required range of Reynolds numbers, two test sections were used in this study. In a series of experiments, the Reynolds number was varied from 800 to 2900, and the heat flux was varied from

250 W/m^2 to 870 W/m^2, for 2 aspect ratios of the duct cross section and the emissivity of internal walls were 0.05 and 0.85. The heated wall temperature ranged from 55 ^oC to 100 ^oC and the cold wall directly opposite to the heated wall was maintained at a uniform temperature.

The flow field within the duct was made visible by a suitable smoke flow visualization method. The results showed that the flow conditions and surface radiation significantly affected the total Nusselt number.

ACKNOWLEDGEMENTS

During the course of my PhD study, numerous people have provided guidance and positive suggestions which has enabled me to perform the enormous task of completing this work, culminating in the production of this thesis. Here I would like to thank and acknowledge these people.

My supervisor Dr. Ramesh Narayanaswamy for providing his expertise in heat transfer, which supported my efforts in studying the mixed convection heat transfer and completing this work. I am grateful for his supervision, guidance and encouragement throughout each step of this journey.

My co-supervisor, Dr. Perumal Kumar for providing me with helpful feedback and assistance at all levels of this research. I appreciate his patience and understanding as well as his assistance in completion of this dissertation.

I would also like to use this opportunity to thank the School of Engineering and Science at Curtin Sarawak for providing the required facilities to carry out this research. Thanks are also due to Curtin University Sarawak for providing me the Miri staff higher degree by research scholarship. Special thanks to Associate Professor Dr. Chua Han Bing for his support.

Most importantly, I express my heartfelt thanks and dedicate this thesis to my wife, Bavani, my parents and my children, whose love and support kept me going throughout the period of my studies. My sincere thanks also go to all my friends and colleagues, especially Mr. Lenin Gopal, Ms. Carrie Ho Lee Ing, Dr. Agus Saptora, Dr. Ramasamy Nagarajan, Mr. Murali Krishnan and Mr. Sanjayvarman Ravindran for their support throughout my work. Lastly I thank Almighty GOD for giving me the health, determination and energy to overcome all obstacles and to march towards my goal of completing this thesis.

LIST OF PUBLICATIONS

JOURNAL PUBLICATION

1. **G. Rajamohan**, N. Ramesh and P. Kumar. Study on Mixed Convection Heat Transfer in Vertical Ducts with Radiation Effects. World Academy of Science, Engineering and Technology, Vol: 81, ISSN 2070-3740, p 737-747, Singapore, 2011.

CONFERENCE PUBLICATIONS

2. **G. Rajamohan**, N. Ramesh, G. Alexander and P. Kumar. An Experimental Study on Mixed Convection Heat Transfer for Thermally Developing Flow in Horizontal Ducts with Radiation Effects. ASME/JSME 8^{th} Thermal Engineering Joint Conference, AJTEC 2011, Honolulu, Hawaii, USA, 2011.
3. **G. Rajamohan**, N. Ramesh and P. Kumar. Study on mixed convection heat transfer for hydrodynamically developed and thermally developing flow in horizontal ducts with radiation effect. 21^{st} National and 10^{th} ISHMT-ASME Heat and Mass Transfer Conference, IIT Madras, India, 2011.

TABLE OF CONTENTS

APPENDIX

LIST OF FIGURES

LIST OF TABLES

NOMENCLATURE

AR duct aspect ratio, W/H

A_s area of hot wall surface, m^2

D_h hydraulic diameter, $D_h = 2(W\ H) / (W+H)$

H height of the duct, m

k_m thermal conductivity of air, W/m-K

L length of the test section, m

Le length of the entrance section, m

N_u Nusselt number, $N_u = h\ D_h/k$

U_{in} air entry velocity to the test section, m/s

q heat flux, W/m^2

Q heat flow, W

Re Reynolds number, $R_e = U_{in} D_h / \nu$

T temperature, K

T_h hot wall temperature, K

T_c cold wall temperature, K

T_{in} air entry temperature to the test section, K

T_m mean temperature $(T_{in}+T_{out})/2$, K

T_{out} air exit temperature from the test section, K

W width of the duct, m

Z dimensionless z-coordinate, $Z = z/D_h$

z distance from inlet of the test section, m

Greek Symbols

ε emissivity

ν kinematic viscosity, m^2/s

μ dynamic viscosity of fluid, kg/ms

Subscripts

con convection

in inlet

m mean

out outlet

rad radiation

tot total

CHAPTER 1
INTRODUCTION

1.1 Background

Heat transfer phenomena in which natural and forced convection mechanisms interact is termed 'combined' or mixed convection. Mixed convection heat transfer in horizontal and vertical ducts is encountered in a wide range of thermal engineering applications such as cooling of electronic equipment, compact heat exchangers, solar collectors and thermal-energy conversion devices. The performance of thermal energy conversion devices depends on the energy exchange that takes place through various heat and fluid flow processes prevailing in these devices. An understanding of the various fluid flow and heat exchange processes enables efficient design of these devices. Therefore, research on flow and heat transfer through ducts requires significant attention. The amount of heat energy transported by the working fluid in a duct is dependent on the geometry of the duct, nature of the flow, and the thermal boundary conditions of the duct. Air is a common working fluid, and is widely preferred as the medium for cooling of electronic equipment, due to the advantages in handling air and its cost effectiveness. The application potential of mixed convection in horizontal and vertical ducts in the presence of surface radiation underscores the importance of the present study.

A careful review of the literature shows that experimental work is still required to be done to examine the characteristics of the transport mechanisms due to the interaction of surface radiation and mixed convection in horizontal and vertical ducts. The radiative interaction between the walls of the duct and its effect on mixed convection heat transfer are of great importance in the design of these systems. The emissivity of the walls of the duct and the surface radiation from the walls of the duct will affect the overall heat transfer coefficient in duct flows.

In the case of enclosures and cavities, even at moderate temperatures, surface radiation does significantly affect free convection heat transfer rates. Radiation and convection effects without considering their interaction leads to significant errors as radiation and convection effects are competingly important. The importance of the surface radiation effects is identified in this research, and accounted for, in the analysis of flow and heat transfer involving horizontal and vertical ducts.

This experimental research considers multimode heat transfer such as, mixed convection (combined free and forced) in laminar airflow in the duct and surface radiation from the internal walls of the duct. The duct considered in this study has differentially heated isothermal (hot and cold) walls and adiabatic walls. The major parameters considered in this work include surface radiation effects (through wall emissivity), Reynolds number, thermal and geometric parameters, and aspect ratios. The emissivities of internal walls are considered to be 0.05 and 0.85 and the two aspect ratios considered are 0.5 and 1. Based on the orientation of the duct, the research is divided into two major divisions, the first part dealing with surface radiation and mixed convection heat transfer in the horizontal orientation of the duct, and the second part dealing with surface radiation and mixed convection heat transfer in the vertical orientation of the duct.

1.2 Aim and Objectives

The aim of this research is to investigate the heat transfer characteristics of mixed convection heat transfer in horizontal and vertical ducts heated from side walls along with the effect of radiation heat transfer from the internal walls of the duct. A systematic experimental study considering the effect of surface radiation in mixed convection has not been done so far, for this class of problems. The objectives of this work are to design and construct test sections suitable for the horizontal and vertical orientation of the duct with instrumentation, perform systematic experiments, including flow visualization for a range of flow rates, thermal and geometric parameters to investigate the flow and heat transfer phenomena. The analysis of

results provide more physical insight and a deeper understanding of the effects of the interaction of surface radiation on convection heat transfer rates. An understanding of the multi-mode interactions provide new knowledge useful in the design of thermal energy conversion devices involving fluid flow and heat transfer.

1.3 Research Methodology

The study is carried out by conducting experiments for surface radiation and mixed convection heat transfer in horizontal and vertical ducts of suitable sizes. The experimental study involves the design, fabrication and construction of a suitable test rig for mixed convection heat transfer in horizontal and vertical ducts. The experimental data was analysed to obtain various heat transfer quantities due to mixed convection and surface radiation heat transfer from the hot vertical wall of the duct. To obtain the radiation heat transfer from the hot wall, a numerical modelling scheme using the computational fluid dynamics solver FLUENT was developed to create a simulation model for analysis. The experimentally observed temperatures of the heated wall were used as input quantities in the numerical modelling, thereby providing a most accurate prediction of results when modelling radiation heat transfer.

1.4 Structure of the Thesis

The outline of the thesis is presented below:

Chapter 1 provides a brief introduction of mixed convection heat transfer in ducts with radiation effects and the objectives of this study.

Chapter 2 of this thesis reviews the relevant literature published in both experimental and numerical studies on mixed convection heat transfer in horizontal and vertical ducts.

Chapter 3 describes the experimental methodology of mixed convection heat transfer measurements in horizontal and vertical ducts and the computation of surface radiation heat transfer rates.

Chapter 4 presents the results and discussion of heat transfer in thermally developing flow in horizontal ducts (CS1).

Chapter 5 presents the results and discussion of heat transfer in hydrodynamically developed and thermally developing flow in horizontal ducts (CS2).

Chapter 6 presents the results and discussion of heat transfer in thermally developing flow in vertical ducts (CS3).

Chapter 7 presents the results and discussion on the comparison of the three case studies: CS1, CS2, and CS3.

Chapter 8 summarizes the major findings of this study, and provides conclusions of the research work.

1.5 Summary

This chapter has provided an introduction of the problem and the objectives of the research. The structure of the thesis is also presented to give an overview of the contents of the thesis. In the next chapter, the literature review and scope of the present work will be presented in detail.

CHAPTER 2

LITERATURE REVIEW

2.1 Introduction

The review of previous studies in the area of mixed convection heat transfer in horizontal and vertical ducts is presented in this chapter. Mixed convection heat transfer in horizontal and vertical ducts are encountered in a wide range of thermal engineering applications. The amount of heat energy transported by the working fluid in a duct is dependent on the geometry and orientation of the duct, nature of the flow, and the thermal boundary conditions of the duct.

Experimental studies on the effect of mixed convection and surface radiation heat transfer in duct flows with two differentially-heated isothermal walls and two adiabatic walls is scarce. This literature review covers both experimental and numerical work carried out on mixed convection heat transfer in duct flows with surface radiation effects. Most of the studies carried out earlier have been done using air as the fluid medium. Different heating configurations generate different fluid flow and heat transfer characteristics; therefore, a systematic literature study on mixed convection heat transfer in duct flows with surface radiation effects are required. Details of mixed convection heat transfer in the review of duct flows is divided into three sections- the first section dealing with thermally developing flow in horizontal ducts; the second section dealing with hydrodynamically developed and thermally developing flow in horizontal ducts, and the third section dealing with thermally developing flow in vertical ducts.

2.2 Mixed Convection Heat Transfer for Thermally Developing Flow in Horizontal Ducts

Mixed convection heat transfer in a horizontal duct has been investigated by many researchers, especially the configuration wherein the flow is heated from the one of the walls. A review of literature relevant to mixed convection heat transfer for thermally developing flow in horizontal ducts that are heated from the one of the walls is given below.

Osborne and Incropera [1] performed an experimental investigation to examine the laminar flow mixed convection heat transfer for flow between horizontal parallel plates with uniform asymmetric heat fluxes. For the range of heat fluxes considered, the top and bottom plate flow conditions were found to be independent of the heat flux at the opposite plate. Correlations were formulated for Rayleigh number, Grashof number and Graetz number. Their results showed that the bottom plate conditions strongly influenced the buoyancy driven flow than the top plate conditions. Forced convection heat transfer was found to be dominating at the top plate.

Incropera and Maughan [2] experimentally studied laminar flow mixed convection heat transfer through parallel plates heated by uniform heat flux from the bottom plate. They studied the variation of the average Nusselt number for $125 < Re < 500$, $7 \times 10^3 < Gr^* < 1 \times 10^6$, and for both horizontal and inclined channel (up to 30^0). Heat transfer was initially found to be dominated by forced convection and showed rapid decline in the Nusselt number. The onset of thermal instability was detected downstream from the inlet, and was found to eventually enhance the heat transfer. Further study resulted in correlations [3].

Huang et al. [4] investigated the combined effects of radiation and laminar mixed convection in the entrance region of an isothermal rectangular channel. The mixed convection and radiation were formulated by the vorticity-velocity formulation of Navier-Stokes equation and integral formulation for radiation equation. Gray fluid

was used in the mixed convection flow regime. The study reported that buoyancy forces led to significantly improvement of the heat transfer in the entrance region.

Smyth and Salman [5] carried out experiments on the combined free and forced convection of air flow in a horizontal rectangular duct of aspect ratio 5:1. The investigation was made with one or both of the horizontal upper and lower plates heated uniformly and the vertical walls were unheated. Velocity and temperature profiles obtained showed that the secondary flow created by free convection heat transfer caused significant influence on the flow behavior and the heat transfer rate from the bottom plate.

Balaji and Venkateshan [6] performed a numerical study of natural convection in a square enclosure using a finite-volume method with a 21 x 21 non-uniform grid. The interaction of surface radiation with free convection was studied in great detail. A radiation model was included in the analysis to study the effect of surface radiation and takes into account different emissivities on the heat transfer characteristics of the enclosure. The results showed the dual effect of radiation (i.e. contributing to the overall heat transfer as well as decreasing the convective component).

Huang and Lin [7] conducted a numerical study of mixed convection in a rectangular channel with bottom heated and top cooled boundary conditions. For a wide range of Gr/Re^2 values, they covered the flow regime from steady laminar longitudinal vortex flow to unsteady chaotic flow. They concluded that the buoyancy induced flow can cause chaotic flow in the downstream for Gr/Re^2 values form 25 to 40, for Re and aspect ratio of 500 and 2 respectively.

Ingham et al. [8] numerically investigated mixed convection in a horizontal parallel plate duct. Laminar combined convection flows bounded by two very long wide horizontal parallel plates was the topic of the interest. They conducted three case studies; namely, heated lower wall, heated upper wall, and both walls heated. Results

were obtained for a fixed Prandtl number of 7.02 at low and moderate values of the Reynolds number over a wide range of values for the ratio of the Grashof number to the square of the Reynolds number. They observed that when applying heat at the upper wall, a thermally stratified flow was generated, and when the fluid was heated from the lower wall, a transversely oriented recirculation was predicted.

Lin and Lin [9] experimentally studied airflow in a bottom heated horizontal rectangular duct. Their results established the onset of thermal instability detected in a previous study. This instability was found to move upstream for higher Grashof numbers, or to be delayed for a larger Reynolds number. The flow regime map and correlations were presented.

Yan [10] conducted a numerical study of combined buoyancy effects on laminar forced convection and mass transfer in a horizontal rectangular duct. Air was used as the cooling medium in the simulation study over a range of parameters. The vorticity-velocity method was used with the Du Fort Frankel scheme to solve the governing equations for flow, heat and mass transfer. In this work, the Rayleigh number was varied from 0 to 10^5 for aspect ratios 0.5, 1 and 2 with buoyancy ratios ranging from 0.8 to 2.0. The results showed that the distribution of local Nusselt (Sherwood) number was characterized by the entrance effect. As a result, the buoyancy-driven secondary flow distorts the axial velocity, temperature and concentration distributions and the nature of the distribution depends on the magnitude of Rayleigh number and buoyancy ratio.

Silekens et al. [11] performed a study of mixed convection in a horizontal square channel. Water was used as the fluid medium passing through a rectangular duct heated symmetrically from side walls. Their study was carried out by both experimental and numerical methods with Reynolds number (Re = 500) and Grashof number was varied around 10^5. Their results showed that the resulting secondary flow induced by buoyancy forces caused a substantial increase in the heat transfer.

Yan and Lee [12] numerically studied the effect of wall transpiration on laminar flow mixed convection and heat transfer in the entrance region of horizontal ducts. The mixed convection heat transfer was formulated by the vorticity-velocity method. Both thermal conditions of uniform heat flux and uniform wall temperature were considered. The predicted results showed that either wall injection or wall suction had considerable impact on the flow structure and heat transfer performance.

Wei et al. [13] studied laminar mixed convection flow and heat transfer in a radially rotating square duct with consideration of rotation induced buoyancy and thermal radiation effects. The vorticity-velocity method was used to solve the three-dimensional parabolic governing equations and the radiative transfer equation was solved by the discrete ordinates method. The results were focused on the effects of the rotational number, rotational Grashof number, Reynolds number, conduction to radiation parameter, optical thickness and wall emissivity on the flow and heat transfer. The result showed that radiation presented significant effect on the axial distributions of the total Nusselt number and reduced the centrifugal buoyancy effects.

Gau et al. [14] investigated mixed convection heat transfer in the rectangular channel heated from a side with the remaining three walls insulated. They studied the flow conditions for a range of Re from 317 to 2000, and buoyancy parameter Gr/Re^2, from 0 to 20,000. The results found that the heated buoyant flow accumulates in the upper region of the channel, which grows in size as the buoyancy parameter increases. The accumulated flow was found to be thermally stable with slower motion which could reduce the heat transfer enhancement by the buoyancy force. Their experimental results were correlated for Nusselt number as a function of the buoyancy parameter.

Ramesh and Merzkirch [15] experimentally investigated combined convective and radiative heat transfer in side-vented open cavities with an isothermal heated vertical and the remaining walls were insulated. Air was used as the fluid medium. An optical

measurement technique was used to obtain the local value of the convective heat transfer coefficient along the heated wall of the cavity and radiative heat transfer rates were estimated by a numerical procedure. Their results presented systematic experiments and highlighted the effect of the interaction of the different modes of heat transfer.

Ramesh and Venkateshan [16] conducted experiments on laminar natural convection heat transfer in a square enclosure using air as the medium. This study included differentially heated isothermal vertical walls and adiabatic horizontal walls with uniform heat flux. The experimental study was carried out using a Differential Interferometer. The experiments achieved adiabatic conditions for top and bottom walls of the enclosure and the results were correlated for average convective Nusselt number for a wide range of parameters to understand the effect of the interaction of surface radiation on natural convection. Their experimental analysis provided valuable information for researchers, particularly for those using numerical methods in analyzing problems of this type.

Leong et al. [17] performed a numerical study on mixed convection heat transfer from a bottom heated open cavity subjected to an external flow. They studied a wide range of governing parameters (i.e., $1 \leq Re \leq 2000$, $0 \leq Gr \leq 10^6$) for cavities with various aspect ratios (A = 0.5, 1, 2 and 4). They found that the Reynolds number and the Grashof number control the flow pattern and the occurrence of re-circulating cells while the aspect ratio had a significant influence on the orientation of these cells. In the mixed convection regime, the heat transfer rate was reduced, and flows become unstable. Their study presented a unique heat transfer correlation which covered all the three convection regimes.

Premachandran and Balaji [18] performed a numerical study to investigate the conjugate convection with radiation from a horizontal channel with protruding heat sources. They considered laminar, incompressible, hydrodynamically and thermally

developing airflow as the working fluid. The effect of parameters such as Re_s, $Gr^2_{s,}$ k_p/k_f, $k_s/k_{f,}$ ε_p *and* ε_s on the fluid flow and heat transfer was studied. Correlations were developed for the non-dimensional maximum temperature. As the emissivity of the protruding heat sources and substrate increased, the non-dimensional maximum temperature decreased. The radiation contribution increased from 12 % to 20 %, as the emissivity of protruding heat source increased from 0.1 to 0.85 at $Re_s = 250$.

Han et al. [19] studied numerically, the mixed convection heat transfer in horizontal rectangular ducts with radiation effects. The study was focused on the interaction of thermal radiation with mixed convection for a gray fluid in rectangular horizontal ducts. The vorticity-velocity method was used to solve the three-dimensional Navier-Strokes equations and energy equation simultaneously. The attention of the results was focused on the effects of thermal buoyancy and radiative heat transfer on the development of temperature; the development on temperature was accelerated by radiation effects. The results showed that radiation effects have considerable impact on the heat transfer and would reduce the thermal buoyancy effects.

Yang et al. [20] experimentally studied the channel divergence on the flow and heat transfer in horizontal ducts with one of the side plates heated uniformly and opposite plate well-insulated. They studied the flow conditions for a range of Re from 316 to 1500, and buoyancy parameter Gr/Re^2 from 0 to 20,000 and Pr of the airflow was 0.707. The effect of the Reynolds number and the buoyancy parameter on the heat transfer was presented and discussed. Their result showed that the small divergence of the duct had a significant effect on both the flow and the local heat transfer.

The above literature review on horizontal ducts shows that significant research has been carried out to study mixed convection heat transfer. Most of the research focused on forced convection in a channel with prescribed heat fluxes on temperature distribution on the wall surfaces. The results show that the buoyancy driven flow is strongly influenced by the wall conditions and causes a substantial increase in heat

transfer rate. The papers that deal with numerical analysis shows that the radiation effect has a considerable impact on the heat transfer and would reduce the thermal buoyancy effects. However, systematic experiments using air as a medium to analyze heat transfer through a duct is found to be lacking. Therefore the present research becomes important.

2.3 Mixed Convection Heat Transfer for Hydrodynamically Developed and Thermally Developing Flow in Horizontal Ducts

Laminar flow mixed convection heat transfer for hydrodynamically fully developed airflow in horizontal duct with the effect of entrance region (different inlet geometries) has been investigated by many researchers. The effect of entrance section on laminar airflow combined convection heat transfer inside a horizontal duct is found to be one of the main regions of interest in this class of problems. Some selected studies of mixed convection heat transfer for fully developed airflow in horizontal ducts with entrance region effects are reviewed below.

Incropera et al. [21] experimentally and theoretically studied forced convection heat transfer from discrete wall sources in a rectangular channel. The problem showed that the single flush mounted heat source and an in-line, four-row array of 12 flush-mounted heat sources were correlated in terms of Nusselt and Reynolds numbers. Correlations were obtained for the turbulent flow regime ($5000 < Re_D < 14{,}000$). The predicted model was in good agreement with measurements for turbulent flow but significantly under-predicted data for laminar flow. The result of average convection coefficient for the rows of the array decreased by 25 % from first to second row and by less than 5 % from the third to the fourth row.

Chiu and Rosenberger [22] investigated the entrance effects in the mixed convection flow from two horizontal differentially heated parallel plates. The study was conducted for nitrogen gas by Laser Doppler Anemometry for a range of $1368 < Ra < 8300$, and $15 < Re < 170$. Two entrance lengths were used for velocity profiles:

first for the onset of instability, and second for the full development of the mixed flow. Further study was carried out [23] to obtain the fully developed velocity profiles in the range of $2472 < Ra < 8300$, and $15 < Re < 150$. Their result showed that transverse velocities of the longitudinal convection rolls were independent of the forced flow.

Lei and Trupp [24] experimentally investigated laminar water flow in the entrance region of a horizontal semicircular duct with uniform heat input. The measurements consisted of axial and circumferential wall temperature variations together with pressure drop across the heated section. In their study, the Reynolds number was varied from 400 to 1600 and the Rayleigh numbers up to 4.6×10^8. The local and fully developed Nusselt number results showed substantial circumferential variations and increased with increasing heat flux level. The laminar mixed convection flow regime correlations were provided which helped to reveal some key features of the problem.

Nyce et al. [25] experimentally and numerically studied mixed convection in a rectangular channel with a bottom heated wall by using Doppler Anemometry technique using nitrogen as the fluid. For a Rayleigh number of 22200, they reported that unsteady flows were found even for a Reynolds number of 18.75. The heat conduction at the side walls was also included in the study. The results showed that transverse velocities were found to be independent of Re.

Lin and Lin [26] carried out experiments on combined flow visualization and conjugate heat transfer analysis of the axial evaluation of the buoyancy-induced secondary vortex flow in a mixed convection air flow in bottom heated horizontal rectangular duct. For the conjugate analysis, the unsteady three dimensional Navier-Strokes and energy equations for the flow were coupled with the unsteady two dimensional conduction equations for the solid walls. Results were obtained for Reynolds number ranging from 35 to 102, and Grashof number from 1600 to 5.8

x 10^5. Both experimental and numerical results showed that the generation of longitudinal vortex rolls in the entry half of the duct, and the merging of these rolls downstream. These experimentally observed vortex flow structure were in good agreement with conjugate heat transfer analysis.

Chang and Lin [27] experimentally studied the effects on longitudinal vortex flow for mixed convection of air in a horizontal rectangular duct. In their study, combined flow visualization and temperature measurement were carried out to investigate the effects of the aspect ratio on the spatial and temporal structures of the vortex flow induced in a mixed convection of air in a bottom heated rectangular duct. In their study, the Reynolds number was varied from 2.5 to 50, the Rayleigh from 3000 to 20,000 and the aspect ratio from 2 to 12, covering the steady and unsteady longitudinal vortex flow. Reducing the Reynolds number in a higher aspect ratio duct was found to cause the vortex flow to progress from a steady to an unsteady state with more frequent roll splitting and merging.

Barletta and Zanchini [28] numerically studied the effect of the choice of reference fluid temperature on the solutions of fully-developed mixed convection in a plane vertical channel. The boundary conditions of uniform wall temperature and uniform heat flux on the opposite wall were considered. The results showed that the choice of reference temperature affects both the velocity profiles and the axial change of the difference between the pressure and hydrostatic pressure.

Dogan et al. [29] conducted experimental studies on mixed convection heat transfer in a rectangular channel with discrete heat sources at the top and at the bottom. The channels were equipped with 8 x 4 flush mounted heat sources subjected to uniform heat flux. The study was done for an aspect ratio 6, the flow conditions range of Re from 955 to 2220 and modified Grashof numbers $Gr^* = 1.7 \times 10^7$ to 6.7×10^7. They found that the surface temperatures increased with increasing Grashof number. The increase in the buoyancy affected secondary flow and the onset of instability.

Iskra and Simonson [30] performed experiments to determine the convective mass transfer coefficient for evaporation in a horizontal rectangular duct with an aspect ratio of 14.5:1. In their study, a short pan of water formed the lower panel of the long duct where a hydrodynamically fully developed laminar or turbulent airflow passes over the surface of water. The range of Reynolds number 570 to 8100, Rayleigh number 6300 to 83,000, inverse Graetz numbers 0.003 to 0.04, and dimensionless operating conditions factors -3.6 and -1.4 were considered. Their findings concluded that the measured convective mass transfer coefficients increased as Re, Ra and Gz increased, and these effects were included in the Sherwood number correlations presented in this paper.

Mohammed and Salman [31] experimentally studied mixed convection heat transfer for hydrodynamically fully developed, thermally developing and thermally fully developed laminar air flow in a horizontal circular cylinder. Reynolds number within the laminar region ranging from 400 to 1600, the heat flux varied from 60 W/m^2 to 400 W/m^2 and with cylinder inclination angle of $\theta = 0^0$ (horizontal) was examined. Four entrance lengths were used, and for all entrance sections, it was found that the Nusselt number values increased as the heat flux increased. The study was extended [32 &33] to investigate the effects of different entrance sections on mixed convection heat transfer inside a horizontal circular cylinder. The average heat transfer results were correlated with an empirical correlation in terms of dependent parameters of Grashof, Prandtl and Reynolds numbers.

Dogan and Sivrioglu [34] experimentally investigated mixed convection heat transfer from longitudinal fins in a horizontal channel. A parametric study was conducted to investigate the effects of fin spacing, fin height and magnitude of heat flux on mixed convection heat transfer from a rectangular fin array heated from below in a horizontal channel. Air was used as the working fluid and the velocity of fluid entering channel was kept constant. Experiments were conducted for modified Rayleigh numbers $3 \times 10^7 < Ra < 8 \times 10^8$ and Richardson number $0.4 < Ri < 5$. The

result showed that the optimum fin spacing that yielded the maximum heat transfer was S = 8-9 mm and optimum fin spacing was dependent on the value of Ra*.

Chandratilleke et al. [35] performed a numerical investigation on airflow through a heated horizontal rectangular duct with combined modes of natural and forced convection heat transfer and thermal radiation form duct walls. The duct periphery was differentially heated using isothermal vertical walls and adiabatic horizontal walls having uniform heat flux. In this study, the air flow enters into the duct hydrodynamically fully developed and thermally developed within the duct. This study considered several temperature profiles on the two vertical side walls, range of flow rates, duct aspect ratios and surface emissivity. The result showed that mixed convection heat transfer rates were well above those achievable from forced convection dominated flow. The surface radiation significantly affected the wall equilibrium temperature and generated thermal instability under certain conditions.

Pirasaci et al. [36] conducted experimental studies on laminar mixed convection heat transfer in a top and bottom heated rectangular channel with protruded discrete heat sources. The lower and upper surfaces of the channel were equipped with 80 x 4 protruded heat sources subjected to uniform heat flux. An experimental study was made for Height/Width (H/W) ratios of (1/2), (1/4), (3/20) at various Reynolds number and modified Grashoff numbers. From experimental measurements, row-average surface temperature and Nusselt number distributions of the discrete heat sources were obtained and effects of Reynolds and modified Grashoff numbers on these distribution were investigated. The result show that the buoyancy affected secondary flow is more effective at the greater values of H/W ratios.

Considerable experimental research has been carried out by many researchers on the bottom heated horizontal duct, horizontal circular cylinder, aspect ratio effects in horizontal duct and rectangular channel with discrete heat sources at the top and bottom. Their results showed that the secondary flow induced by the thermal

buoyancy force can significantly enhance the heat transfer and also concluded that the effects of buoyancy would tend to decrease the thermal entrance length. The results were correlated with an empirical correlation in terms of the dependent parameters such as Grashof, Prandtl and Reynolds numbers.

2.4 Mixed Convection Heat Transfer for Thermally Developing Flow in Vertical Ducts

Mixed convection heat transfer for thermally developing airflow in vertical ducts has been of special interest recently due to application areas such as cooling of electronic equipment, compact heat exchangers, solar collectors and thermal-energy conversion devices. Much work, both theoretical and experimental, has been done on mixed convection heat transfer in vertical duct flows. A review of published literature relevant to the present study is given below.

Jackson et al. [37] presented a comprehensive review of experimental and theoretical studies of mixed convection heat transfer in internal flows. The aim of their study was to provide up to date review of works concerned with mixed convection heat transfer in vertical tubes. The review was divided into two sections; the first dealing with laminar flow; and, the second dealing with turbulent flow. Further subdivisions were made according to the theoretical and experimental work. Their study provided valuable information for many researchers with some general comments and recommendations.

Huang et al. [38] carried out experiments on mixed convection flow and heat transfer in a vertical convergent channel. One of the side vertical position wall was heated uniformly and the opposite wall was insulated with a convergent angle of 3^0. The ratio of the height to the width at the inlet of the channel was 15. They studied the Reynolds number range from 100 to 4000, and the buoyancy parameter Gr/Re^2 range from 0.3 to 907. Temperature fluctuations at different locations were measured and used to indicate oscillations and fluctuations of the reversed flow. The effect of the

buoyancy parameter on the reversed flow structure and the Nusselt number was presented and discussed. The Nusselt numbers were correlated in terms of the relevant non-dimensional parameters for both pure forced and mixed convection.

Lee et al. [39] numerically studied mixed convection heat transfer in a vertical rectangular duct with film evaporation along the porous wall. The Boussinesq approximation was involved to take into account the buoyancy effect induced by thermal and mass diffusion. The numerical results were presented including the development of velocity, temperature, concentration, Nusselt number, Sherwood number and friction factor. Predicted results showed that the influences of the combined buoyancy force of thermal and mass diffusion on the flow, heat and mass transfer were significant. Due to film evaporation along the wetted wall, the mass transfer was found to enhance the heat transfer rate along the wetted wall.

Pu et al. [40] experimentally studied mixed convection heat transfer in a vertical channel with asymmetric heating. The experiments were conducted under a wide range of $2 < Pe < 2200$ and $700 < Ra < 1500$. The measured temperature distribution showed the presence of secondary convective cell in the mixed convection regime. The experimental data was correlated for Nusselt number in terms of Peclet number and Rayleigh numbers. The correlation equation agreed well with the experimental data.

Wei et al. [41] performed a numerical study to investigate the effects of thermal radiation with laminar mixed convection for a gray fluid in a vertical square duct. They used the vorticity-velocity method, three-dimensional Navier-Strokes equations and energy equations. The radiative heat transfer equation was solved by the discrete ordinates method. The thermal radiation effects are emphasized thermal buoyancy and radiative transfer on the development of velocity and temperature field, the friction factor and the Nusselt number. The results showed that radiation significantly affects the total Nusselt number Nu_t and tends to reduce the buoyancy effects.

Rao et al. [42] studied numerically the problem of two dimensional, steady, incompressible, conjugate, laminar mixed convection with surface radiation in a vertical parallel plate channel, provided with a flush mounted discrete heat source in each wall. Air was used as the cooling medium. The effect of surface emissivity, aspect ratio, discrete heat source position and modified Richardson number on the fluid flow and heat transfer characteristics was investigated. Correlations were developed for the maximum temperature of the left and the right channel walls and the mean friction coefficient.

Barletta et al. [43] conducted a numerical study on combined forced and free flow in vertical rectangular duct with a prescribed uniform wall heat flux using the Galerkin finite element method. Different heat flux values for each plane wall were considered. The numerical solution provided the dimensionless velocity and the temperature distributions, together with the values of the Fanning friction factor, Nusselt number, momentum flux correction factor and the kinetic energy correction factor. These dimensionless parameters were reported as functions of the aspect ratio and the ratio between the Grashof number, and the Reynolds number.

Krishnan et al. [44] proposed a correlation for combined natural convection and radiation between parallel vertical plates. In this experimental study, air was used as the fluid medium between parallel plates. The results were presented in a correlation equation form, and reported that the non-dimensional temperature excess of the heated plate was due to the effect of radiation heat transfer.

Krishnan et al. [45] studied experimentally and numerically the problem of combined free convection and surface radiation between parallel plate vertical channels. The radiative heat transfer rate at the hot surface was computed by the radiosity-irradiation method. Experiments were done for six plate spacings ranging from 12.66 to 52.2 mm, and for an order of magnitude range of wall to ambient temperature difference. The analysis showed that the significance of radiation heat

transfer rate even at a low temperature of 310 K. Correlations were developed for the average convective Nusselt number in terms of Grashof number and the aspect ratio based on 133 data points for a Grashof number range $2370 < Gr < 872700$.

Huang et al. [46] numerically examined the mixed convection heat and mass transfer in vertical rectangular ducts with film evaporation and condensation. The work focused on the effect of aspect ratio of the duct, wetted wall temperature, Reynolds number of the flow and the inlet relative humidity on momentum, heat and mass transfer. The numerical result showed the distribution of dimensionless axial velocity, temperature and concentration distributions. Nusselt number as well as Sherwood number was presented for moist air mixture system with different wall temperatures and aspect ratios of the ducts. Their result showed that the latent heat transport with film evaporation and condensation tremendously enhanced the heat transfer rate.

Barletta et al. [47] studied the fully developed mixed convection flow with frictional heat generation in a vertical channel bounded by isothermal plane walls. The local mass, momentum and energy balance equation was developed according to the Boussinesq approximation, without fixing explicitly the reference temperature. Their results revealed that neither the velocity field nor the temperature field was influenced by the choice of the reference temperature. On the other hand, a choice of the reference temperature was needed in order to determine the axial pressure gradient. Finally the mechanical and thermal characteristics of the dual flow regimes were discussed in detail both analytically and numerically.

Grosan and Pop [48] numerically investigated the effect of radiation on the steady mixed convection flow in a vertical channel. The Rosseland approximation method was used in the modeling of the conduction radiation heat transfer and temperature of the walls were assumed constants. The results revealed that there was a decrease in reverse flow with an increase in the radiation parameters.

Molla and Hossain [49] investigated the effect of thermal radiation on a steady two dimensional mixed convection laminar flow along a vertical wavy surface. The governing boundary layer equations of motion were transformed into a non-dimensional form and the resulting non-linear systems of partial differential equations were solved numerically by two methods namely Keller box method and straightforward finite difference method. The numerical results for streamline and skin friction coefficient, local, average and total number for a range of radiation conduction parameters, surface heating parameter, amplitude of wavy surface and the Richardson number were presented.

Rao and Narasimham [50] studied numerically laminar flow conjugate mixed convection in a vertical channel with protruding heat generating ribs attached to substrates forming channels. The substrates with rib form a series of vertical parallel plate channels. The heat sources and substrates simulate integrated circuit package attached to printed circuit boards. The Reynolds number variation was based on the fan velocity component rather than the combined natural and forced convection velocity. The result showed that simple adiabatic boundary condition for the substrate and isothermal condition for the heat source portions are not appropriate and that the conjugate nature of the problem should be duly considered taking into account the heat conduction in both the components and the substrate. They also found that the lower thermal conductivity substrate could be very effective in terms of heat removal and redistribution of the heat from the components.

Mohammed and Salman [51] experimentally studied mixed convection heat transfer for assisting thermally developing flow in a uniformly heated vertical circular cylinder. Reynolds number within the laminar region ranged from 400 to 1600, the heat flux varied from 60 W/m^2 to 400 W/m^2 and the effect of the cylinder inclination angle on the mixed convection process was examined. Four entrance lengths were used, the entrance section pipes having the same diameter as test section pipe but with variable lengths. Their result showed that the surface temperature values

decreased as the cylinder inclination angle moved from vertical to horizontal. The average heat transfer results were correlated with an empirical correlation in terms of dependent parameters of Grashof, Prandtl and Reynolds numbers.

Balaji et al. [52] numerically studied turbulent mixed convection from vertical parallel plate channels. The treatment of turbulent mixed convection as a parameter perturbation problem in Richardson number was demonstrated. Temperature wall functions for natural and forced convection were suitably blended in order to arrive at a wall function for mixed convection. Asymptotic consideration provided the credibility and the much needed physical basis for derivations. Their analysis clearly showed the need for more direct numerical solution results for mixed convection.

From the review of the literature presented above, it can be inferred that numerical study of mixed convection heat transfer in the vertical channel geometry has received considerable attention. Also no study has considered the experimental analysis of mixed convection with surface radiation in vertical ducts with differentially heated walls. Most of the papers focused on mixed convection heat transfer in rectangular ducts, surface radiation between parallel vertical plates, vertical rectangular ducts with film evaporation and condensation and conjugate mixed convection in a vertical channel with protruding heat source. The results showed that radiation significantly affects the total Nusselt number and tends to reduce the buoyancy effects. Moreover, the correlated results were developed for the average convective Nusselt in terms of Grashof number, temperature of the channel walls and Reynolds number.

2.5 Summary

From a careful review of the published literature, it is clear that although several studies on mixed convection are reported in literature, no experimental studies have been published on mixed convection and radiation heat transfer in duct flows and also no experimental study has so far considered the analysis of mixed convection in horizontal and vertical ducts provided with differentially heated walls.

In addition, most of the studies reported in the literature investigated the combined effect of radiation only for gray fluids. So far, it is found that several researchers have neglected the effect of surface radiation heat transfer among the inside surfaces of the walls of the duct due to the assumption that it had small or negligible effects. The surface radiation from the walls of the duct will affect significantly affect free convection heat transfer rates. Air is a radiatively non-participating fluid, and is commonly used as the preferred medium in industrial heat transfer applications. Only little information is known about the surface radiation contributions due to air temperatures affecting the heat transport process. Hence, it is very important that the surface radiation effect is identified, and accounted for the analysis of flow and heat transfer through ducts. Furthermore, the literature review in this chapter underscores the importance of the present research, highlighting the research objectives outlined in Chapter 1.

CHAPTER 3

EXPERIMENTAL METHODOLOGY

3.1 Introduction

A comprehensive review of literature relevant to the present work was presented in Chapter 2. The experimental methodology for mixed convection heat transfer experiments in horizontal and vertical ducts with radiation effects carried out in the present research is presented in this chapter. To obtain the radiation heat transfer from the hot wall, a numerical modeling scheme using the computational fluid dynamics solver FLUENT [53] was developed, in order to simulate the test section and to carry out heat transfer analysis. All experiments were carried out at the Thermodynamics Laboratory at the Miri campus of Curtin University in Malaysia.

3.2 Problem Statement

The experimental work considered in this thesis is divided in to 3 Case Studies, as follows: (i) mixed convection heat transfer in thermally developing flow in horizontal ducts (CS1); (ii) hydrodynamically developed thermally developing flow in horizontal ducts (CS2), and (iii) thermally developing flow in vertical ducts (CS3). The major parameters considered in this work are wall heat flux, emissivity of walls, Reynolds number and aspect ratios. The surface radiation of the walls is brought in through the wall surface emissivity (ε), which has two values: 0.05 and 0.85. In order to cover the wide range of emissivity, a low value of 0.05 and high emissivity value of 0.85 were selected. These emissivity values represent the weak and strong radiation respectively, and cover the full range of practically available surfaces. The heat flux is varied from 250 W/m^2 to 870 W/m^2.

The Reynolds number is varied from 800 to 2900. The variation of Reynolds number is same for both cases of square and rectangular ducts so as to enable a meaningful comparison. Table 3.1 shows the Reynolds numbers for square and rectangular ducts considered in the study. The thermally developing section length 270 mm is calculated based on five times the height of the test section [16].

Table 3.1 Table of Reynolds numbers

Aspect Ratio (AR)	Cross-sectional duct size (height x width) mm	Hydraulic Diameter mm	Airflow Velocity m/s	Reynolds number Re
1	54 X 54	54	0.24	858
1	54 X 54	54	0.50	1788
1	54 X 54	54	0.80	2861
0.5	54 X 27	36	0.36	858
0.5	54 X 27	36	0.75	1788
0.5	54 X 27	36	1.20	2861

The duct sizes are represented by aspect ratio, which is defined as width divided by the height of the duct. Two aspect ratios 1 and 0.5 are considered to study the effect of duct size on the heat transfer characteristics. The aspect ratio 1 and 0.5 represents the square and rectangular duct respectively. The length and height are the same for both cases, except the width.

The design of the test section was such that it can be removed or attached as and when required from the rest of the hardware. The test sections were made of two differentially heated isothermal walls and two adiabatic walls. The heated wall temperature ranged from 55 ^{o}C to 100 ^{o}C and the cold wall directly opposite to the heated wall was maintained at a uniform temperature, and was always ensured to be equal to the inlet temperature of air entering the duct. The other two walls of the duct were insulated, and hence no heat transfer took place across these two walls.

3.3 Description of the Test Rig

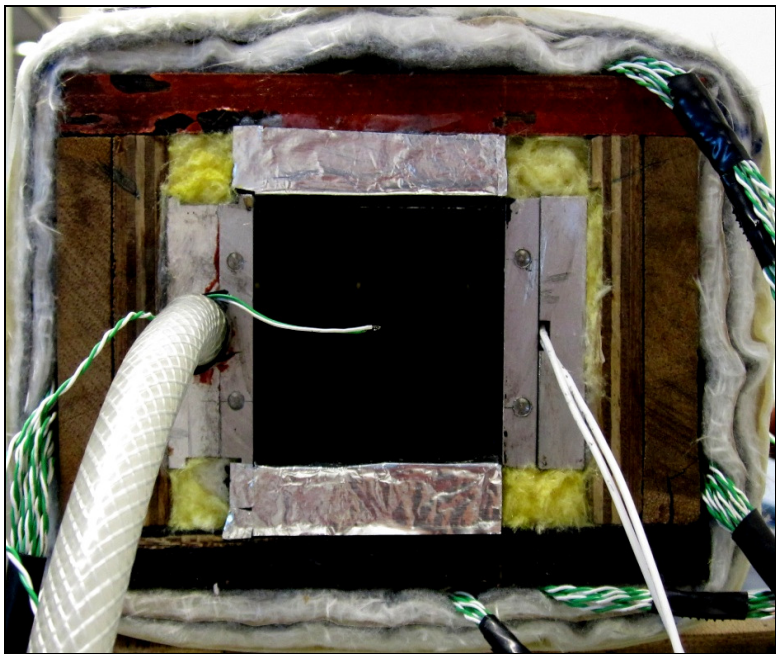

Figure 3.1 Photograph of the square test section.

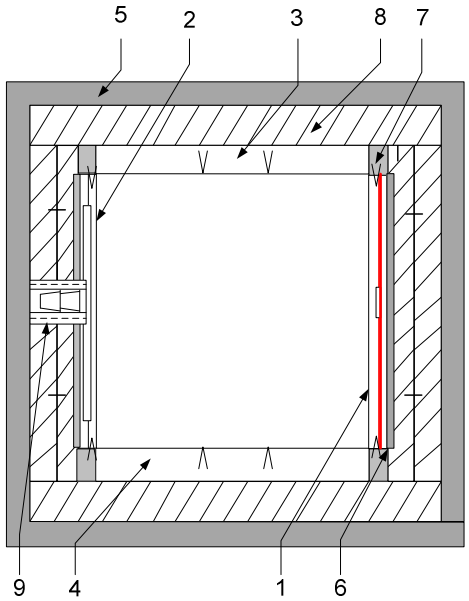

Figure 3.2 Schematic of the 54 mm x 54 mm (square) experimental test cell (1 and 2. isothermal hot and cold walls respectively, 3 and 4. adiabatic walls, 5. insulation, 6. electric heater, 7. thermocouples, 8. wood, 9. water circulation port).

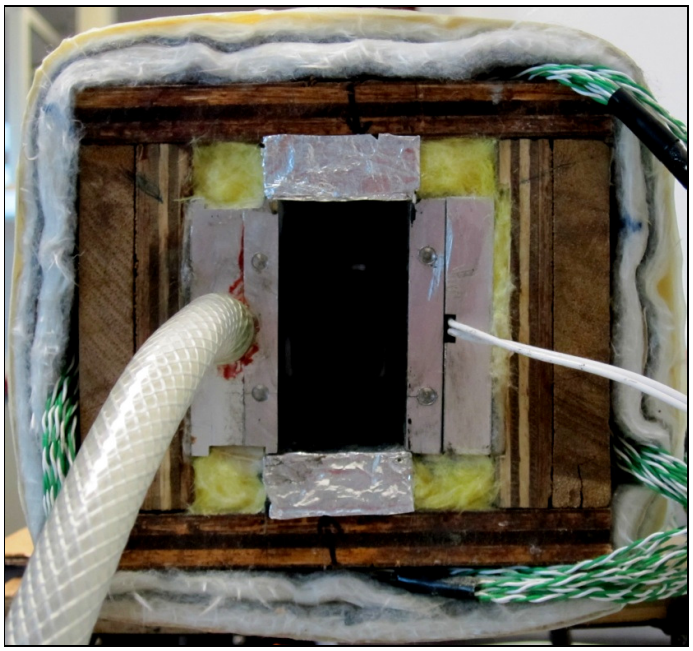

Figure 3.3 Photograph of the rectangular test section.

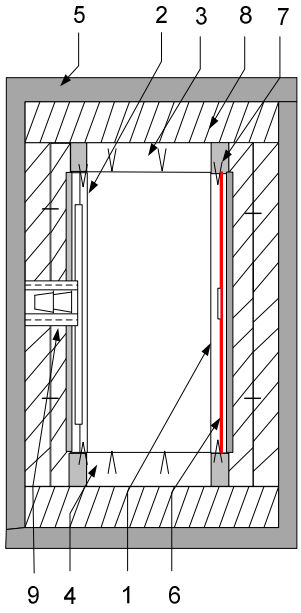

Figure 3.4 Schematic of the 54 mm x 27 mm (rectangular) experimental test cell (1 and 2. isothermal hot and cold walls respectively, 3 and 4. adiabatic walls, 5. insulation, 6. electric heater, 7. thermocouples, 8. wood, 9. water circulation port).

The test rig consists of the square and rectangular test sections, heater, blower and instrumentation. In this section the test section and the other components of the test rig are described in detail. Square and rectangular test sections are used in the present study in order to cover the required range of Reynolds numbers and other controlling parameters. The photograph and schematic of the square test section are shown in Figure 3.1 and 3.2, respectively. The square test section has inner dimensions of 270 mm (length) x 54 mm (width) x 54 mm (height). The photograph and schematic of the rectangular test section are shown Figure 3.3 and 3.4 respectively. The rectangular test section has inner dimensions of 270 mm (length) x 27 mm (width) x 54 mm (height). Both test sections are of same length and height, but have different widths to enable two different aspect ratios as mentioned earlier.

The test sections were made of two differentially heated isothermal vertical walls and two adiabatic horizontal walls. The isothermal hot and cold walls were made of aluminum. The hot wall incorporated an electrical heater made of silicon rubber, which formed the heat source for the duct. The heater was embedded in between the aluminum plates. A 5 mm glass-wool insulation and 20 mm wooden plate was glued to the backside of the hot wall. Alternating Current (AC) power supply with a suitable regulator was used to provide the electrical energy for producing the desired heat flux for the heater. Two thin film heat flux sensors (Model HFS-4) from Omega Engineering, attached to the heated wall surface within the duct were used to measure the heat flux on the surface of the heated wall. It was located midway from the centre of the heated wall, and between the inlet and outlet sections of the duct; approximately 20 mm away from the entry and exit of the center of the heated wall surface.

The cold wall consisted of a milled-channel to circulate constant temperature water provided by a thermostat with fuzzy control system (WiseCircu Fuzzy Control System, flow rate – 6 l/min, ± 0.05 ^{o}C) to act as a constant temperature sink. For better insulation, glass-wool and 20 mm wood as insulations were glued to the

backside of the cold wall. The cold wall temperature was always maintained to be equal to the inlet air temperature throughout the experiment, and for all experiments considered in this study. The inside surface of the cold wall and the hot wall were highly polished in order to achieve a mirror finish, to have a low emissivity of 0.05, or coated with blackboard [A3] paint to have an emissivity of 0.85. An emissometer [A4] was used to measure the surface emissivity of the internal walls of the duct. K-type thermocouples were provided in the hot and cold wall at various locations along the length (inlet to outlet), for measuring the respective wall temperatures. The distance between the two neighboring thermocouple rows was 15 mm, and the spacing between the neighboring columns was 30 mm. Ten thermocouples were fixed in the walls in each row.

The top and bottom walls made of Perspex were milled, based on the design requirement for the two different aspect ratios. In assembling the test section, one of the most important considerations was to make sure that there was no physical contact between the walls. Slots were provided at all corner of the test section such that there was no conduction heat transfer across the walls. Glass-wool insulation material was filled in all corners of the test section to avoid air circulation in the slots. During the fabrication of test section, a 0.5 mm clearance between the edges was provided to ensure that the edges of the hot and cold walls did not touch the top and bottom walls. Thermocouples were embedded in the top and bottom wall at various locations along the length (inlet to outlet) direction, for measuring the respective wall temperatures. The distance between the two neighboring thermocouple rows was 15 mm, and the spacing between the neighboring columns was 54 mm; totally 6 thermocouples fixed in each row. This was done in order to obtain the temperature distribution along the inside of the top and bottom horizontal walls. The top and bottom walls were painted black (on the inside surface) in order to obtain a surface emissivity of about 0.85 or provided with very thin aluminum foil (on the inside surface) so as to obtain a surface of emissivity of about 0.05.

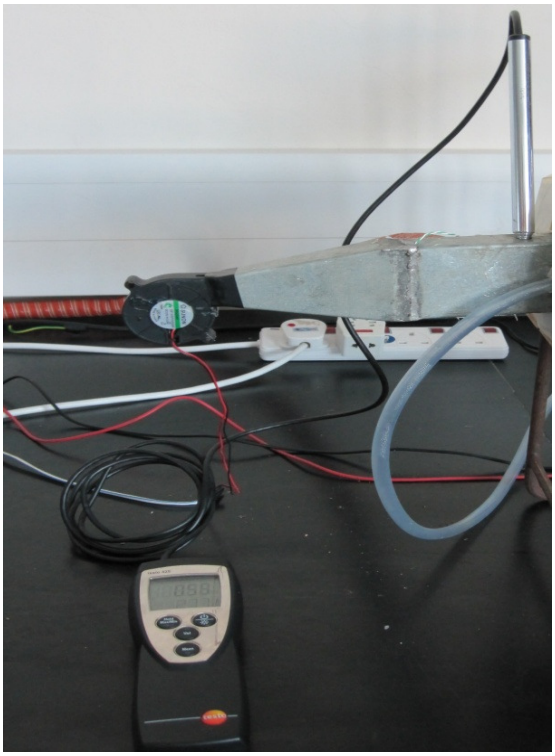

Figure 3.5 Photograph of the blower with Anemometer used in experiments.

Figure 3.5 shows the photograph of the blower with the anemometer [A5] used in this experiment. The blower provided air through the test section from the inlet of the test section to the exit, with an operating range of 3 -12 V DC, and had a diameter of 36 mm. The blower was connected to the laboratory DC power supply with a regulator to provide the desired voltage. The flow rate was measured by using an anemometer (Testo 425) with an accuracy of ± 1.5 %. The anemometer probe was inserted from a small hole of 7 mm diameter located on the top side of the test section to measure the airflow velocity within the duct.

To avoid conduction heat loss and air leakage from the test section, the outside of the test section was fully wrapped with two layers of glass wool insulation having total thickness of 12 mm. A typical experimental run consisted of maintaining the desired temperatures for the hot and cold walls, starting the blower, attaining steady state conditions and then recording a set of data.

3.4 Data Analysis

The following steps are used to characterize the heat transfer process for air flow in a duct when the heated surface (in this case, one of the walls of the duct) is subjected to a constant heat flux boundary condition.

The convection heat flow from the hot wall surface is obtained as

$$Q_{conv} = Q_{tot} - Q_{cond} - Q_{rad} \tag{3-1}$$

where, $Q_{cond.}$is the heat loss by conduction along the heated wall. Q_{rad} is the radiation heat transfer rate from the heated wall, which is obtained from the computational analysis using FLUENT [53]. For all cases considered in this study, the conduction heat loss across the hot wall was estimated using the composite wall conduction heat transfer analysis for modeling the heated vertical wall, and the thickness of the insulation. The conduction heat loss from the heated wall was found to be very small and negligible. In this experimental study, thin film heat flux sensor (Model HFS-4) was used to measure the total heat flux directly from the hot wall, which was further used in the calculations to obtain the total heat transfer (Q_{tot}).

The convection heat flux from the heated wall surface (within the duct) is calculated using the relation:

$$q_{conv} = \frac{Q_{con}}{A_S} \tag{3-2}$$

where

$$A_s = H \times L$$

The average convective Nusselt number at the heated wall is calculated based on the hot wall surface temperature and the mean temperature of air as follows:

$$Nu_{conv} = \frac{q_{con} D_h}{(T_h - T_m) k_m} \tag{3-3}$$

where

$$T_m = \frac{(T_{in} + T_{out})}{2} \tag{3-4}$$

The average radiative Nusselt number at the hot wall is given as

$$Nu_{rad} = \frac{q_{rad} D_h}{(T_h - T_m) k_m} \tag{3-5}$$

The total Nusselt number at the heated vertical wall is then obtained as the sum of the convective and radiative Nusselt numbers [15], and is given as

$$\mathrm{Nu}_{\mathrm{total}} = \mathrm{Nu}_{\mathrm{conv}} + \mathrm{Nu}_{\mathrm{rad}} \tag{3-6}$$

Table 3.2 Range of parameters considered in the present study

Parameter	Range
T_h (^oC)	55 - 100
T_c (^oC)	27 - 32
T_{in} (^oC)	21 - 24
U_{in} (m/s)	0.2 - 1.30
AR	0.5, 1
ε	0.05, 0.85
H (m)	0.054
W (m)	0.054, 0.027
L (m)	0.270
Re	800 - 2900

Table 3.2 provides the range of parameters covered in the experimental study. The total heat transfer from the duct is influenced by the temperature of the walls, emissivity of walls, the aspect ratio of the duct cross section, and the flow rate of air through the duct.

3.5 Temperature Measurement

For measuring the duct wall surface temperatures, Type K (Chromel – Alumel) thermocouples from RS components were assembled in the duct walls at various locations along the length (inlet to outlet) direction. The thermocouples were made of 0.3 mm diameter wire, and were embedded in holes drilled close to the surface of the duct walls. To prepare the thermocouple wire for beads, about 10 mm of the insulation around the wires were removed and twisted together, then the twisted wire

were made of small beads. For consistent and accurate temperature measurement, the bead sizes were maintained the same for all thermocouples. All the thermocouples used in the present study were calibrated over the range of interest using a precision thermometer as reference and a constant temperature bath. The uncertainty in temperature measurements is estimated to be within ± 0.04 ^{o}C; the details of the calibration of Type K thermocouples are provided in Appendix A1. Additionally, two thermocouples were placed at the beginning and end of the test section to measure the entry (T_{in}) and exit (T_{out}) air temperatures from the test section. Four thermocouples were fixed outside of the insulated wall to obtain wall temperatures used for estimation of conduction heat loss to the ambient from the duct wall. For all the cases considered in this study, the conduction heat transfer rate across the hot wall was estimated using the composite wall conduction heat transfer analysis for modeling the heated vertical wall, and the thickness of the insulation. As mentioned earlier, this was found to be very small and negligible.

3.6 Flow Visualization

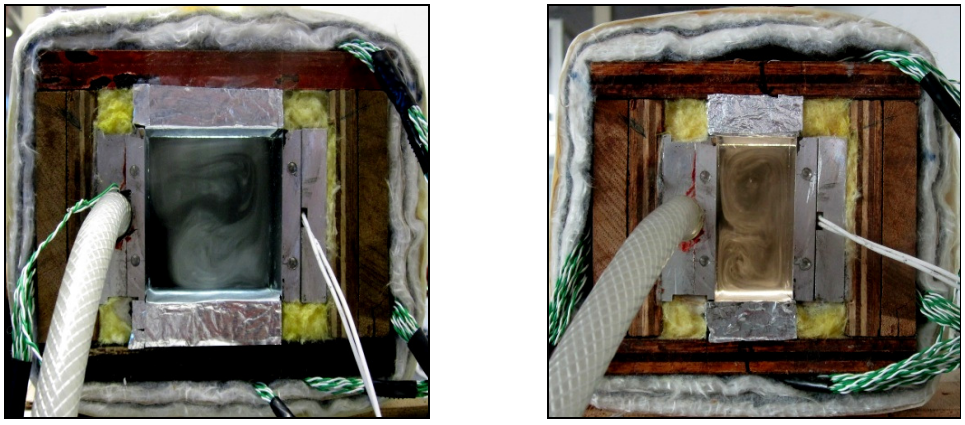

(a) (b)

Figure 3.6 Photograph of the flow visualization at a cross section of the duct.

Figure 3.6 (a) and (b) show the photograph of the test section for visualizing the mixed convection flow structure for the square and rectangular duct respectively.

Flow visualization experiment was conducted to observe the qualitative flow patterns within the duct due to natural and mixed convection. A smoke generator (Rocket Smoke Fluid Aerosols (PS23), Pea Soup Ltd) was used to supply smoke to the test section through a 1.5 mm slot created at the side of the test section entrance at a suitable location closer to the exit of the duct. When illuminated through the top wall by an illuminator (LB Cold beam 5W Illuminator) and viewed from the end of the front test section, a sharp contrast was achieved between walls and the smoke. Flow visualization photographs were obtained using a Cannon digital (IXUS 100 IS) camera with suitable settings. The smoke particle size (mass median diameter) range was between 0.2 - 0.3 micron and this smoke was able to trace the flow in the duct.

3.7 Experimental Methodology for Thermally Developing Flow in Horizontal Ducts

A photograph and schematic diagram of the experimental test rig is shown in figure 3.7 and 3.8, respectively. The experimental work represents the case of mixed convection heat transfer for thermally developing flow in horizontal ducts with radiation effects (CS1). The test set-up consisted of a centrifugal blower with speed-regulator control, test section, measuring probes, data acquisition system, and a power supply unit. Voltage regulator and digital voltmeter were used to control and measure the input power to the heater and the blower. The blower provided air through the horizontal duct and the airflow passed through the test without a developing section. In the current work, the Reynolds number ranged from 800 to 2900, the range was selected suitably for both cases of square and rectangular duct. When the fluid enters the duct, convection heat transfer occurs and thermal boundary layer begins to develop. In addition, if the heated wall surface condition is fixed by imposing either a uniform temperature or a uniform heat flux a thermally fully developing wall heat flux is reached.

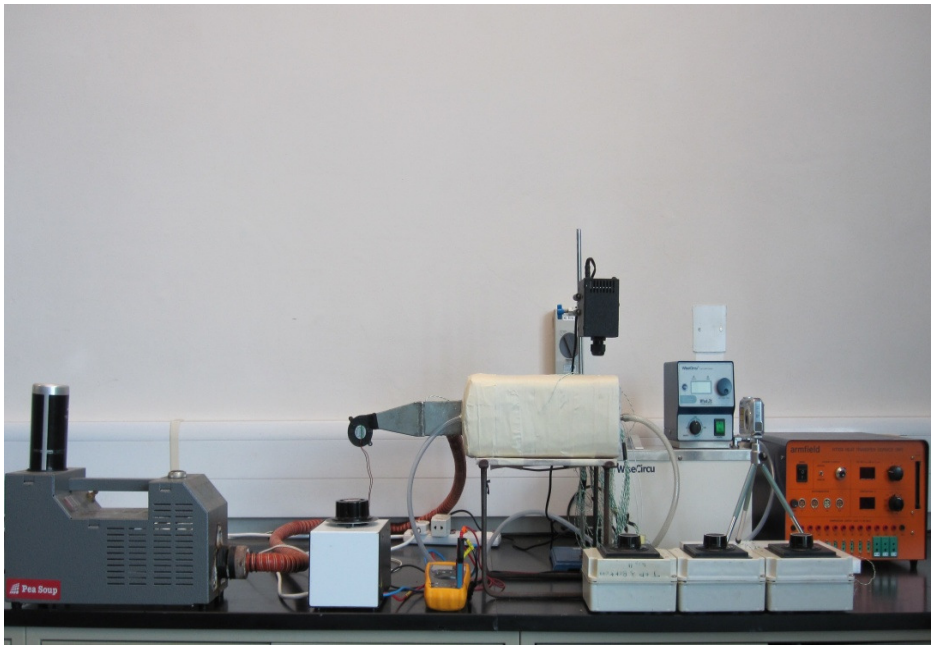

Figure 3.7 Photograph of the experimental test rig for horizontal duct.

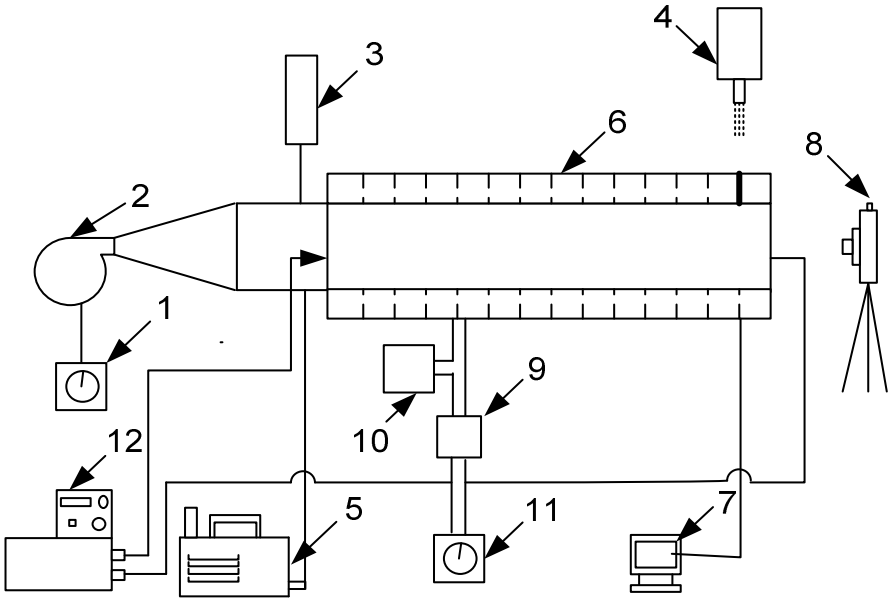

Figure 3.8 Schematic of the experimental rig shown with various components (1. dc power supply, 2. blower, 3. anemometer, 4. illuminator, 5. smoke generator, 6. test section, 7. data acquisition system, 8. camera, 9. voltmeter, 10. ammeter, 11. ac power supply, 12. water bath).

For the experimental work described in this thesis, the square and rectangular test sections were separately investigated. These test sections had the facility to be removed or attached as and when required. The details of the test section were described in Section 3.3 and other parameters followed in this experiment were mentioned in the Section 3.2. Two different wall surface emissivities were considered in this study, which had two values: 0.05 and 0.85, to represent for weak and strong radiation effects, respectively. A typical experimental run consisted of maintaining the desired temperatures for the hot and cold walls, starting the blower, attaining steady state conditions and then recording a set of data. The cold wall temperature was always maintained to be equal to the inlet air temperature throughout an experiment, and for all experiments considered in this study. Flow visualization was conducted to observe qualitative pattern of the flow from the horizontal ducts; the details of the flow visualization set up was described in Section 3.5.

3.8 Experimental Methodology for Hydrodynamically Developed and Thermally Developing Flow in Horizontal Ducts

Figure 3.9 (a) - (c) shows the photograph of the experimental test rig and figure 3.10 show the schematic diagram of experimental test rig. The experimental work represented the case of mixed convection heat transfer for hydrodynamically developed and thermally developing flow in horizontal ducts with surface radiation effects (CS2). The test set-up consisted of a centrifugal blower with speed-regulator control, flow developing channel, test section, measuring probes, data acquisition system, test cell, and a power supply unit. Voltage regulator and digital voltmeter were used to control and measure the input power supply. The investigation covered two Reynolds numbers (Re = 858 and 1788) the range has been selected to be suitable for both cases of square and rectangular duct.

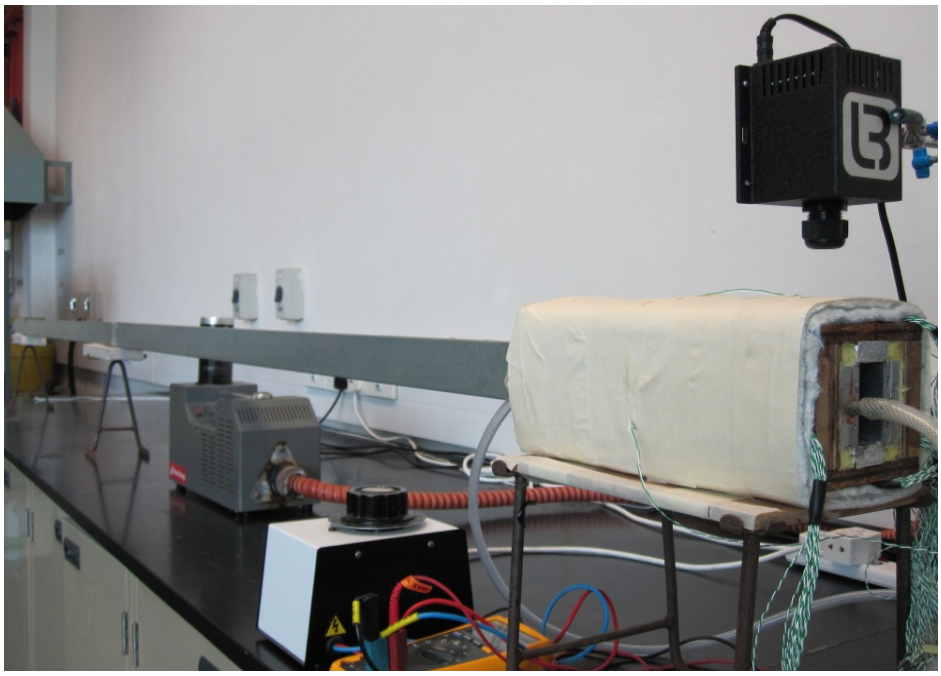

Fig 3.9 (a)

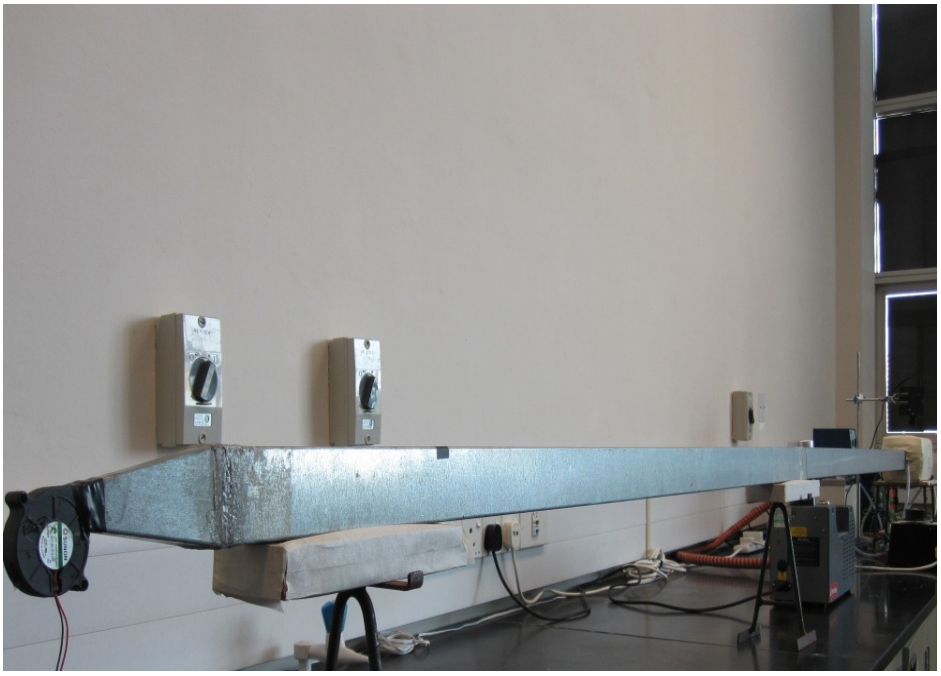

Fig 3.9 (b)

Fig 3.9 (c)

Figure 3.9 (a, b, c) Photograph of the experimental test rig for hydrodynamically developed flow in horizontal duct.

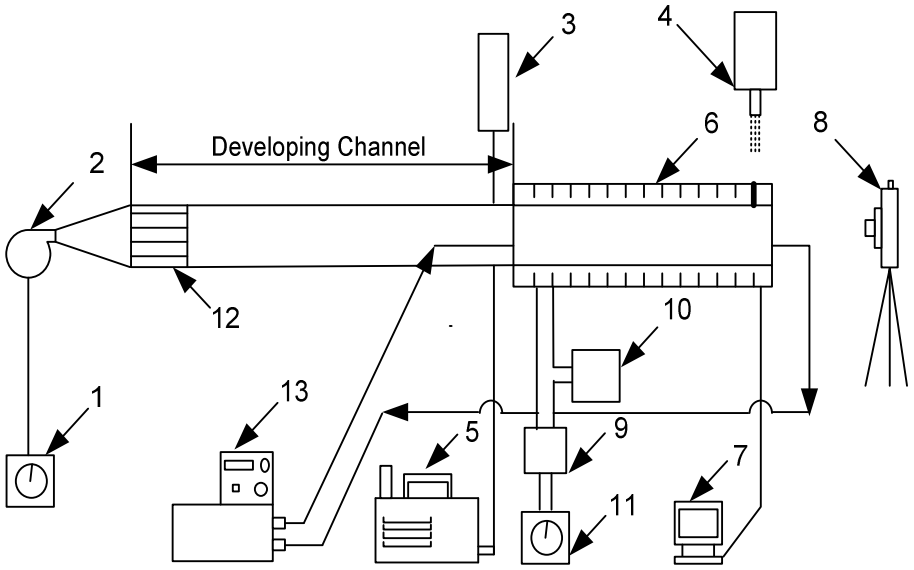

Figure 3.10 Schematic of the experimental rig shown with various components (1. dc power supply, 2. blower, 3.anemometer, 4. illuminator, 5. smoke generator, 6. test section, 7. data acquisition system, 8. camera, 9. voltmeter, 10. ammeter, 11. ac power supply. 12. flow straightener, 13. water bath).

The blower provided forced air flow through the developed duct to the test section. The flow rate was measured using an anemometer. Measurements were made to ensure fully developed flow at the entrance of the test section with no heat input from the heated wall. The work included using four entrance sections with different lengths in which the flow was hydrodynamically fully developed at the entrance section of the heat transfer in horizontal ducts with length and height of the test section is 270 mm and 54 mm respectively. This condition is represented by the duct with long and short lengths at entrance having the same dimension of test section. These test sections and entrance sections could be removed or attached as and when required. Table 3.3 shows the dimensions of the test rig with the entrance section length. The developing channel length had been calculated based on Equation 3-7. The hydrodynamic entry length for a laminar flow is given by Langhaar [56] as,

$$\frac{L_e}{D_h} = 0.05\,\mathrm{Re} \qquad 3\text{-}7$$

The Reynolds number range from 800 to 2900 is selected for CS1 and CS3 but the current work (CS2) due to the entrance length constraints in the lab, the Reynolds number was restricted to be 858 and 1788. The length of the entrance section was higher for higher Reynolds numbers.

Table 3.3 Entrance length for fully developed flow, based on Langhaar [56]

Aspect Ratio (AR)	Cross-sectional Duct size (height x width) mm	Hydraulic Diameter mm	Airflow Velocity m/s	Reynolds number Re	Length of the entrance section (Le) m
1	54 X 54	54	0.24	858	2.3
1	54 X 54	54	0.50	1788	4.8
0.5	54 X 27	36	0.36	858	1.5
0.5	54 X 27	36	0.75	1788	3.2

At the channel entrance, a flow straightener was used in order to achieve steady, laminar flow conditions with a uniform velocity distribution at the channel entrance.

The flow straightener was made of 10 mm diameter, 100 mm long plastic tubes. To act as a flow straightener in the horizontal and vertical ducts considered in this research, 16 such tubes were assembled in the square duct and 8 such tubes were assembled in the rectangular duct.The fluid entered the developed channel at a uniform temperature less than the surface temperature. Two different wall surface emissivities (0.05 and 0.85) are considered in this study. A typical experimental run consisted of maintaining the desired temperatures for the hot and cold walls, starting the blower, attaining steady state conditions and then recording a set of data. This was described earlier in Section 3.7. Flow visualization was conducted to observe qualitative pattern of the flow from the horizontal ducts, as was described in Section 3.6.

3.8.1 Fully Developed Velocity Profile

The main flow was investigated to check its fully developed condition at the entrance of test section with no heat input. Figure 3.11 and 3.12 show the sampled data for square and rectangular duct from the thermal anemometer respectively. The experimental data was taken at the center line of vertical length, 54 mm. The results clearly indicate that at the entrance of the test section inlet parabolic velocity profile is fully developed. These profiles are further validated with analytical solutions for laminar fully developed flow in duct provided by Marco and Han [55]. The present work included the use of four entrance sections with different lengths in which the flow is hydrodynamically fully developed at entrance section of the heat transfer in horizontal ducts with length and height of the test section is 270 mm and 54 mm respectively.

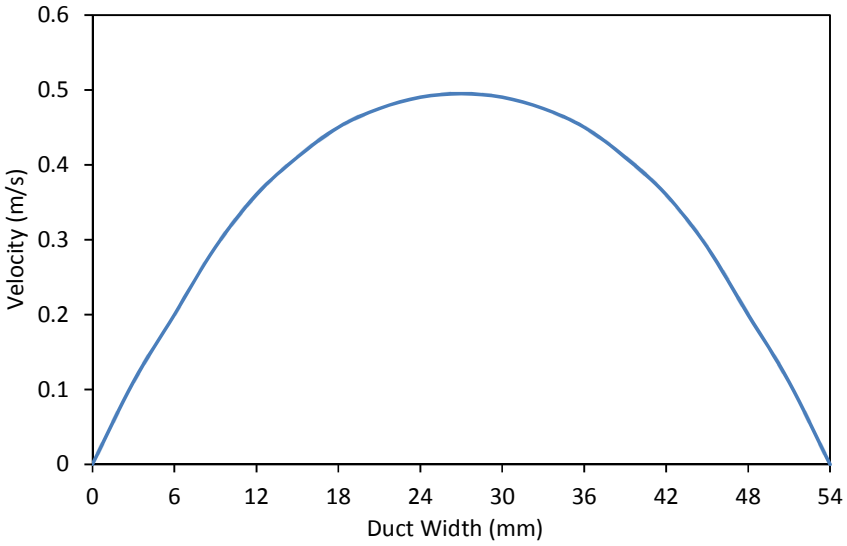

Figure 3.11 Fully developed velocity profile for Re = 1788 (AR = 1).

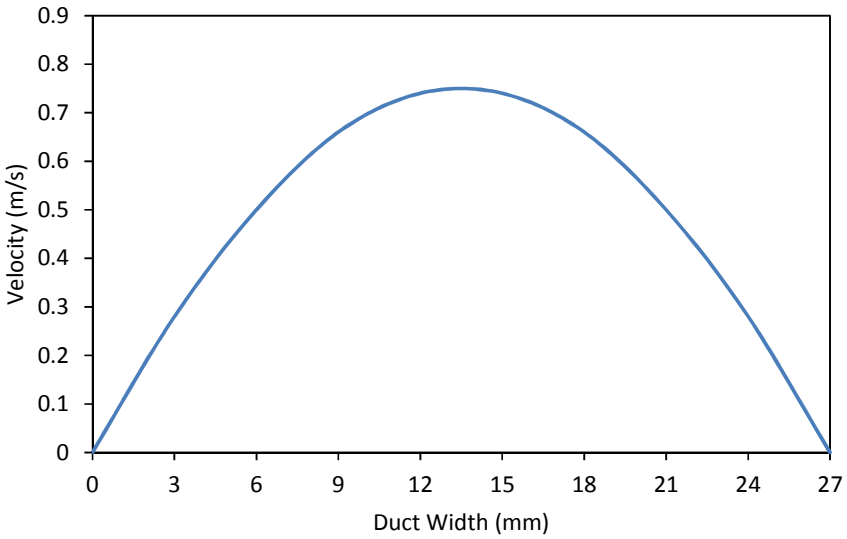

Figure 3.12 Fully developed velocity profile for Re = 1788 (AR = 0.5).

3.9 Experimental Methodology for Thermally Developing Flow in Vertical Ducts

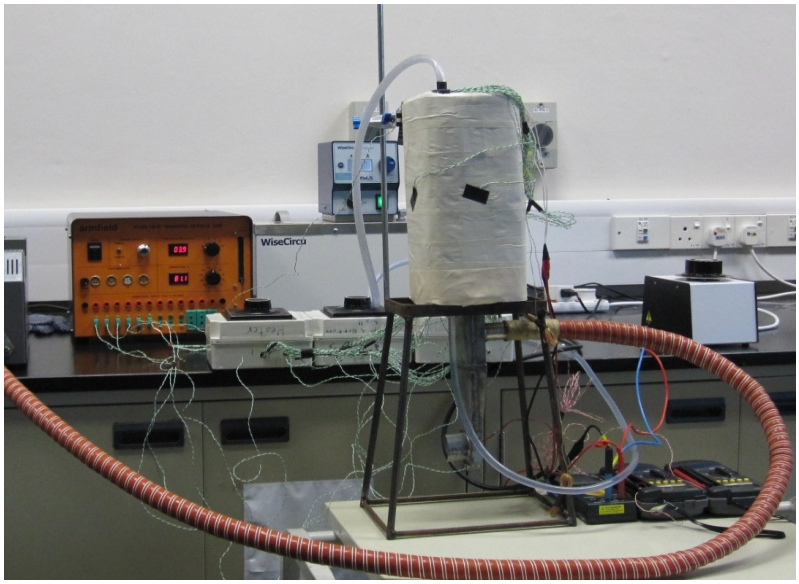

Fig 3.13 (a)

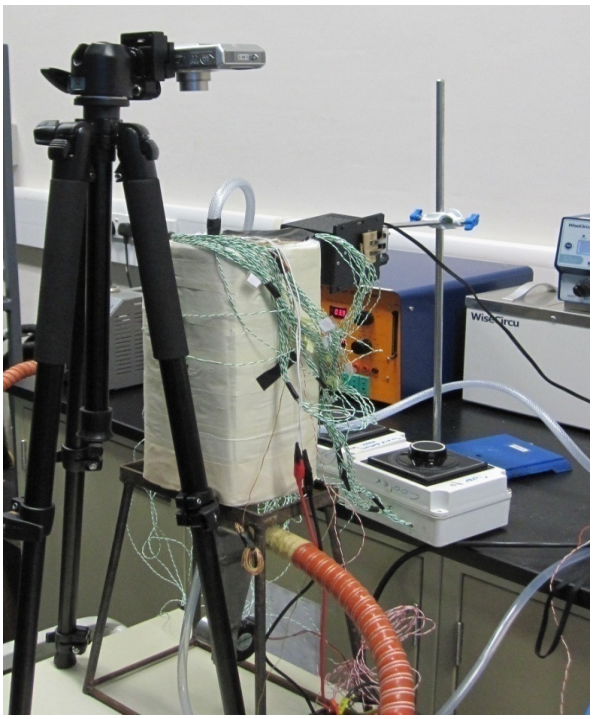

Fig 3.13 (b)

Figure 3.13 (a, b) Photograph of the experimental test rig for the vertical duct.

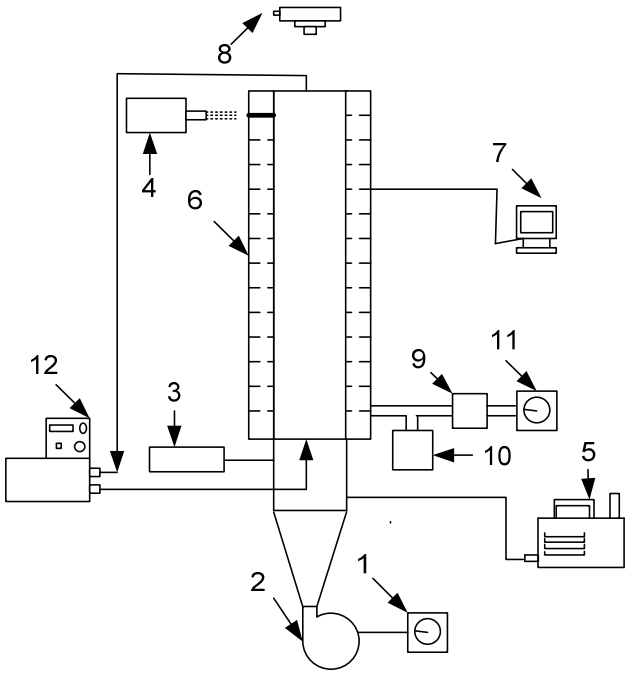

Figure 3.14 Schematic of the experimental rig shown with various components (1. DC power supply, 2. blower, 3. anemometer, 4. illuminator, 5. smoke generator, 6. test section, 7. data acquisition system, 8. camera, 9. voltmeter, 10. ammeter, 11. AC power supply, 12. water bath).

Figure 3.13 (a) and (b) show the photograph of the experimental test rig and figure 3.14 shows the schematic diagram of experimental test rig. The experimental work represents the case of mixed convection heat transfer for thermally developing flow in vertical ducts with radiation effects (CS3). In this study, the experimental methodology and procedure all are same as for thermally developing flow in horizontal ducts with radiation effects (CS1). This was described in section 3.6. The difference between the two case studies is the orientation of the duct; the all other parameters considered in this work are the same as was done for CS1.

3.10 Experimental Procedure

The experimental procedure consisted of the following sequence. To maintain natural convection, first the heater was switched on, then set the heater and water circulator

temperature. After that, run the test section for four hours without the fan. Within four hours, the heated wall reaches the steady state temperature. Once steady state is reached, heat flux is measured from the heat flux gauge and the wall temperatures are noted down. The average temperature of test section walls is used as the input values in FLUENT for the calculation of radiative flux. After the steady state period, the fan is switched on for one hour to maintain forced convection. A thermal anemometer inserted from a small hole of 7 mm diameter located on the top side, at the start of the test section is used to measure the airflow velocity. After one hour, all the temperatures from the thermocouples are noted down including the inlet and exit temperature of the air. The above procedure is repeated for all cases of the experiments, different Reynolds numbers, emissivities and heat fluxes.

3.11 Computation of Surface Radiation Heat Transfer

The experimental data was analyzed to obtain various heat transfer quantities due to mixed convection and surface radiation heat transfer from the hot vertical wall of the duct. To obtain the radiation heat transfer from the hot wall, a numerical modeling scheme using the computational fluid dynamics solver FLUENT [53] was chosen to create a geometrical simulation of the enclosure. The geometry of the duct was constructed by GAMBIT [54] and exported to the CFD solver FLUENT where the boundary conditions and other parameters were applied. The numerical modeling scheme involved the creation of a geometric model of this duct. Experimentally measured temperatures were used as input quantities for wall surface temperatures. Air being a non-participating medium, the surface to surface radiation model was used to obtain radiant energy interchange among the walls of the duct. The numerical model provided an estimate of the radiation flux at the heated wall of the duct. Using these values of the radiation flux, and Equation 3-5, the radiation Nusselt number was calculated. Using the experimentally observed temperatures of the heated wall as input quantities in the numerical modeling provides the most accurate modeling in this class of problems. The numerical results obtained were analyzed and presented in terms of the radiative Nusselt number from the heated wall.

3.12 Uncertainty Calculation

In this research, there are two types of measurement quantities associated with the present experiments that contribute to the overall uncertainty in the final results. These are the uncertainties in the velocity and temperature measurements. The accuracy of experimental results depended upon the accuracy of the individual measuring instruments. In order to determine the accuracy and reliability of the experimental results, an uncertainty analysis was conducted on all measured quantities calculated from the measured results. Uncertainties were estimated according to the procedure outlined in Coleman and Steele [57]. The uncertainty of the temperature measurements was estimated to be within ± 0.04 ^{o}C; the detailed uncertainty analysis is provided in Appendix A2. The flow rate was measured by using an anemometer with an accuracy of ± 1.5 %. The overall uncertainty in the estimated Nusselt number from the hot vertical wall of the test section was found to be less than ± 3 %, for the range of Reynolds numbers considered in this study.

3.13 Summary

The description of the experimental methodology for all cases (CS1, CS2 and CS3) was presented in this chapter. The constructional details of the experimental rig and the test sections representing the three case studies were separately described and the use of different instruments for acquiring data, flow visualization, test section, temperature measurement, flow measurement and the experimental procedure was also described. In the next chapter, the results obtained from mixed convection heat transfer for thermally developing flow in horizontal ducts (CS1 configuration) will be presented and discussed.

CHAPTER 4

RESULTS AND DISCUSSION

CASE STUDY 1: THERMALLY DEVELOPING FLOW IN HORIZONTAL DUCTS (CS1)

4.1 Introduction

In this chapter, the results of mixed convection heat transfer for thermally developing flow in horizontal ducts with radiation effects is presented. The duct cross section is made of two differentially heated isothermal vertical walls and two adiabatic horizontal walls. The Reynolds number was varied from 800 to 2900, and the heat flux was varied from 256 W/m^2 to 863 W/m^2, for two aspect ratios of the duct cross section. The hot wall temperature ranged from 27 ^{o}C to 100 ^{o}C, and the emissivity of internal walls were 0.05 and 0.85. The results presented here show the effect of surface radiation and mixed convection on the total heat transfer rate within the duct. The flow field within the duct was also visualized using the smoke flow visualization method.

4.2 Thermally Developing Flow in Horizontal Ducts

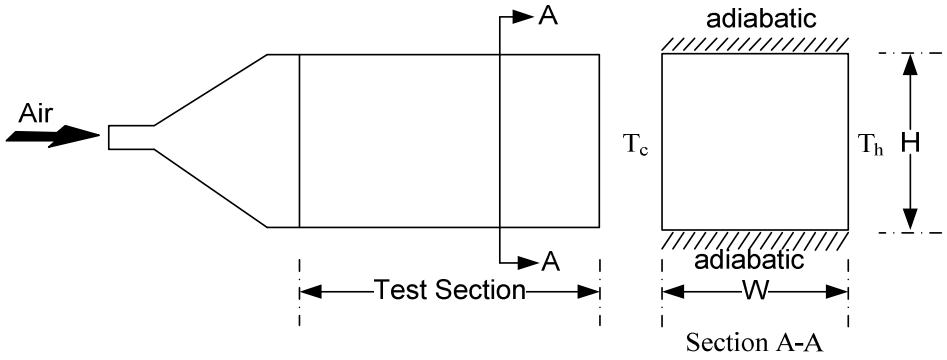

Figure 4.1 Schematic of the horizontal square test section.

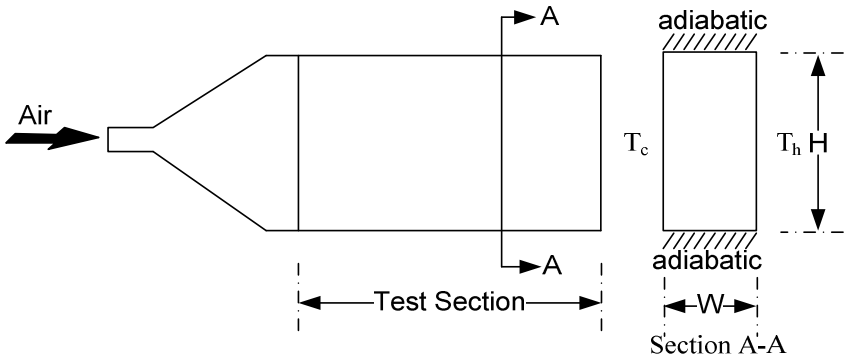

Figure 4.2 Schematic of the horizontal rectangular test section.

Figures 4.1 and 4.2 show the schematic diagrams of the horizontal duct with square (AR = 1) and rectangular (AR = 0.5) cross sections that were considered for the analysis of a thermally developing flow. The test section shown here was made of two differentially heated isothermal vertical walls and two adiabatic horizontal walls. The hot vertical wall incorporated an electrical heater made of silicon rubber, which formed the heat source for the duct. For all the cases, the cold wall temperature was maintained to be equal to the inlet air temperature. The inside surface of the cold wall and the hot wall were highly polished in order to achieve a mirror finish with, a low emissivity of 0.05, or coated with blackboard paint to have an emissivity of 0.85.

4.3 Surface Temperature Distribution along the Duct Walls

4.3.1 Surface Temperature Distribution on the Heated Wall

Figures 4.3 and 4.4 show the distribution of the surface temperature on the vertical heated wall as a function of the horizontal distance from the inlet of the test section to the exit of the test section for different wall heat flux values with a fixed Reynolds number of 1788. It was found that the square (AR = 1) test section had the highest heated wall average surface temperature of 88.9 ^{o}C (Fig 4.3) for highly polished walls ($\varepsilon = 0.05$) corresponding to a high heat flux q = 862 W/m², whereas for the duct with black wall (internal) surfaces ($\varepsilon = 0.85$) the surface temperature is 79.9 ^{o}C

corresponding to a high heat flux q = 728 W/m². The average wall temperature between the two surfaces differed by about 9 °C. Figure 4.4 shows that for a rectangular test section, the highest heated wall average surface temperature of 89.7 °C is obtained for the case of a duct having highly polished walls (ε = 0.05) with high heat flux q = 862 W/m². Similarly, for the case of a duct having black surface walls (ε = 0.85) with high heat flux q = 728 W/m² the corresponding temperature was found to be 81.3 °C. The average wall surface temperature between the two surfaces differed by about 8.4 °C.

Considering the surface emissivity, the polished heated wall surface temperature is higher than the black wall surface temperature. The temperature of the polished and black surfaces differed by about 10.1 % and 9.3 % for the case of square and rectangular duct respectively. When comparing the aspect ratios of the duct, the rectangular duct heated wall temperature is higher than square duct. The temperature difference between the square and rectangular duct is about 0.9 % and 1.7 % for the case of polished and black surfaces respectively. The surface temperature is slightly lower at the entrance and the exit of the test section due to the entrance and exit effects.

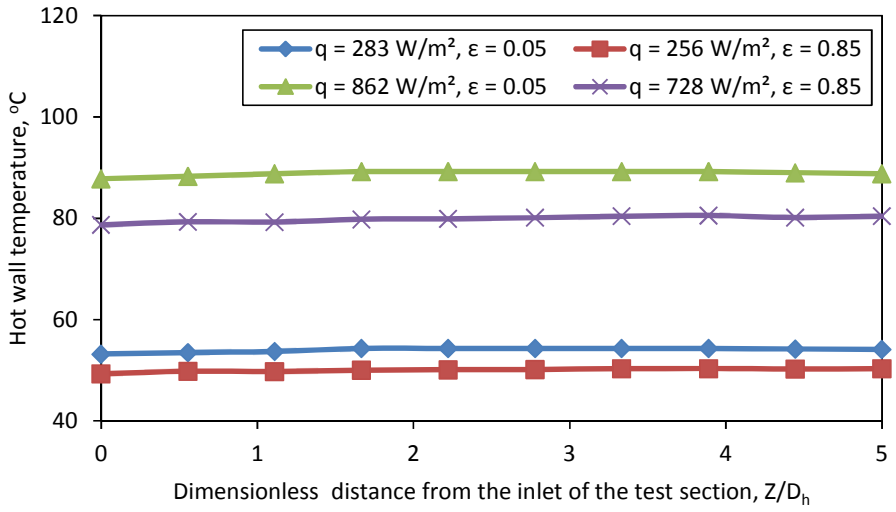

Figure 4.3 Variation of the surface temperature on the heated wall (Re = 1788, AR = 1).

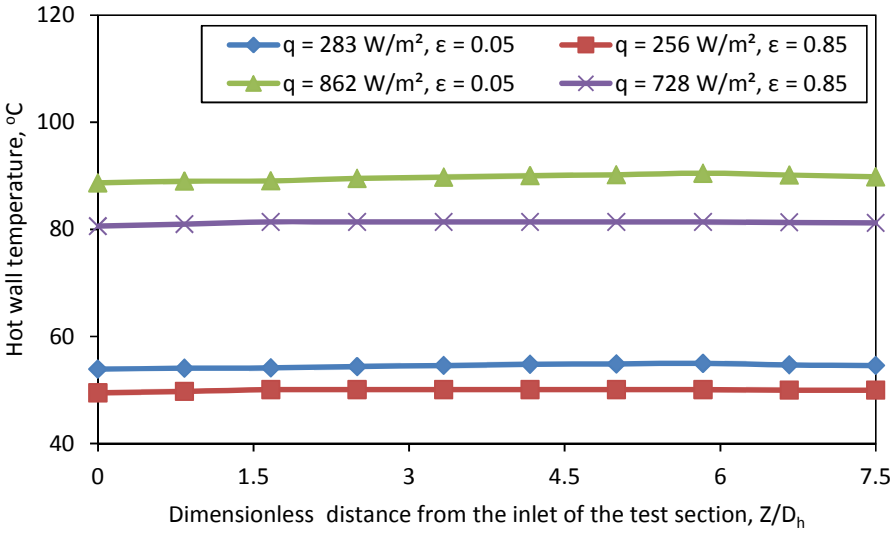

Figure 4.4 Variation of the surface temperature on the heated wall (Re = 1788, AR = 0.5).

4.3.2 Surface Temperature Distribution on the Cold Wall

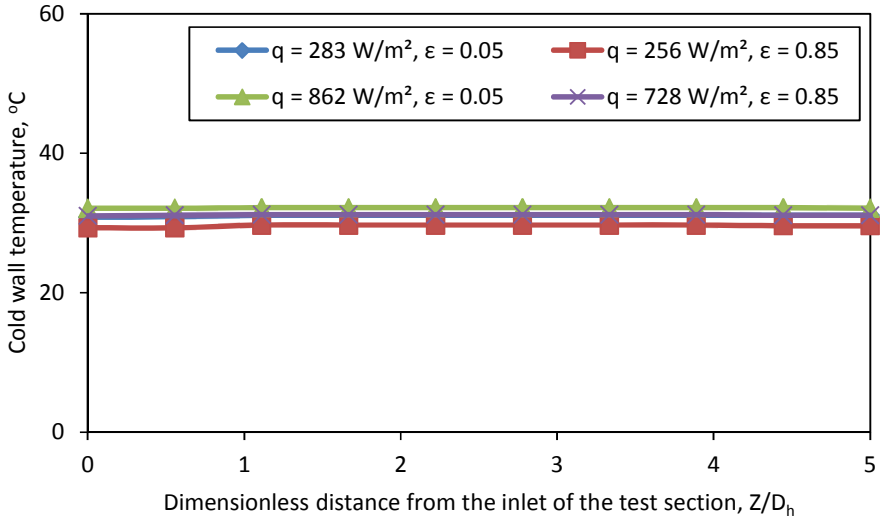

Figure 4.5 Variation of the surface temperature on the cold wall (Re = 1788, AR = 1).

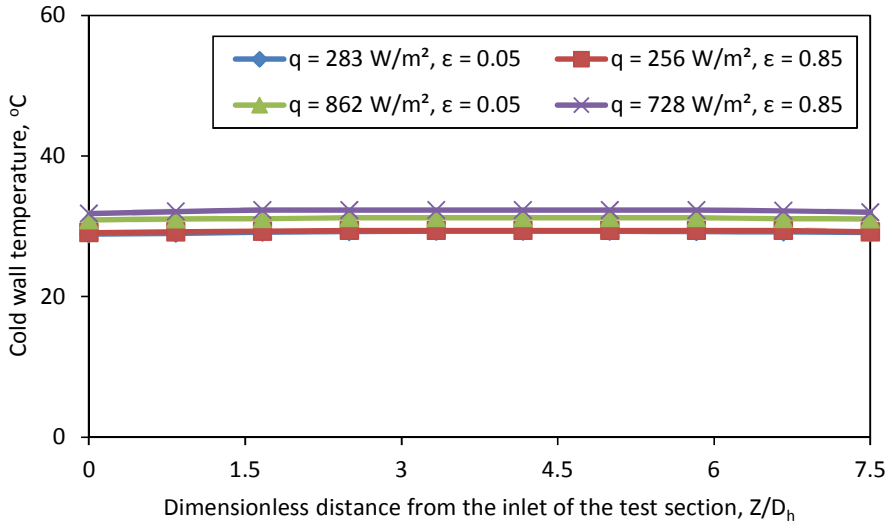

Figure 4.6 Variation of the surface temperature on the cold wall (Re = 1788, AR = 0.5).

Figures 4.5 and 4.6 show the variation of the cold wall surface temperature. The temperature of the cold wall is always maintained to be equal to the inlet air temperature for all cases.

4.3.3 Surface Temperature Distribution on the Top Wall

Figures 4.7 and 4.8 show the variation of the top wall temperature as a function of the horizontal distance. It can be seen that the highest average surface temperature of 53 ^{o}C is obtained for polished wall (ε = 0.05) of square test section with high heat flux. For the black surface (ε = 0.85) wall temperature decreases by about 9.1 ^{o}C. Similar observations can also be made with the rectangular test section (Fig.4.8). Due to the high heat flux applied to the hot wall, the average top wall temperature is almost independent of the surface emissivity of the duct walls. In this case, the top wall average temperature was higher for the polished surface, when compared to the black surface. When considering the aspect ratio, the rectangular test section top wall temperature was higher compared to that of a square test section. For a particular value of the input wall heat flux, the temperature drop per unit length of the test section from the inlet to the outlet of the duct is found to be the same for all cases.

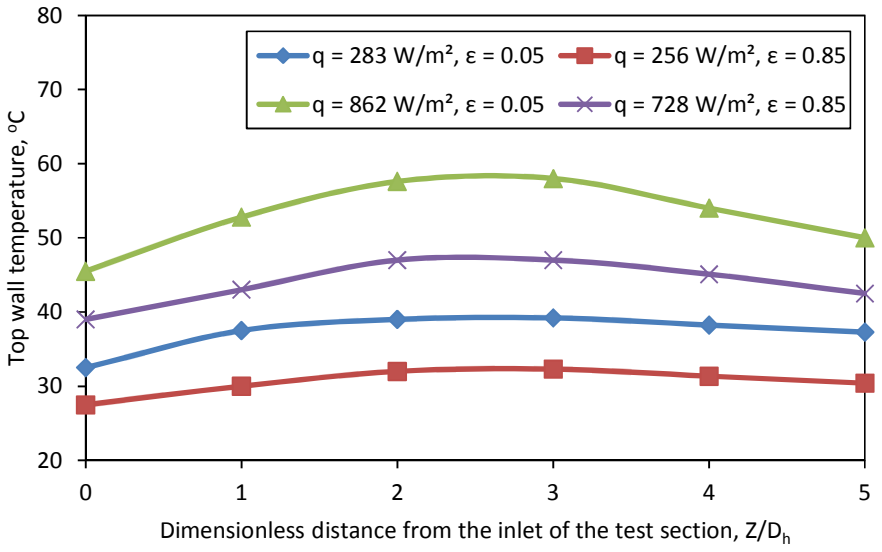

Figure 4.7 Variation of the surface temperature on the top wall (Re = 1788, AR = 1).

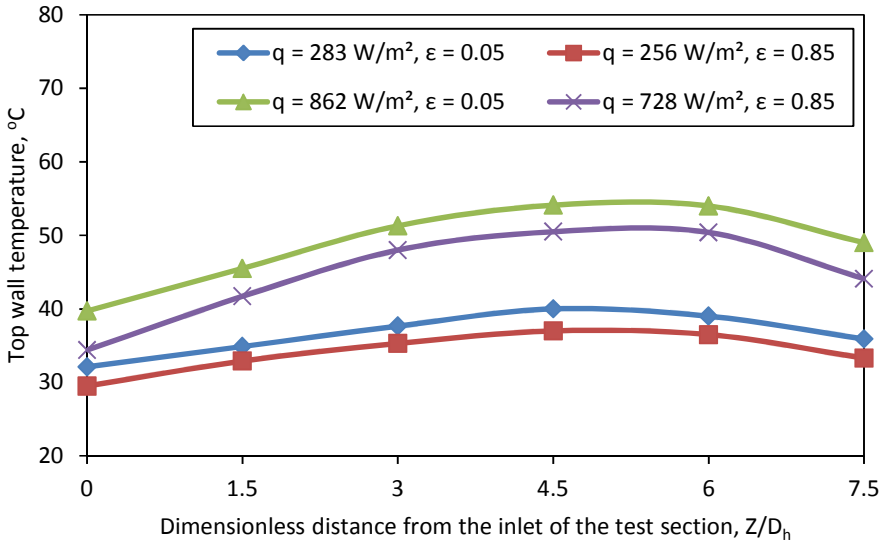

Figure 4.8 Variation of the surface temperature on the top wall (Re = 1788, AR = 0.5).

4.3.4 Surface Temperature Distribution on the Bottom Wall

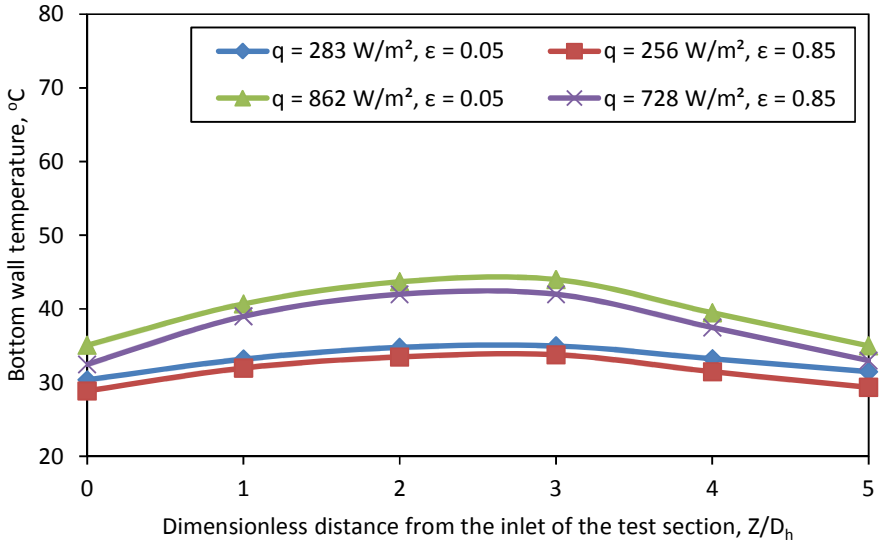

Figure 4.9 Variation of the surface temperature on the bottom wall (Re = 1788, AR = 1).

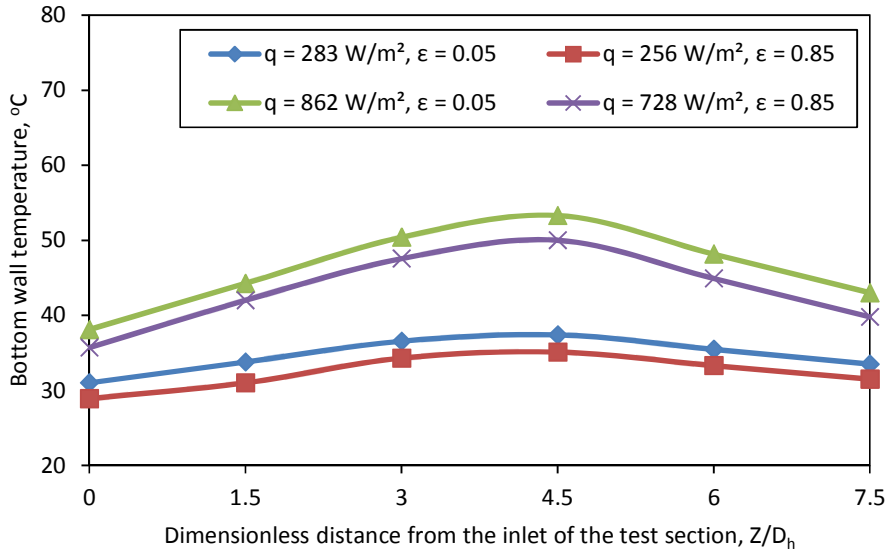

Figure 4.10 Variation of the surface temperature on the bottom wall (Re = 1788, AR = 0.5).

Figure 4.9 shows the highest bottom wall average surface temperature of 39.7 °C for square test section with polished wall (ε = 0.05) and 37.7 °C for black surface wall (ε

= 0.85). Similarly Figure 4.10 shows the highest top wall average surface temperature of 46.2 ^{o}C for a rectangular test section with polished walls (ε = 0.05) and 43.3 ^{o}C for the case of a duct having black surface walls (ε = 0.85). In comparison with Figure 4.7 and 4.8, it can be inferred from Figure 4.9 and 4.10 that the change in the bottom wall temperatures from the inlet to the outlet of the test section is only marginal. These differences in the top and bottom wall temperatures are due to the result of the interaction of the mixed convection and surface radiation. For mixed convection cases having a strong natural convection heat transfer component, the average top wall temperature is always found to be higher than the average bottom wall temperature. The difference between top and bottom wall has a range of 14 % to 25 % and 4 % to 14 % for the case of polished and black surface respectively. Therefore, it can be concluded from the foregoing results and discussion that the surface temperature along the duct wall depends on the heat flux, emissivity of walls, the flow Reynolds number, and the length of the test section.

4.4 Combined Forced and Natural Convection Heat Transfer

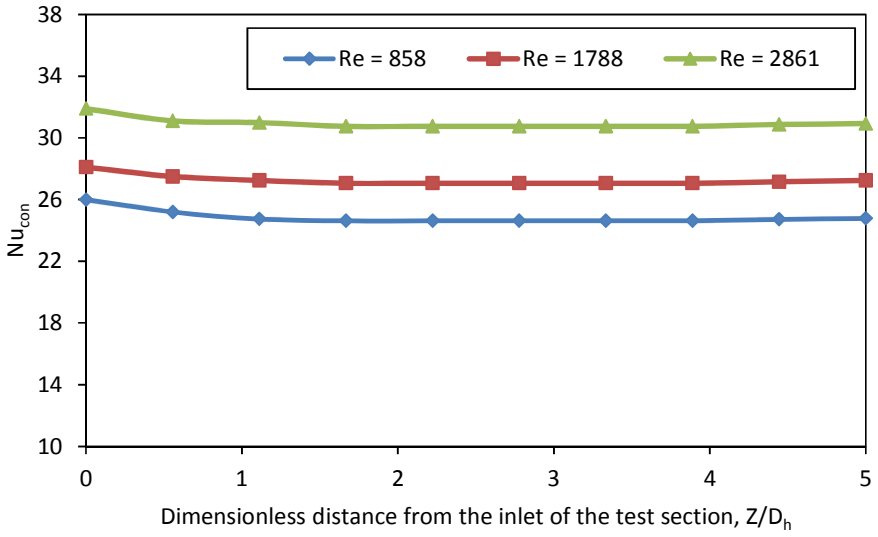

Figure 4.11 Effect of Reynolds number on the average convective Nusselt number at the heated wall (q = 862 W/m², AR = 1, ε = 0.05).

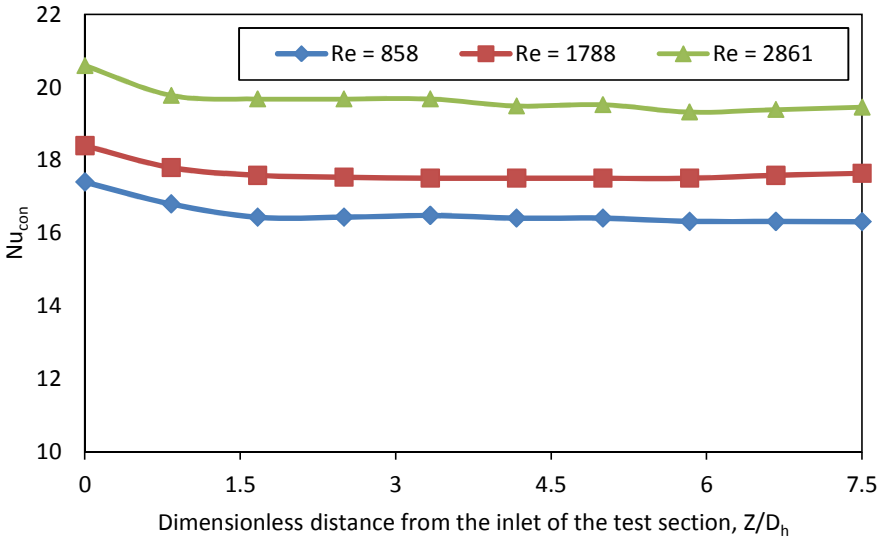

Figure 4.12 Effect of Reynolds number on the average convective Nusselt number at the heated wall (q = 862 W/m², AR = 0.5, ε = 0.05).

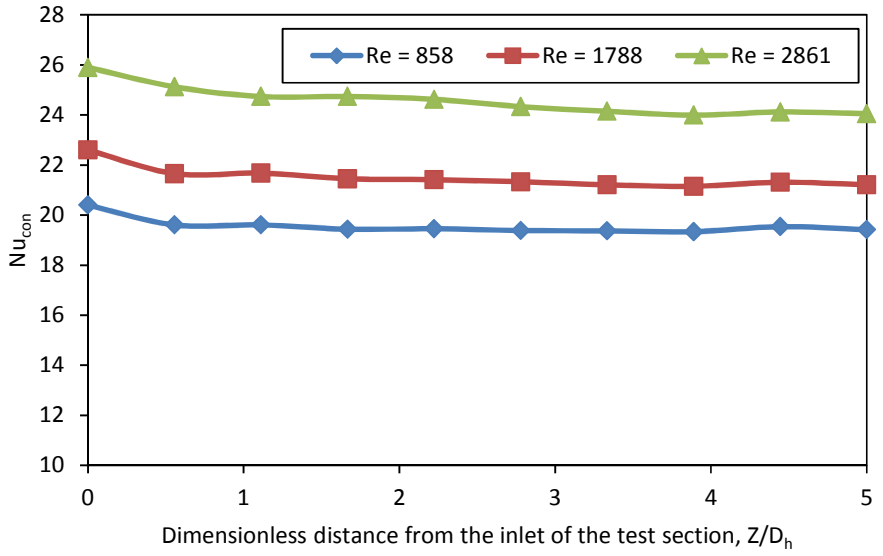

Figure 4.13 Effect of Reynolds number on the average convective Nusselt number at the heated wall (q = 728 W/m², AR = 1, ε = 0.85).

The variation of the local average convective Nusselt number with horizontal distance from the inlet of the test section to the exit is plotted for typical runs in figures 4.11 to 4.14. The variation of Nusselt number reveals that the Nusselt number

is high near the inlet of the test section and decreases slightly due to the thermal boundary layer development near the inlet. The rate of Nusselt number drop near the inlet for all the cases were found to be in the range of 2 to 3 %.

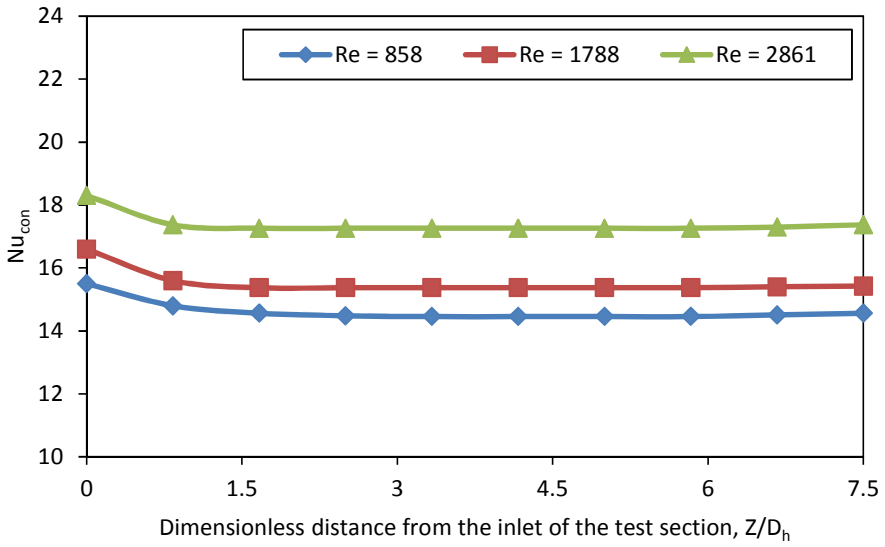

Figure 4.14 Effect of Reynolds number on the average convective Nusselt number at the heated wall (q = 728 W/m², AR = 0.5, ε = 0.85).

Figures 4.11 and 4.12 show the effect of Reynolds number on the Nusselt number for polished (ε = 0.05) surface with heat flux q = 862 W/m². In this case the square test section average convective Nusselt number was found to be 24.9 and 31.0 for the case of low (Re = 858) and high (Re = 2861) Reynolds number. The average convective Nusselt number between the low and high Reynolds number differed by about 19.6 %. For the rectangular test section, the average convective Nusselt number was found to be 16.5 and 19.7 for the case of low (Re = 858) and high (Re = 2861) Reynolds number respectively. The average convective Nusselt number between the low and high Reynolds number differed by about 16.2 %.

Figures 4.13 and 4.14 show the effect of Reynolds number on the Nusselt number for black (ε = 0.85) surface with heat flux q = 728 W/m². In this case also, the range of average convective Nusselt number percentage was found to be 16 % to 20 %. As the

Reynolds number is reduced, the buoyancy effect increases resulting in improved heat transfer rate. A similar observation was also made with all the other cases. For constant heat flux and high Reynolds number, the average convective Nusselt values give higher results, because of the forced convection domination on the heat transfer process with little effect of buoyancy force for high Reynolds number [31].

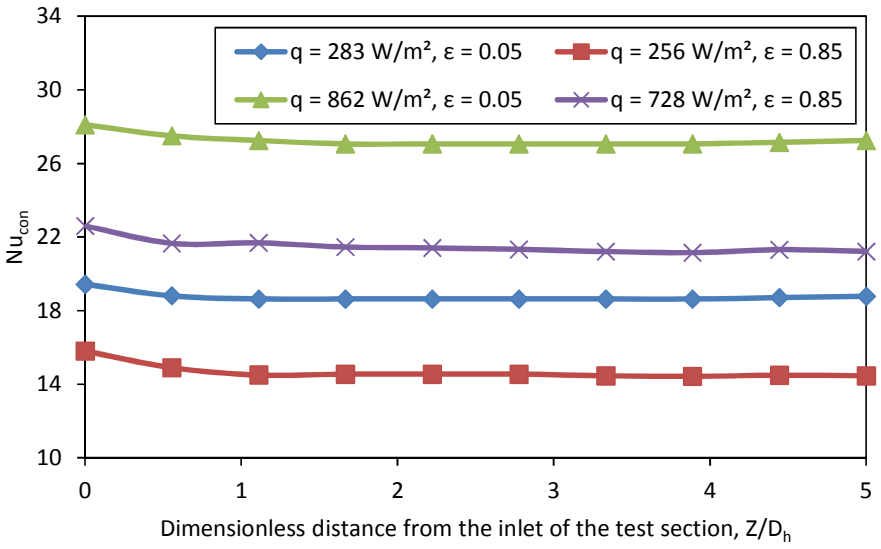

Figure 4.15 Effect of surface emissivity on the average convective Nusselt number at the heated wall (Re = 1788, AR =1).

The variation of the average convective Nusselt number at the heated wall for a duct of square and rectangle cross section (AR=1 & 0.5) with different emissivity of low and high heat flux for Reynolds number (Re = 1788) are shown in Figures 4.15 & 4.16. Considering the effect of emissivity, the average convective Nusselt number for the square test section with high heat flux was found to be 27.3 and 21.5 for polished and black surface respectively. The average convective Nusselt number between the polished and black surface differed by about 21.2 %. Similarly for the rectangular test section the average convective Nusselt number for high heat flux was found to be 17.7 and 15.5 for the case of polished and black surface respectively. The average convective Nusselt number between the polished and black surface differed by about

12.4 %. It was found that for a given wall heat flux, the convective Nusselt number is higher for highly polished surface than black surface; the same trend was observed with both square and rectangular ducts.

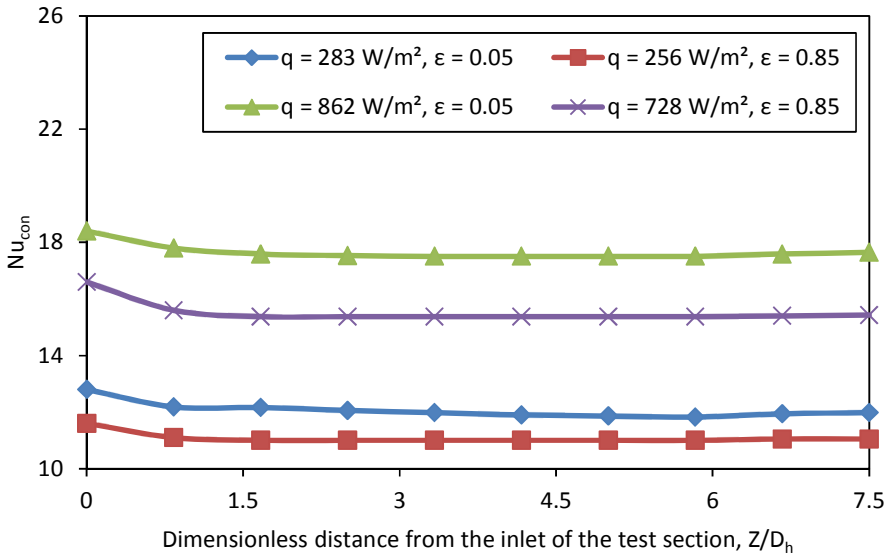

Figure 4.16 Effect of surface emissivity on the average convective Nusselt number at the heated wall (Re = 1788, AR =0.5).

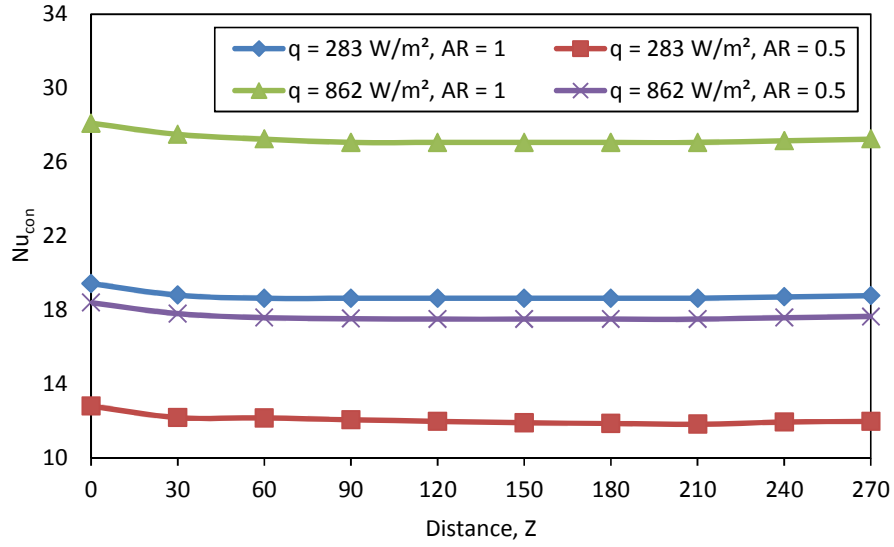

Figure 4.17 Effect of aspect ratio on the average convective Nusselt number at the heated wall (Re = 1788, ε = 0.05).

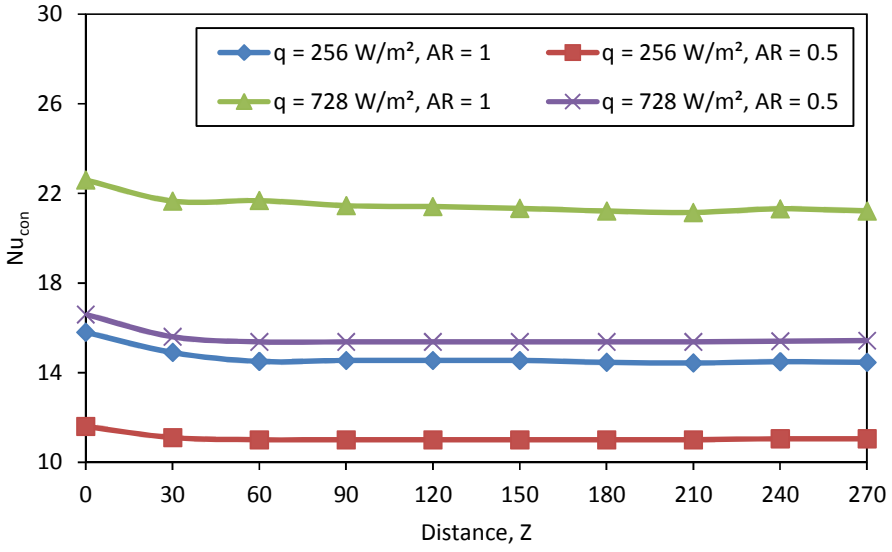

Figure 4.18 Effect of aspect ratio on the average convective Nusselt number at the heated wall (Re =1788, ε = 0.85).

Figures 4.17 and 4.18 show that the effect of aspect ratio on the convective Nusselt number at the heated wall for a certain value of the Reynolds number (Re = 1788) identically maintained for the two aspect ratios. Considering the effect of aspect ratio, the polished surface average convective Nusselt number for high heat flux was found to be 27.3 and 17.7 for the case of square and rectangular test section respectively. The average convective Nusselt number between the square and rectangular test section differed by about 35.1 %. Similarly the black surface average convective Nusselt number for high heat flux was found to be 21.5 and 15.5 for the case of square and rectangular test section respectively. The average convective Nusselt number between the polished and black surface differed by about 27.5 %. It was found that for a given wall heat flux, the convective Nusselt number is higher for aspect ratio 1 compared with 0.5. In the present study, the height of the duct is fixed for both aspect ratios and the higher aspect ratio shows larger distance between two vertical side walls. Higher aspect ratio having more duct volume, allows more amount of air inside the duct. As a result, a higher aspect ratio duct has a better heat transfer rate than a lower aspect ratio duct.

4.5 Radiation Heat Transfer

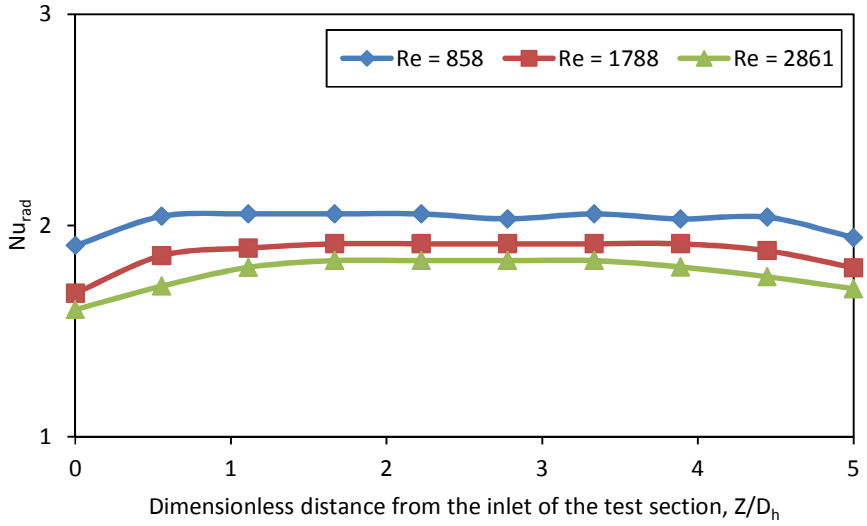

Figure 4.19 Effect of Reynolds number on the average radiative Nusselt number at the heated wall (q = 862 W/m², ε = 0.05, AR = 1).

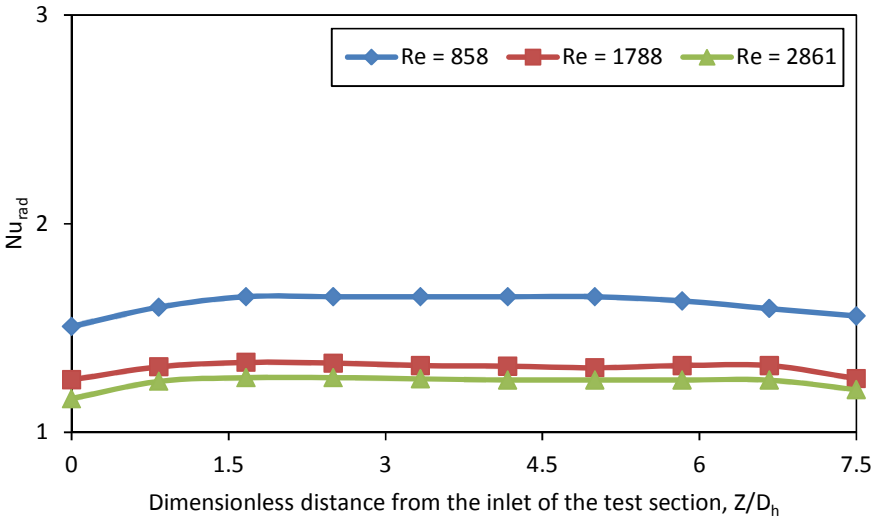

Figure 4.20 Effect of Reynolds number on the average radiative Nusselt number at the heated wall (q = 862 W/m², ε = 0.05, AR = 0.5).

Figures 4.19 and 4.20 show the effect of Reynolds number on the average radiative Nusselt number for polished surface (ε = 0.05) with heat flux q = 862 W/m². In this

case the square test section average radiative Nusselt number was found to be 2.0 and 1.7 for the case of low (Re = 858) and high (Re = 2861) Reynolds number. The average radiative Nusselt number between the low and high Reynolds number differed by about 15 %. Similarly for the rectangular test section, the average radiative Nusselt number was found to be 1.6 and 1.2 for the case of low (Re = 858) and high (Re = 2861) Reynolds number respectively. The average radiative Nusselt number between the low and high Reynolds number cases differed by about 25 %.

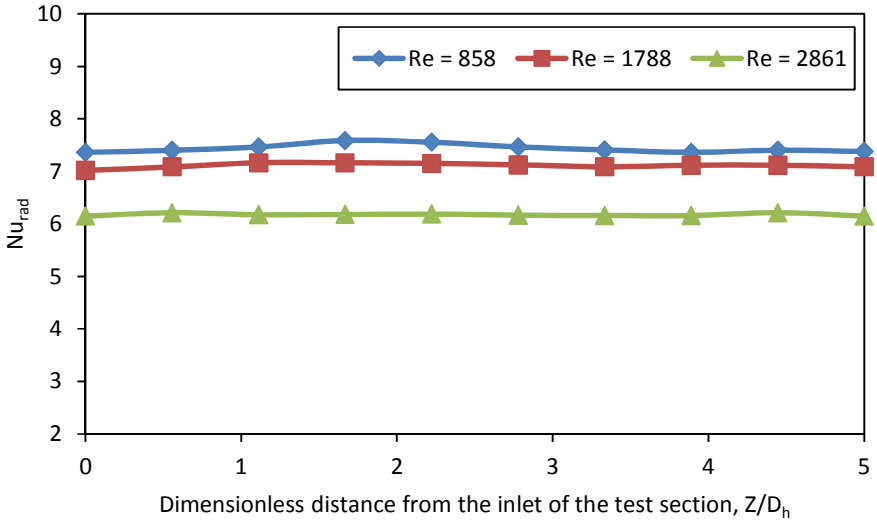

Figure 4.21 Effect of Reynolds number on the average radiative Nusselt number at the heated wall (q = 728 W/m², ε = 0.85, AR = 1).

Figures 4.21 and 4.22 show the effect of Reynolds number on the average radiative Nusselt number for black surface (ε = 0.85) with a heat flux q = 728 W/m². In this case the average radiative Nusselt number difference between the square and rectangular test section was found to be 16.2 % and 38.4 % for low (Re = 858) and high (Re = 2861) Reynolds number respectively.

For a constant heat flux and the high Reynolds number flow, the average radiative Nusselt number values are always lower than the corresponding low Reynolds number case. The radiative heat flux remains constant for most part of the test

section, except at the inlet and the outlet, where some of the radiative energy is lost to the surroundings.

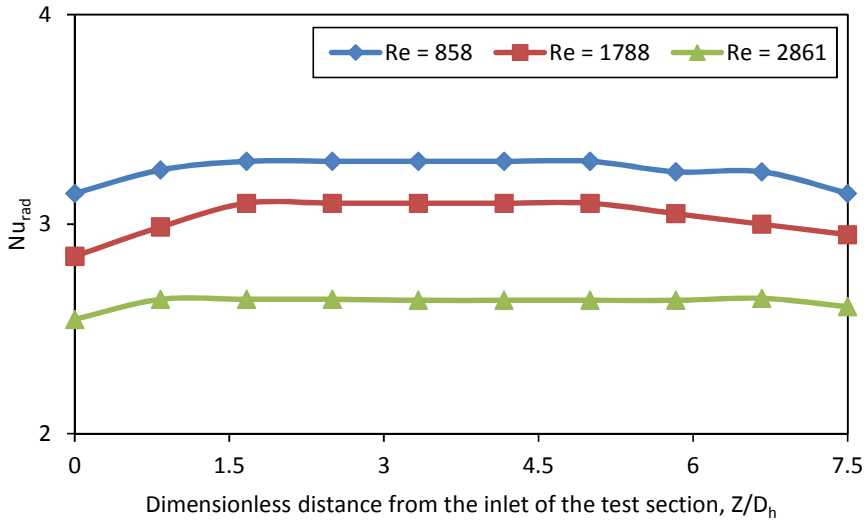

Figure 4.22 Effect of Reynolds number on the average radiative Nusselt number at the heated wall (q = 728 W/m², ε = 0.85, AR = 0.5).

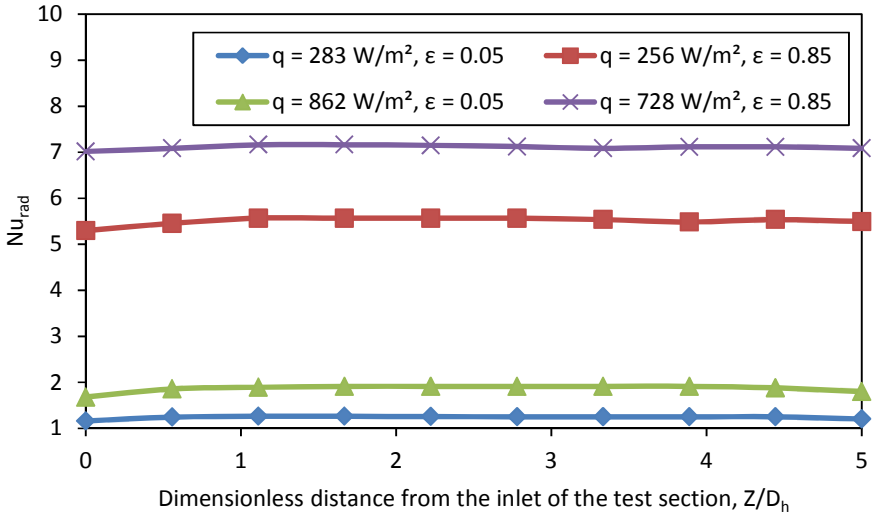

Figure 4.23 Effect of surface emissivity on the average radiative Nusselt number at the heated wall (Re = 1788, AR =1).

The variation of average radiative Nusselt number at the heated wall for a duct of square and rectangle cross section (AR = 1 & 0.5) with different emissivity of low and high heat flux with a fixed Reynolds number at 1788 are shown in Figures 4.23 and 4.24. For square test section the average radiative Nusselt number for high heat flux was found to be 7.1 and 1.9 for the case of black and polished surface respectively. In this case, the average radiative Nusselt number between the black and polished surface differed by about 72.9 %.

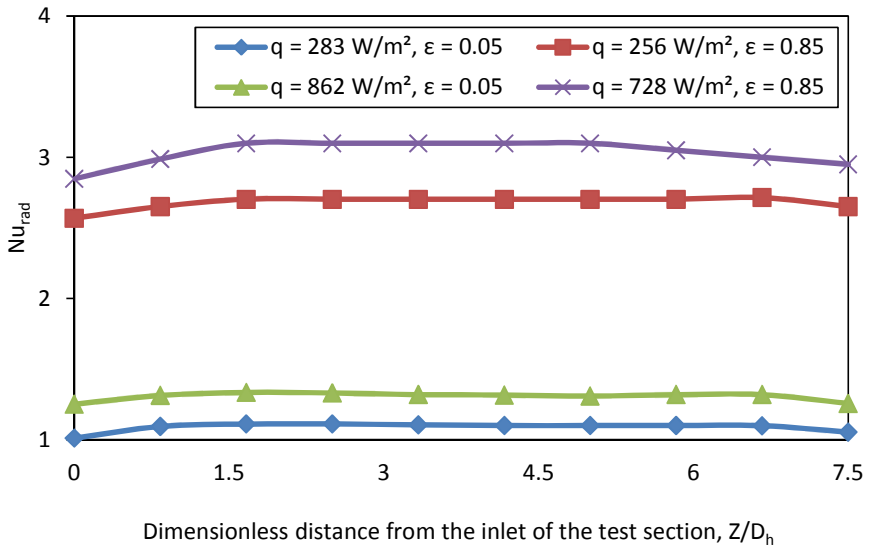

Figure 4.24 Effect of surface emissivity on the average radiative Nusselt number at the heated wall (Re = 1788, AR = 0.5).

The average radiative Nusselt number for the rectangular test section with high heat flux was found to be 3.0 and 1.3 for the case of black and polished surface respectively (Fig 4.24). For high heat flux, the average radiative Nusselt number between the black and polished surface differed by about 56.6 %. It was found that for a given wall heat flux, the radiative Nusselt number is higher for black surface than highly polished surface; the same trend was observed both cases of square and rectangular duct.

It is clearly seen that the average radiative Nusselt number is a very strong function of surface emissivity. Since radiation is a surface phenomenon, dependent on the wall emissivity and the wall temperatures, a reduction in the duct wall temperature causes an attendant reduction in the radiative heat transfer rate. The case of the duct having highly emissive walls, and higher wall fluxes (and temperature) provides a higher value of the average radiative Nusselt number.

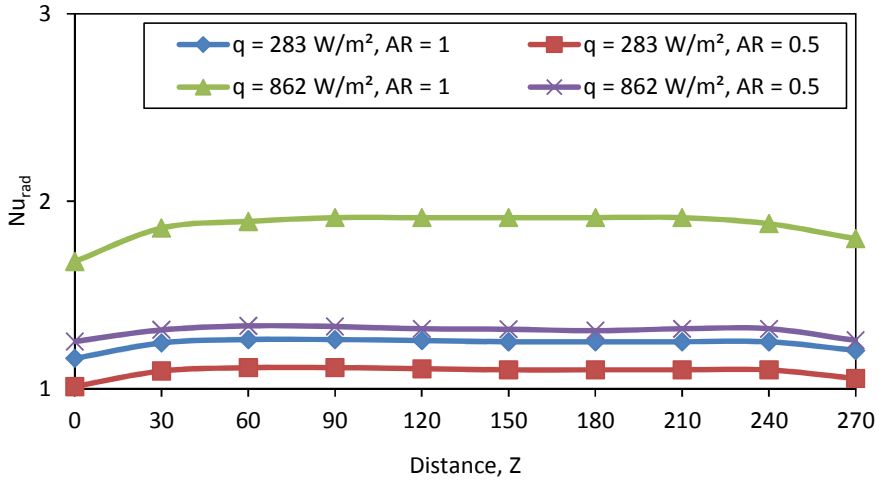

Figure 4.25 Effect of aspect ratio on the average radiative Nusselt number at the heated wall (Re = 1788, ε = 0.05).

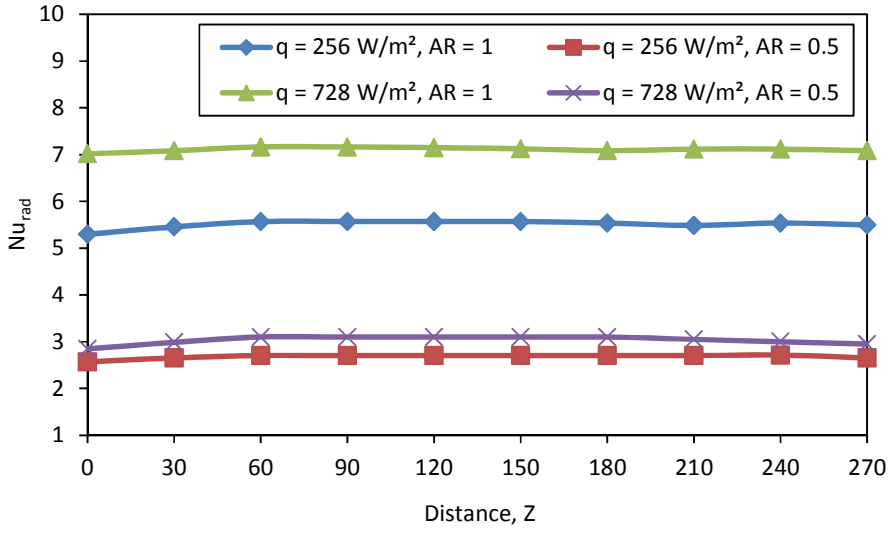

Figure 4.26 Effect of aspect ratio on the average radiative Nusselt number at the heated wall (Re = 1788, ε = 0.85).

Figure 4.25 shows the effect of aspect ratio on the average radiative Nusselt number for polished surface. In this case the average radiative Nusselt number for high heat flux was found to be 1.8 and 1.3 for the case of square and rectangular test section respectively. The average radiative Nusselt number between the square and rectangular test section differed by about 27.7 %. Similarly, Figure 4.26 shows the effect of aspect ratio on the average radiative Nusselt number for black surface. In this case the average radiative Nusselt number for high heat flux was found to be 7.1 and 3 for the case of square and rectangular test section respectively. The average radiative Nusselt number between the square and rectangular test section differed by about 57.7 %. Generally, higher aspect ratio results give higher convective and radiative Nusselt number rates. For a given heat flux and fixed Reynolds number, the radiative Nusselt number values were found to be higher for aspect ratio 1 compared to aspect ratio 0.5. For each aspect ratio, the radiative Nusselt number slightly increases along the length of the duct.

4.6 Combined Convection and Radiation Effect

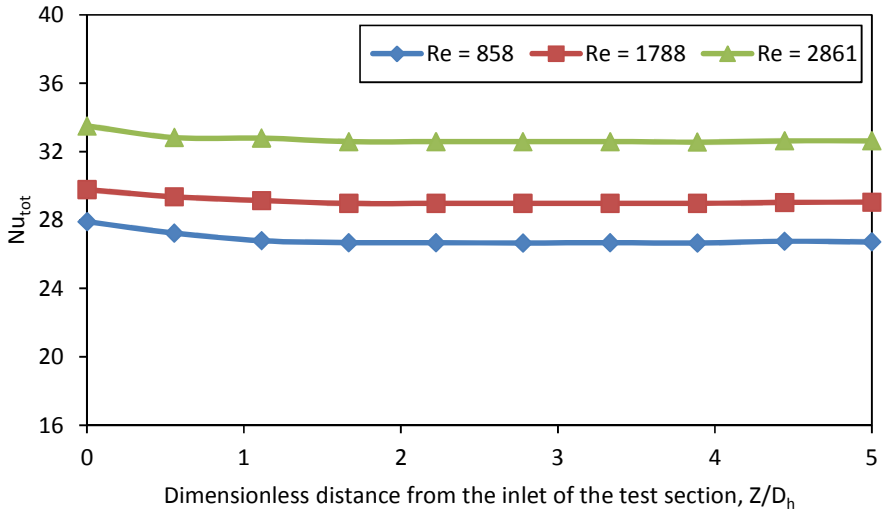

Figure 4.27 Effect of Reynolds number on the average total Nusselt number at the heated wall (q = 862 W/m², ε = 0.05, AR = 1).

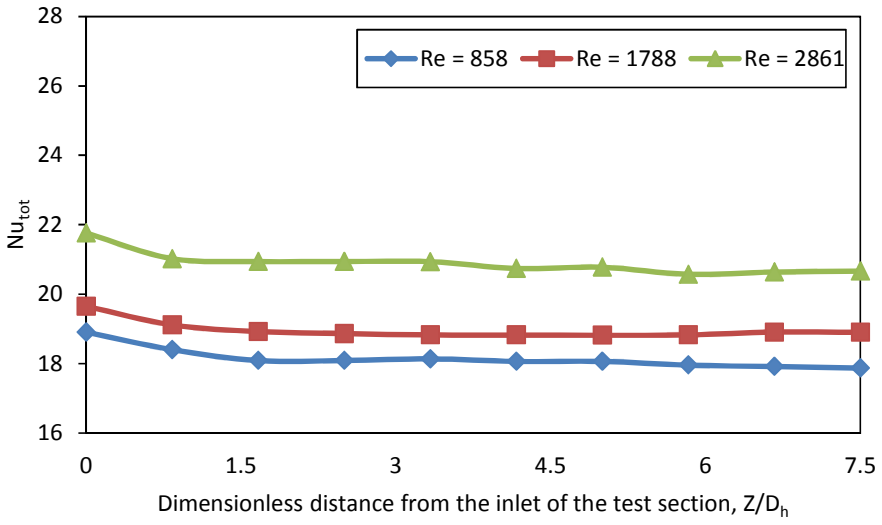

Figure 4.28 Effect of Reynolds number on the average total Nusselt number at the heated wall (q = 862 W/m², ε = 0.05, AR = 0.5).

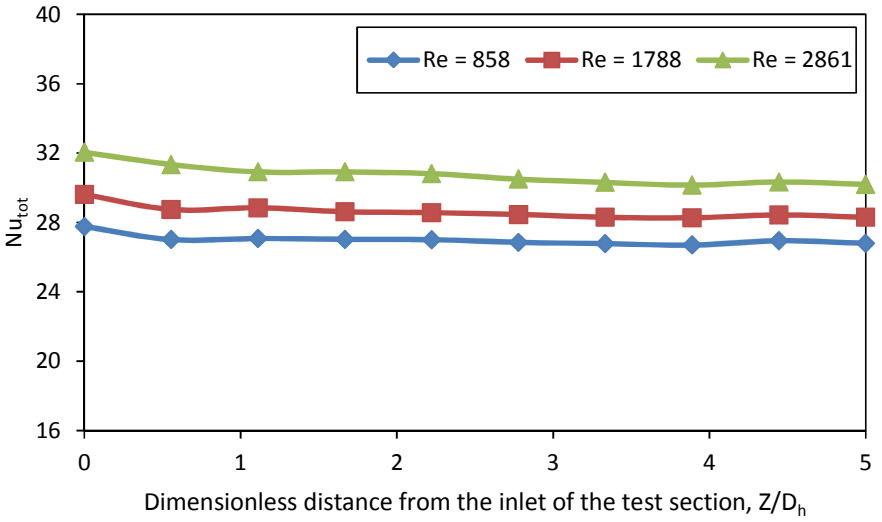

Figure 4.29 Effect of Reynolds number on the average total Nusselt number at the heated wall (q = 728 W/m², ε = 0.85, AR = 1).

Figures 4.27 and 4.28 show the effect of Reynolds number on the average total Nusselt number for polished surface (ε = 0.05) with heat flux q = 862 W/m². In this case the square test section average total Nusselt number was found to be 26.6 and 33.0 for the case of low (Re = 858) and high (Re = 2861) Reynolds number. The

average total Nusselt number between the low and high Reynolds number differed by about 19.3 %. Similarly for the rectangular test section average total Nusselt number was found to be 17.8 and 21 for the case of low (Re = 858) and high (Re = 2861) Reynolds number respectively. The average total Nusselt number between the low and high Reynolds number differed by about 15.2 %.

Similarly Figures 4.29 and 4.30 show the effect of Reynolds number on the average total Nusselt number for black surface (ε = 0.85) with a heat flux q = 728 W/m². In this case, the average total Nusselt number difference between the square and rectangular test section was found to be 19.2 % and 15.1 % for low (Re = 858) and high (Re = 2861) Reynolds number respectively. The above results show the same percentage difference between low (Re = 858) and high (Re = 2861) Reynolds number for both the cases. For constant heat flux and high Reynolds number with higher aspect ratio the average total Nusselt values give higher results. This was explained earlier in Section 4.4.

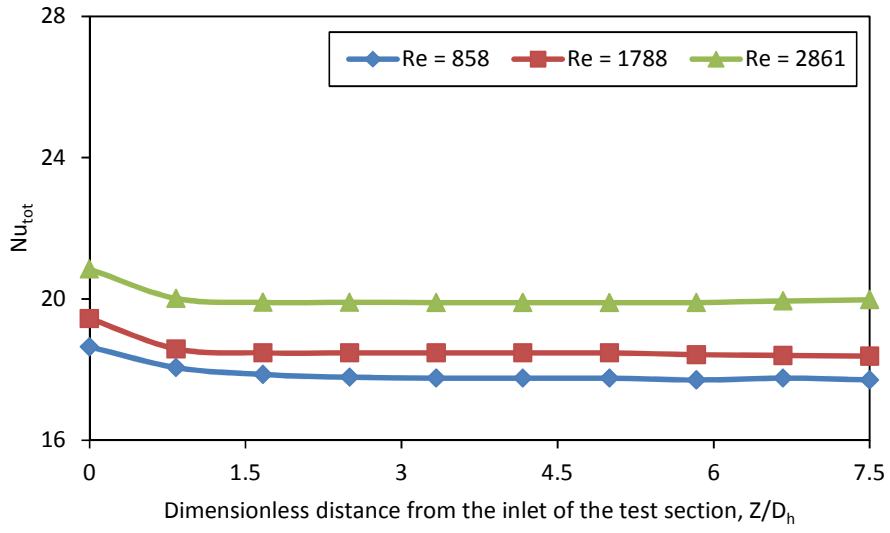

Figure 4.30 Effect of Reynolds number on the average total Nusselt number at the heated wall (q = 728 W/m², ε = 0.85, AR = 0.5).

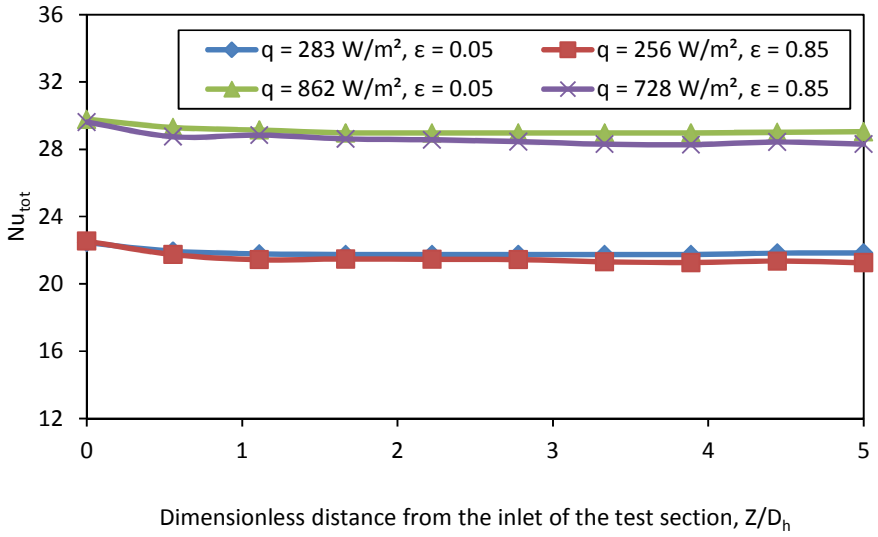

Figure 4.31 Effect of surface emissivity on the average total Nusselt number at the heated wall (Re = 1788, AR =1).

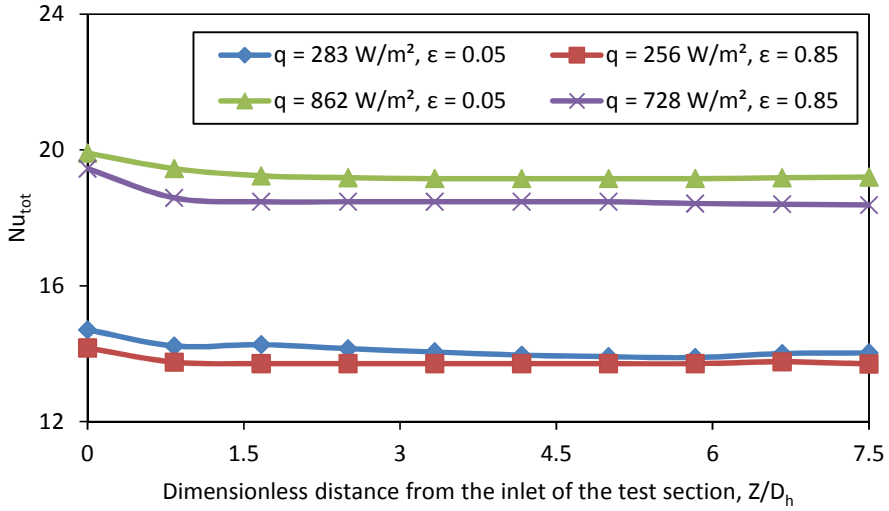

Figure 4.32 Effect of surface emissivity on the average total Nusselt number at the heated wall (Re = 1788, AR = 0.5).

Considering the combined convection and surface radiation effects occurring in a coupled mode, the total heat transfer rate from the heated wall can be represented as the sum of the Nusselt numbers due to convection and radiation. This is shown in Figure 4.31 and 4.32, wherein the variation of the average total Nusselt number is

plotted as a function of emissivity with different heat flux for Re = 1788. It can be observed that the average total Nusselt numbers for strong and weak radiation are comparable.

When separately analyzing the convection and radiation effects, contribution of strong and weak convection and radiation effects is clearly seen. The surface emissivity is found to play a very important role in determining the average total Nusselt number from the heated vertical wall. This is evident from Figure 4.31 and 4.32, as shown by higher values of the total average Nusselt numbers. This confirms the effect of surface radiation in modifying the total heat transfer rate from the hot wall of the duct. Thus, for a given value of the wall heat flux, more heat is transferred from the walls to the fluid for the case of a duct having highly emissive walls. Hence, it is advantageous to have highly emissive walls as a passive heat transfer enhancement mechanism, even in the presence of mixed convection.

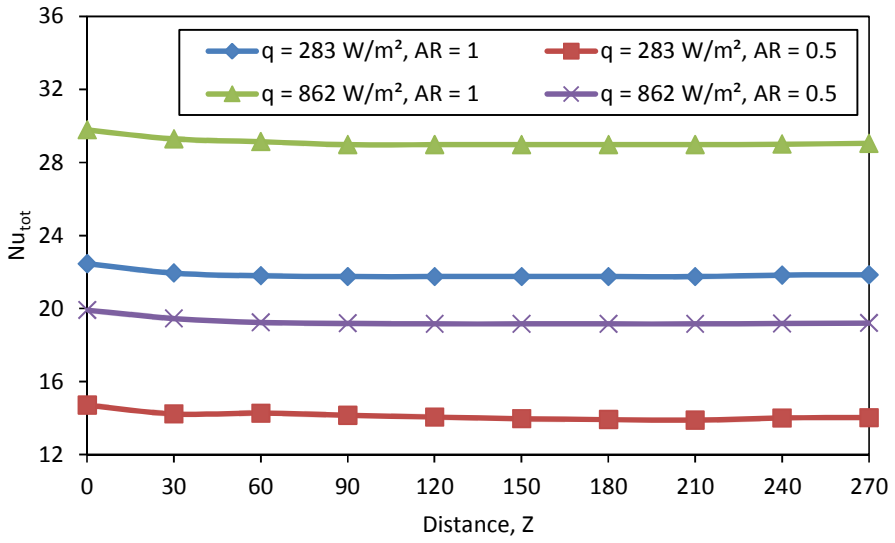

Figure 4.33 Effect of aspect ratio on the average total Nusselt number at the heated wall (Re = 1788, ε = 0.05).

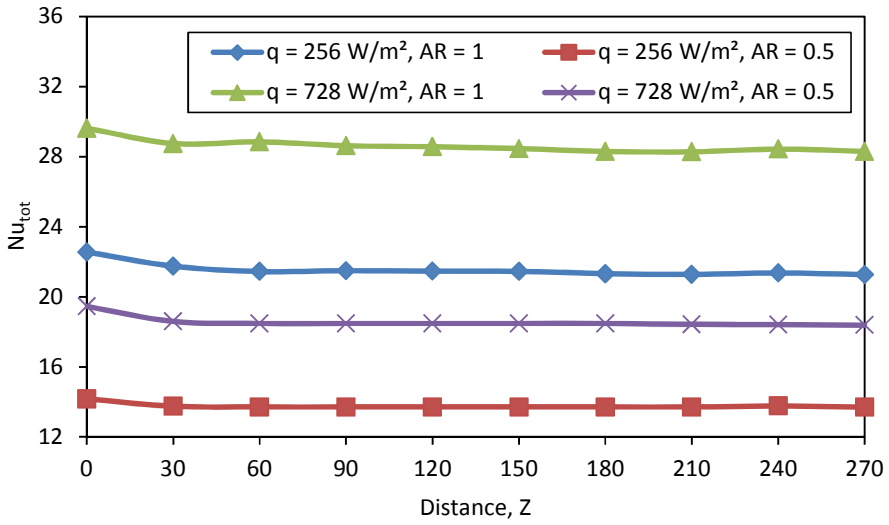

Figure 4.34 Effect of aspect ratio on the average total Nusselt number at the heated wall (Re = 1788, ε = 0.85).

Figures 4.33 and 4.34 show that the effect of aspect ratio on the average total Nusselt number. Considering the effect of aspect ratio, the polished surface average total Nusselt number for high heat flux was found to be 29.1 and 19.3 for the case of square and rectangular test section respectively. The average total Nusselt number between the square and rectangular test section differed by about 33.6 %. Similarly for the black surface, the average total Nusselt number for high heat flux was found to be 28.6 and 18.6 for the case of square and rectangular test sections respectively. The average total Nusselt number between the polished and black surface differed by about 34.6 %. The average total Nusselt number between the surfaces differed by about to 1 %. The same trend was found to be the case for low heat flux. The above results showed that for a given wall heat flux; the average total local Nusselt number is higher for a higher aspect ratio duct with polished and black surface.

4.7 Ratio of Convective and Radiative Nusselt Number to Total Nusselt Number

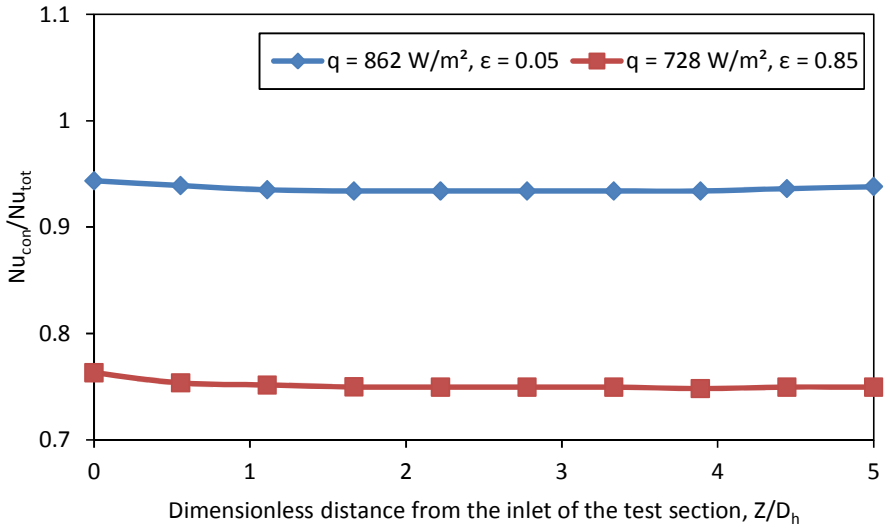

Figure 4.35 Ratio of convective to total Nusselt number(Re = 1788, AR = 1).

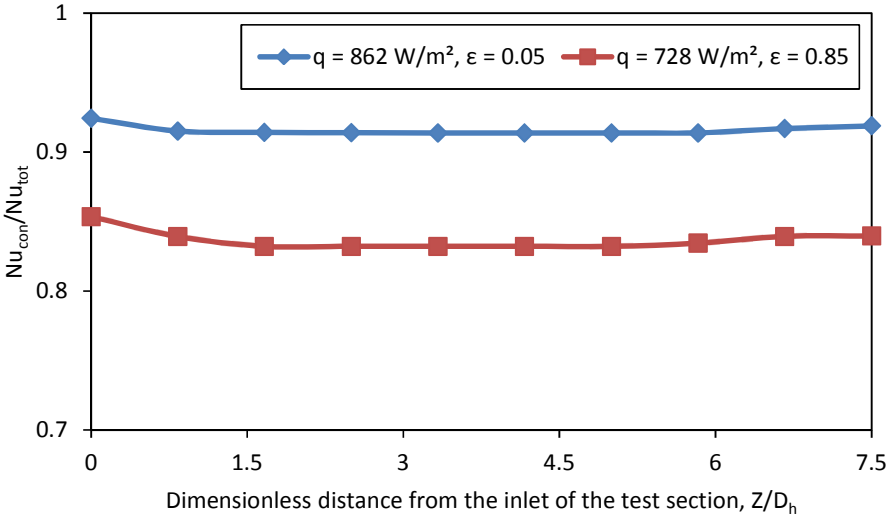

Figure 4.36 Ratio of convective to total Nusselt number (Re = 1788, AR = 0.5).

The ratio of convective and radiative Nusselt numbers to the total Nusselt number are presented in Figures 4.35 to 4.38. Figure 4.35 shows the ratio of convective to the total Nusselt number for the case of aspect ratio 1, in this case the percentage of

convective Nusselt rate is higher for weak radiation (94 %) compared to strong radiation (75 %). Similarly Figure 4.36 shows the ratio of convective to the total Nusselt number for the case of aspect ratio 0.5, in this case also the percentage of convective rate is higher for weak radiation (92 %) compared to strong radiation (84 %) conditions.

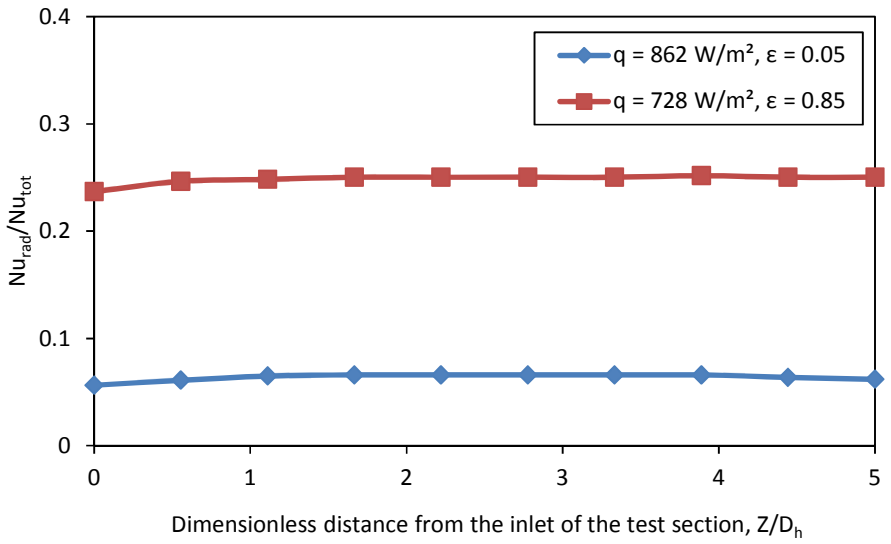

Figure 4.37 Ratio of radiative to total Nusselt number(Re = 1788, AR = 1).

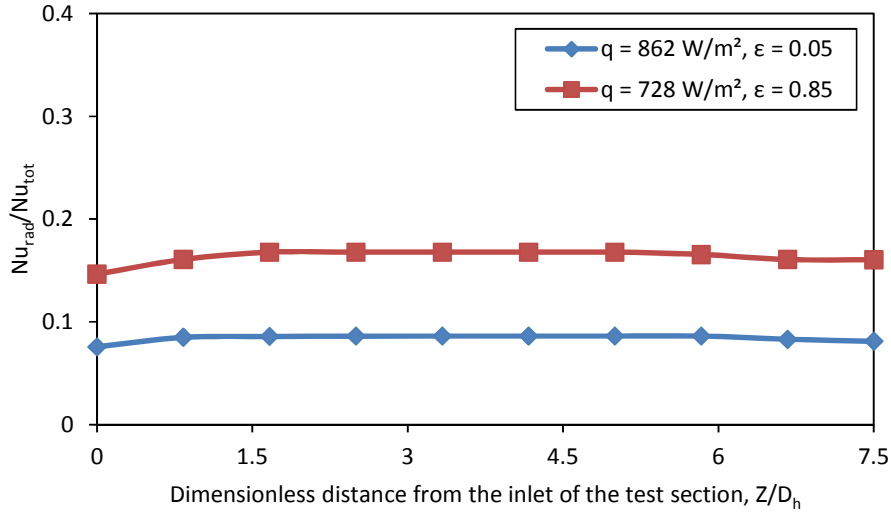

Figure 4.38 Ratio of radiative to total Nusselt number (Re = 1788, AR = 0.5).

Figures 4.37 and 4.38 show the ratio of radiative to the total Nusselt number for the case of aspect ratio 1 and 0.5. In this case the percentage of square duct radiative Nusselt number is higher for strong radiation (25%) compared to weak radiation (6%). Similarly the percentage of rectangualr dcut radiative Nusselt number is higher for strong radiation (16%) compared to weak radiation (8 %). Finally the above results show that the percentage of convection is higher for weak radiation compared to strong radiation and the percentage of radiation is higher for strong radiation compare to weak radiation.

4.8 Natural Convection Flow Visualization

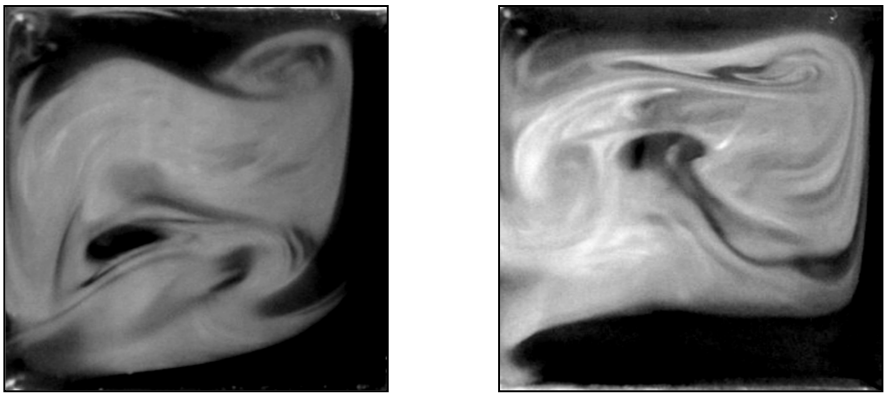

(a) (b)

Figure 4.39 Natural convection flow structure within the square ducts.

The flow visualization photographs provide a very good picture of the flow field as seen at a cross-section of the test section. Figure 4.39 (a) and (b) show the natural convection flow structure for the square duct with polished (q = 862 w/m², ε = 0.05) and black (q = 728 w/m², ε = 0.85) surface respectively, similarly Figure 4.40 (a) and (b) shows the natural convection flow structure for the rectangular duct with polished (q = 862 w/m², ε = 0.05) and black (q = 728 w/m², ε = 0.85) surface respectively.

The density gradient caused by strong natural convection induces the buoyancy force. So the flow slowly moves towards the upper part of the duct. The strength of the circulation depends on the heat flux as can be seen in Fig. 4.39 and 4.40.

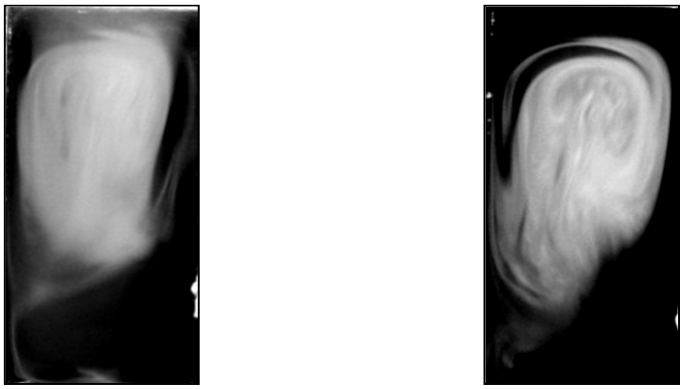

(a) (b)

Figure 4.40 Natural convection flow structure within the Rectangular ducts.

4.9 Mixed Convection Flow Visualization

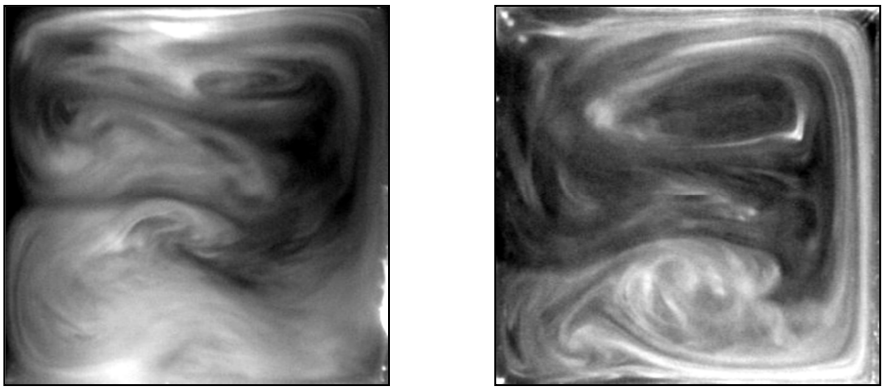

(a) (b)

Figure 4.41 Mixed convection flow structure within the square duct (Re = 858, ε = 0.05, AR = 1).

Figure 4.41 (a) and (b) shows the mixed convection flow structure for the square duct with polished surface for low (q = 283 W/m²) and high (q = 862 W/m²) heat flux respectively. In this case the low heat flux hot wall average temperature was

maintained at 56.7 ^{o}C and the high heat flux hot wall average temperature was maintained at 94.9 ^{o}C. It can be seen that the flow pattern is found to be very similar for both cases. Due to the high heat flux and buoyancy effect, the cold wall side the downward distance of the motion from top wall was maintained slightly higher compare to low heat flux. Similarly Figure 4.42 (a) and (b) show the mixed convection flow structure for the square duct with black surface for low (q = 256 W/m²) and high (q = 728 W/m²) heat flux respectively. In this case the low heat flux the hot wall average temperature was maintained at 52.5 ^{o}C and the high heat flux the hot wall temperature was maintained at 85.9 ^{o}C.

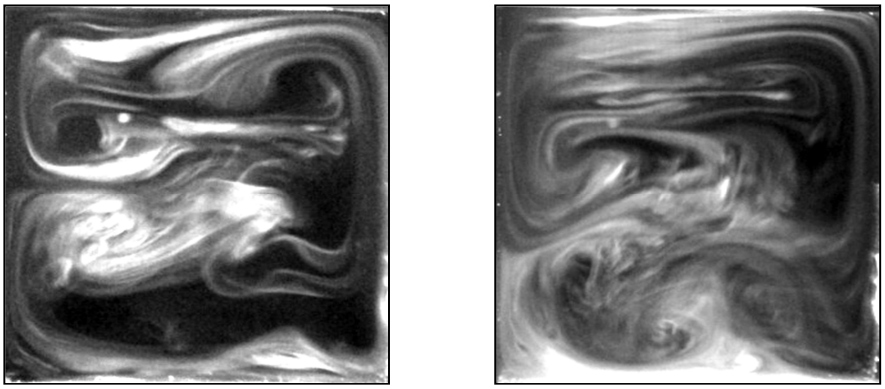

(a) (b)

Figure 4.42 Mixed convection flow structure within the square duct (Re = 858, ε = 0.85, AR = 1).

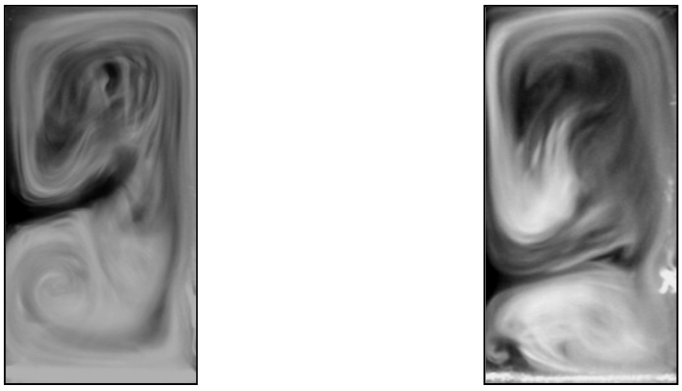

(a) (b)

Figure 4.43 Mixed convection flow structure within the square duct (Re = 858, ε = 0.05, AR = 0.5).

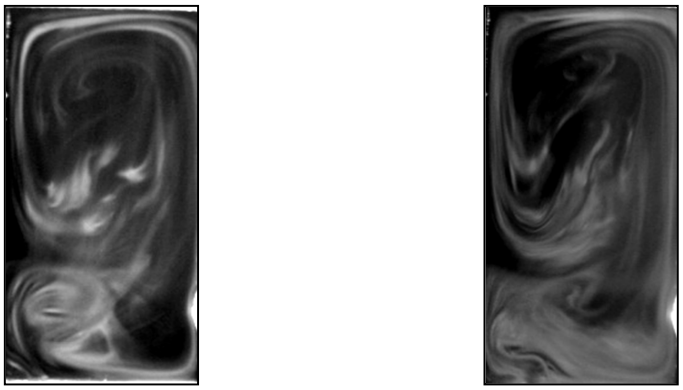

(a) (b)

Figure 4.44 Mixed convection flow structure within the rectangular duct (Re = 858, ε = 0.85, AR = 0.5).

Figure 4.43 (a) and (b) provide the mixed convection flow structure for the rectangular duct with polished surface for low (q = 283 W/m²) and high (q = 862 W/m²) heat flux respectively. In this case the low heat flux the hot wall average temperature was maintained at 58.1 ^{o}C and the high heat flux the hot wall temperature was maintained at 95.9 ^{o}C. Similarly Figure 4.44 (a) and (b) provide the mixed convection flow structure for the rectangular duct with black surface for low (q = 256 W/m²) and high (q = 728 W/m²) heat flux respectively. In this case for the low heat flux, the hot wall average temperature was maintained at 53.4 ^{o}C and the high heat flux the hot wall temperature was maintained at 86.9 ^{o}C.

The flow visualization result shows that the polished surface heated wall temperature is always higher than black surface. When comparing aspect ratio the rectangular duct temperature is always higher than square duct. The above figures (4.41 to 4.44) show that the flow moves upward and accumulates near the top wall adjacent to the hot wall of the duct, and is being circulated to the cold wall on the opposite side. This flow further moves downward and gets as close as to the bottom of the duct depending on the heat flux value. The accumulated flow is thermally stable; the stable conditions can reduce the heat transfer enhancement due to the buoyancy force. Similar trend is observed for all other cases of square and rectangular duct.

Table 4.1 Effect of Reynolds number on the average Nusselt Number at the heated wall for AR = 1

Description	Polished Surface (q = 862 W/m²)			Black Surface (q = 728 W/m²)		
	Reynolds Number			Reynolds Number		
	858	1788	2861	858	1788	2861
Convective Nusselt Number	24.9	27.3	31.0	19.6	21.5	24.6
Radiative Nusselt Number	2.0	1.8	1.7	7.4	7.1	6.2

Table 4.2 Average Nusselt number at heated wall for Re = 1788

Description	Polished Surface (q = 862 W/m²)		Black Surface (q = 728 W/m²)	
	Aspect Ratio (AR = 1)	Aspect ratio (AR = 0.5)	Aspect Ratio (AR = 1)	Aspect ratio (AR = 0.5)
Convective Nusselt Number	27.3	17.7	21.5	15.5
Radiative Nusselt Number	1.8	1.3	7.1	3.0

4.10 Summary

The results of mixed convection heat transfer for thermally developing flow in horizontal square and rectangular ducts with radiation effects are presented in this chapter. The test section consisted of two differentially heated isothermal vertical walls and two adiabatic horizontal walls. The effects of mixed convection, Reynolds number, radiation heat transfer and aspect ratio on the convective, radiative and the total Nusselt number were discussed.

Table 4.1 presents the effect of Reynolds number on the average convective and radiative Nusselt for square test section (AR = 1). The results show that for constant heat flux and high Reynolds number, the convective Nusselt values are higher but the radiative Nusselts are lower. Similar trend was observed for the rectangular duct. The

effect of emissivity and aspect ratios on the average convective and radiative Nusselt for a fixed Reynolds number (Re = 1788) is presented in Table 4.2. This indicates that for a given wall heat flux, the convective Nusselt number is higher for highly polished surface and higher aspect ratio, the radiative Nusselt number is higher for black surface. The same trend was observed for Reynolds numbers 858 and 2861.

The results obtained from this chapter will be used to compare with the hydrodynamically developed thermally developing flow in horizontal ducts and thermally developing flow in vertical ducts. In the next chapter, the results obtained from mixed convection heat transfer for hydrodynamically developed and thermally developing flow in horizontal ducts (CS2 configuration) will be presented and discussed.

CHAPTER 5

RESULTS AND DISCUSSION

CASE STUDY 2: HYDRODYNAMICALLY DEVELOPED AND THERMALLY DEVELOPING FLOW IN HORIZONTAL DUCTS (CS2)

5.1 Introduction

In the previous chapter, the results from the experiment work on mixed convection heat transfer for thermally developing flow in horizontal ducts with radiation effects was presented and discussed in detail. In this chapter, the results of laminar flow mixed convection heat transfer for hydrodynamically fully developed and thermally developing airflow in horizontal ducts with radiation effects is presented. The duct cross section is made of two differentially heated isothermal vertical walls and two adiabatic horizontal walls with aspect ratios 1 & 0.5. The investigation covers two Reynolds numbers (Re = 858 and Re = 1788), the wall heat flux was varied from 256 W/m^2 to 863 W/m^2, hot wall temperature varied from 55 ^oC to 100 ^oC, and the emissivity of internal walls were 0.05 and 0.85. The hydrodynamically fully developed condition was achieved by using an aluminum entrance section having the same cross section as the test section. The entrance length was varied from 1.5 m to 4.8 m depending on the Reynolds number. Flow visualization was also conducted to observe the flow patterns within the duct. The effect of surface temperature variation along the walls was studied to investigate the local Nusselt number variation within the duct.

5.2 Hydrodynamically Developed and Thermally Developing Flow in Horizontal Ducts

Figures 5.1 and 5.2 show the schematic diagram of a horizontal duct with square and rectangular cross sections that were considered for the analysis of a hydrodynamically developed and thermally developing flow. In the present set of experimental analysis, both square (AR = 1) and rectangular (AR = 0.5) test sections

were investigated with the use of four different entrance lengths in which the flow is hydrodynamically fully developed. The test section shown here was made of two differentially heated isothermal vertical walls and two adiabatic horizontal walls. The inside surface of the walls are highly polished in order to achieve a mirror finish with, a low emissivity of 0.05, or coated with blackboard paint to have an emissivity of 0.85. The description of test section was presented in Chapter 3. Table 3.3 shows the range of parameters and calculated length of four entrance lengths.

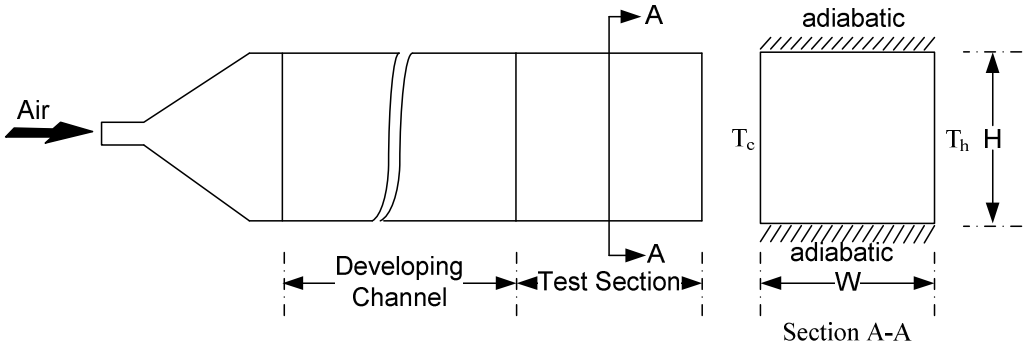

Figure 5.1 Schematic of the developed channel with horizontal square test section.

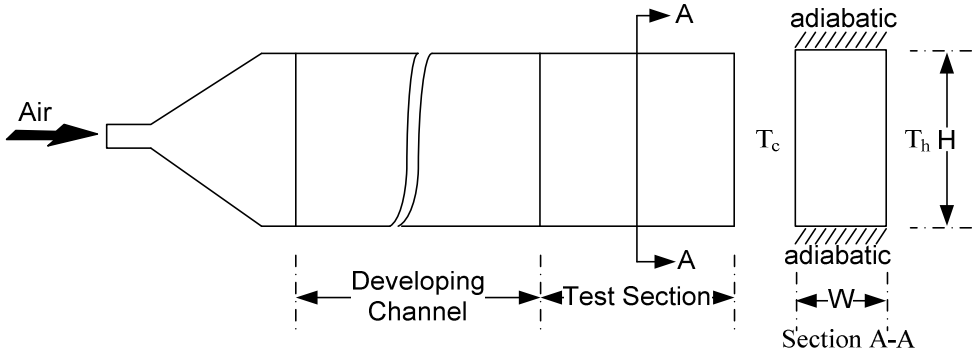

Figure 5.2 Schematic of the developed channel with horizontal rectangular test section.

5.3 Surface Temperature Distribution along the Duct Walls

5.3.1 Surface Temperature Distribution on the Heated Wall

The surface temperature distribution along the duct walls for a few selected experimental runs is shown in Figures 5.3 to 5.10. Figures 5.3 and 5.4 show the variation of surface temperature on the heated wall inside temperature as a function of the horizontal distance from the inlet of the test section to the exit for a low and high heat flux with a fixed Reynolds number of 1788. In this case study, the variation of surface temperature along the duct wall was mainly affected by Reynolds number, hydrodynamically developed flow condition, length of the entrance section, length of the test section and surface emissivity.

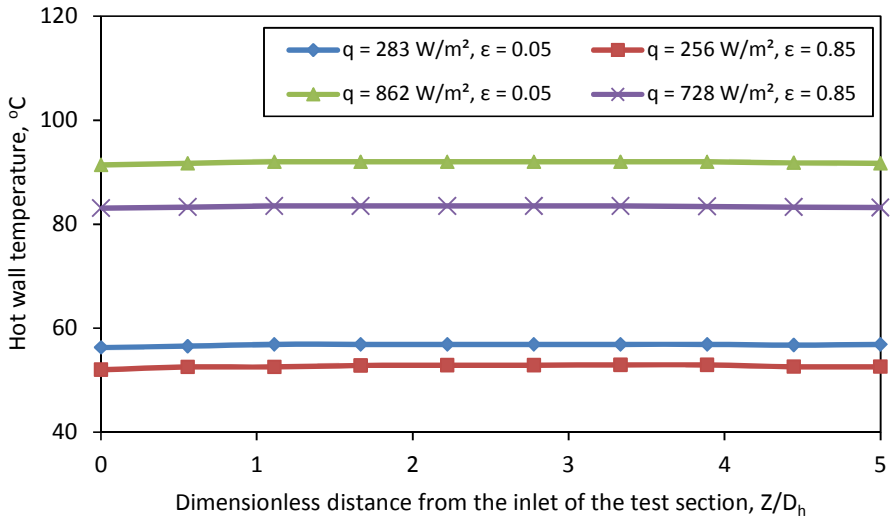

Figure 5.3 Variation of the surface temperature on the heated wall (Re = 1788, AR = 1).

Figure 5.3 shows that the square (AR = 1) test section had the highest heated wall average surface temperature of 91.2 ^{o}C for highly polished walls (ε = 0.05) with high heat flux q = 862 W/m². For black surface walls (ε = 0.85), the highest temperature was 82.8 ^{o}C with high heat flux q = 728 W/m². It can be seen from Figure 5.4 that the highest temperature increases marginally for both polished and black walls.

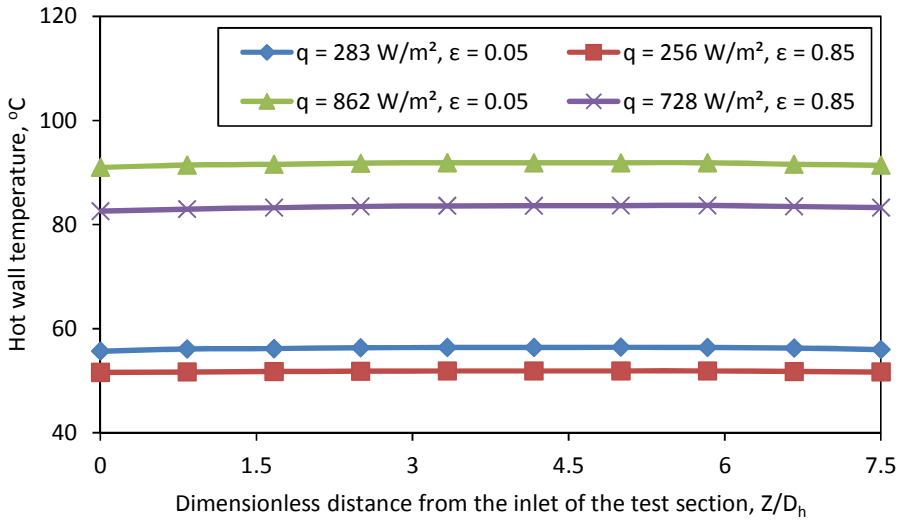

Figure 5.4 Variation of the surface temperature on the heated wall (Re = 1788, AR = 0.5).

Considering the surface emissivity in heated wall, the polished surface temperature is higher than black surface temperature. It can be observed that the variation of the surface temperature along the heated wall was uniform, except slightly lower for the entrance and the exit of test section. Due to the shorter length of test section and developed airflow, the heated wall surface temperature was maintained uniform. Otherwise the air when heated along the duct, its physical properties gradually change with the increasing of temperature. The fully developed air flow helps to extract the heat uniformly from the heated wall, due to that the heated wall temperature is found to be more uniform.

5.3.2 Surface Temperature Distribution on the Cold Wall

Figures 5.5 and 5.6 show the variation of the cold wall surface temperature. For all cases, the cold wall temperature was maintained equal to the inlet air temperature. The cold wall acts as a constant temperature sink and the inside surface of the cold wall faces the hot wall.

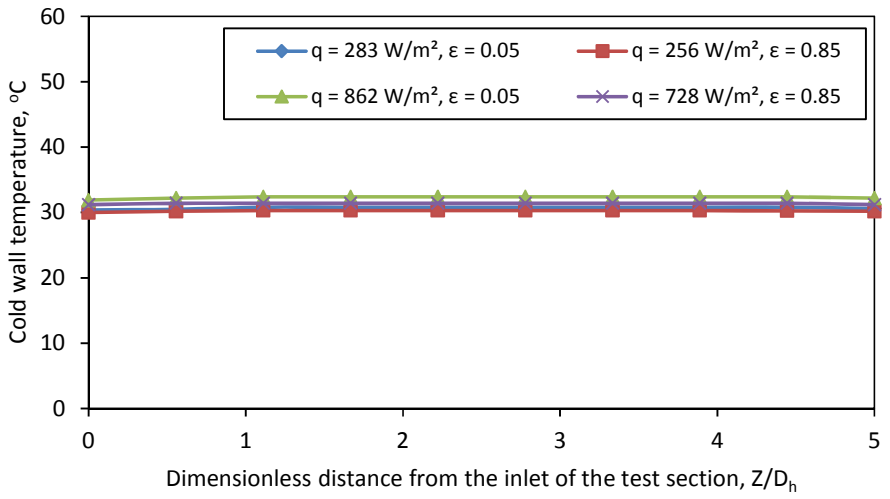

Figure 5.5 Variation of the surface temperature on the cold wall (Re = 1788, AR = 1).

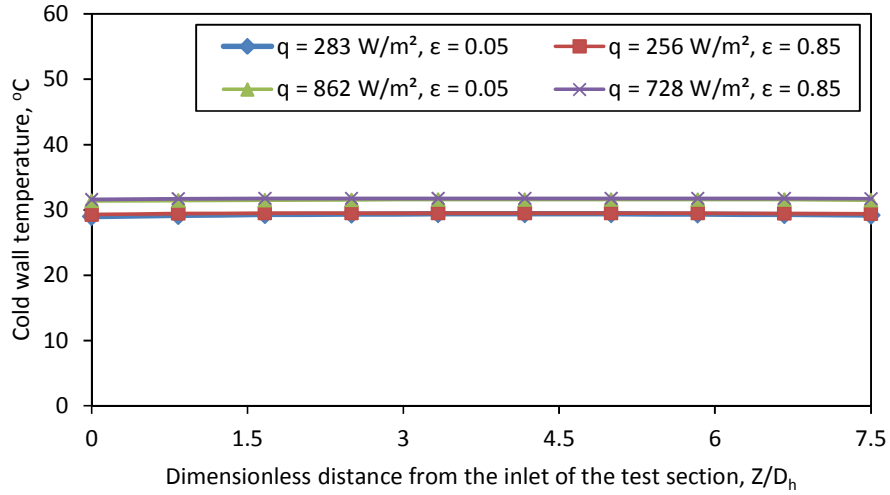

Figure 5.6 Variation of the surface temperature on the cold wall (Re = 1788, AR = 0.5).

5.3.3 Surface Temperature Distribution on the Top Wall

Figures 5.7 and 5.8 show the variation of the top wall inside surface temperature as a function of the horizontal distance for Reynolds number of 1788. The highest top wall average surface temperature of 51.5 ^{o}C and 48.2 ^{o}C is obtained for polished wall (ε = 0.05) and black surface wall (ε = 0.85) of the square test section. Similar

observations were found for the rectangular test section (Fig.5.8). It was observed that the average top wall temperature is marginally higher for the polished surface compared to black surface, in both the square and rectangular ducts. When considering the effect of aspect ratio, the rectangular test section top wall temperature was higher compared to that of the square test section. The temperature drop per unit length of the test section from the inlet to the outlet of the test section was found same for all cases.

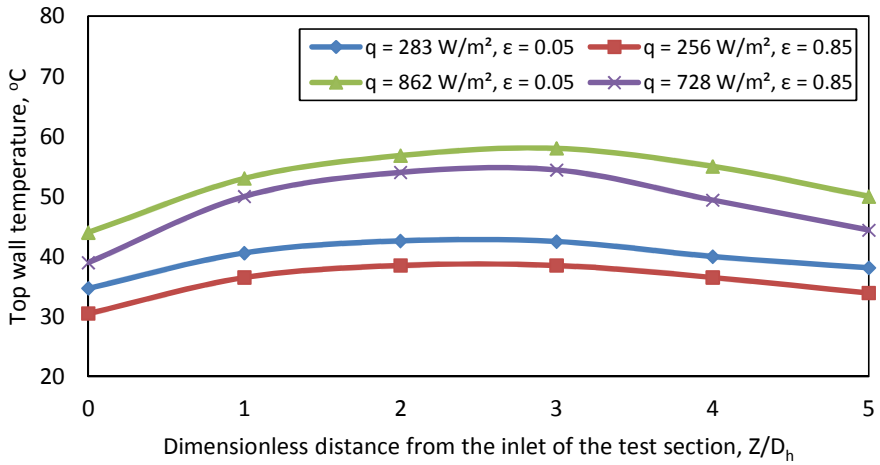

Figure 5.7 Variation of the surface temperature on the top wall (Re = 1788, AR = 1).

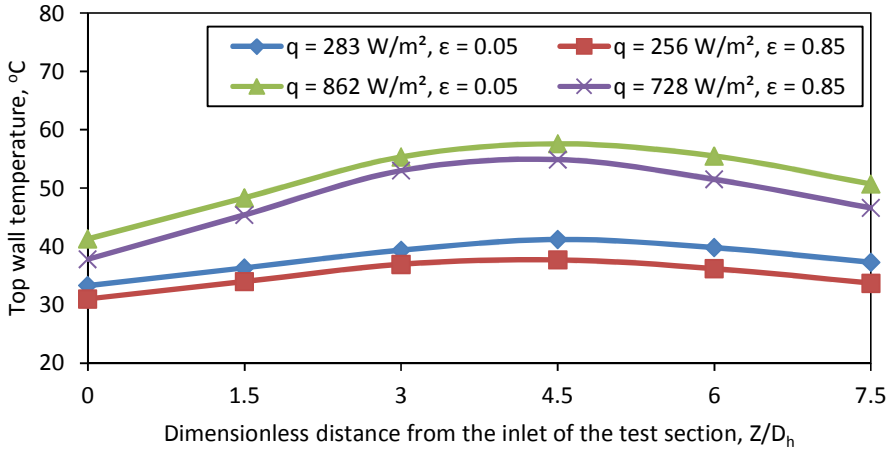

Figure 5.8 Variation of the surface temperature on the top wall (Re = 1788, AR = 0.5).

5.3.4 Surface Temperature Distribution on the Bottom Wall

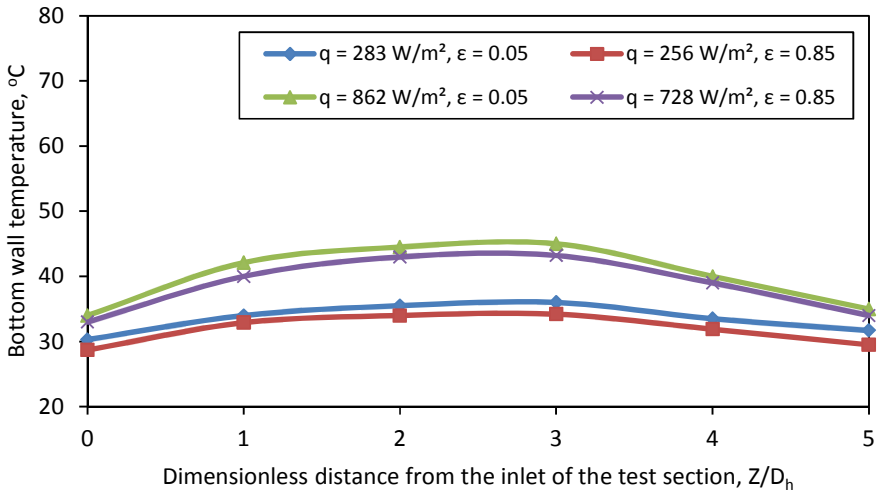

Figure 5.9 Variation of the surface temperature on the bottom wall (Re = 1788, AR = 1).

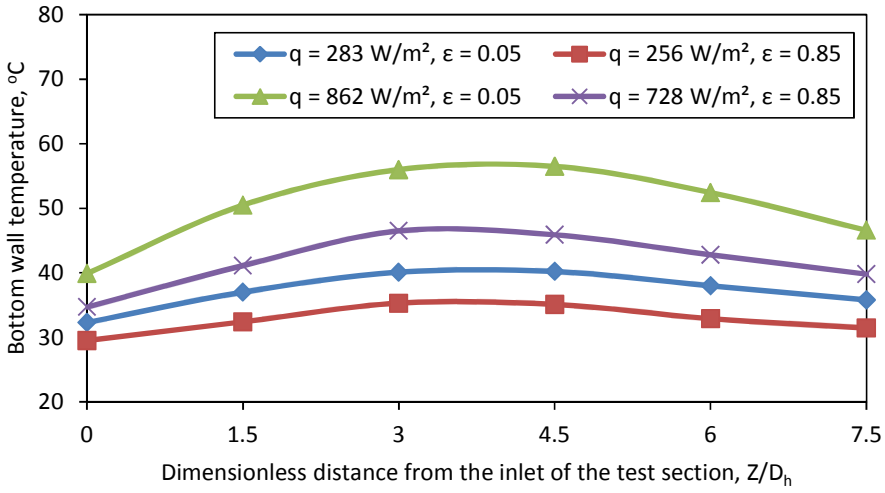

Figure 5.10 Variation of the surface temperature on the bottom wall (Re = 1788, AR = 0.5).

Figure 5.9 and 5.10 show the variation of the bottom wall inside surface temperature as a function of the horizontal distance. For the square test section, the highest bottom wall average surface temperature of 40.1 ^{o}C is obtained for polished wall (ε =

0.05) and an average surface temperature of 38.7 ^{o}C was obtained for black surface wall (ε = 0.85). For the polished surface wall (ε = 0.05) the average temperature increases by about 1.4 ^{o}C. Similar observations can also be made with the rectangular test section (Fig.5.10) and it was found to be at a higher temperature for the polished surface. The above result shows that the polished wall surface temperature is higher than black wall surface temperature. Surface radiation affected the surface temperature differences in the polished and black wall surfaces. For mixed convection cases, the average top wall temperature was always found to be higher than the bottom wall temperature. Generally the fluid with higher temperature moves upward due to the density gradient caused by strong natural convection effect and buoyancy force. The difference between top and bottom wall temperatures had a range of 8 % to 23 % and 4 % to 14 % for the case of polished and black surfaces respectively.

5.4 Combined Forced and Natural Convection Heat Transfer

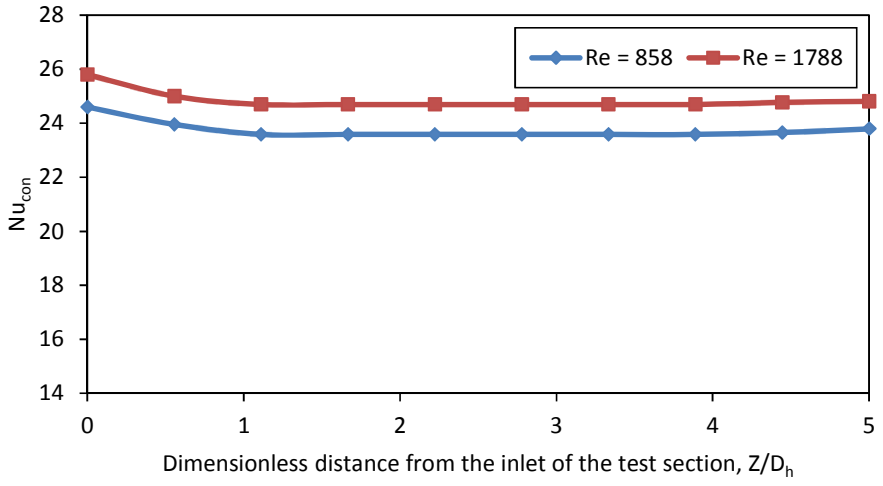

Figure 5.11 Effect of Reynolds number on the average convective Nusselt number at the heated wall (q = 862 W/m², AR = 1, ε = 0.05).

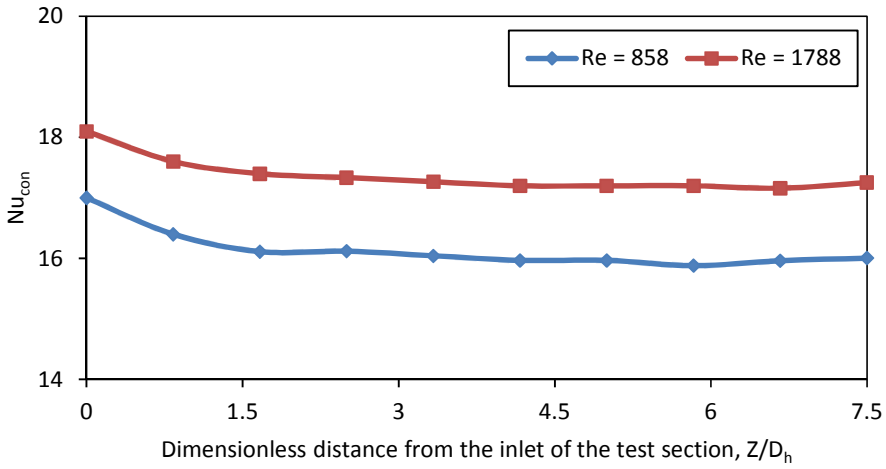

Figure 5.12 Effect of Reynolds number on the average convective Nusselt number at the heated wall (q = 862 W/m², AR = 0.5, ε = 0.05).

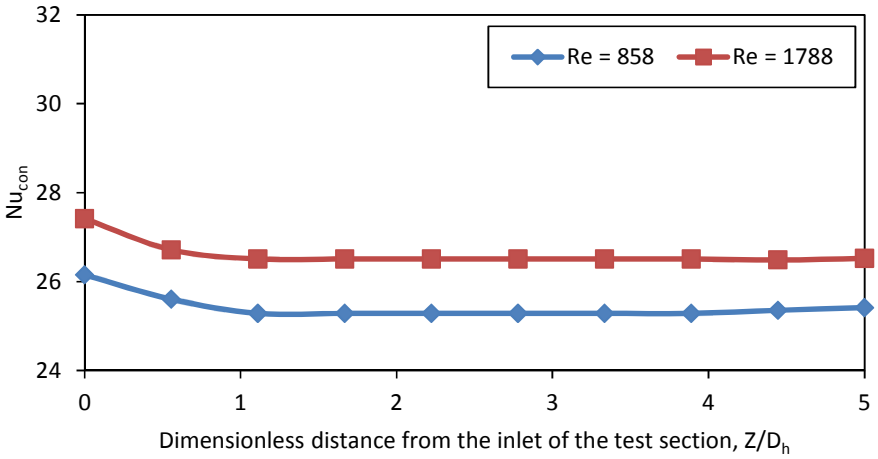

Figure 5.13 Effect of Reynolds number on the average convective Nusselt number at the heated wall (q = 728 W/m², AR = 1, ε = 0.85).

The above results show the effect of Reynolds number on the average convective Nusselt number at the heated wall with the dimensionless distance. Figure 5.11 and 5.12 show the Nusselt number for polished (ε = 0.05) surface with heat flux q = 862 W/m². In this case the square test section average convective Nusselt number was found to be 23.8 and 24.9 for the case of low (Re = 858) and high (Re = 1788) Reynolds numbers respectively. The average convective Nusselt number between the

low and high Reynolds number differed by about by 4.4 %. The rectangular test section average convective Nusselt number was found to be 16.1 and 17.4 for the case of low (Re = 858) and high (Re = 1788) Reynolds number respectively. The average convective Nusselt number is 7.4 % higher for high Reynolds number flow.

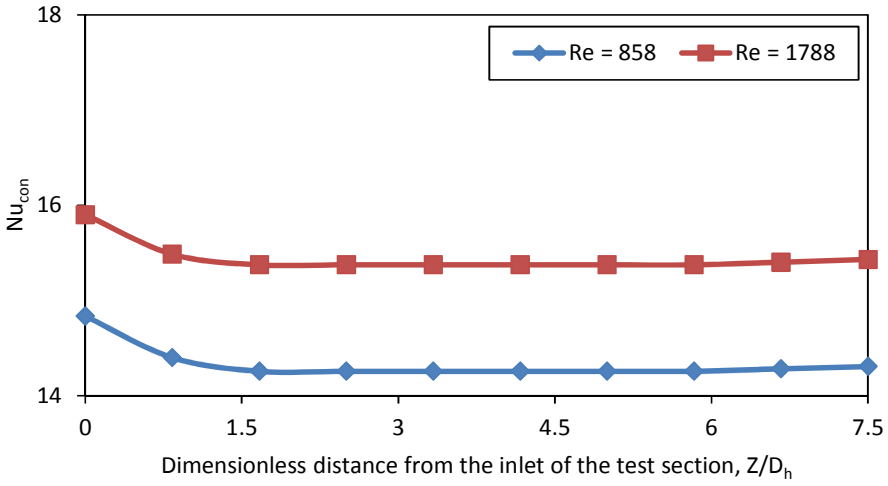

Figure 5.14 Effect of Reynolds number on the average convective Nusselt number at the heated wall (q = 728 W/m², AR = 0.5, ε = 0.85).

Figures 5.13 and 5.14 show the effect of Reynolds number on the Nusselt number for black (ε = 0.85) surface with heat flux q = 728 W/m². The range of average convective Nusselt number percentage was found to be 2.5 % to 7.1 % for the case of aspect ratio 1 and 0.5, respectively. For constant heat flux and high Reynolds number, the average convective Nusselt values give higher results, because of the dominant forced convection heat transfer with little effect of buoyancy force for high Reynolds number. Also it can be observed that, the natural convection to be stronger for slower flows. The pattern of the graph shows higher Nusselt number near the inlet of the test section. When the air flow is fully developed, it helps to extract the heat uniformly from the heated wall, due to the boundary layer development. The rate of convective Nusselt number drop near the inlet for all the cases was found to be in the range of 2.4 to 3.5 %.

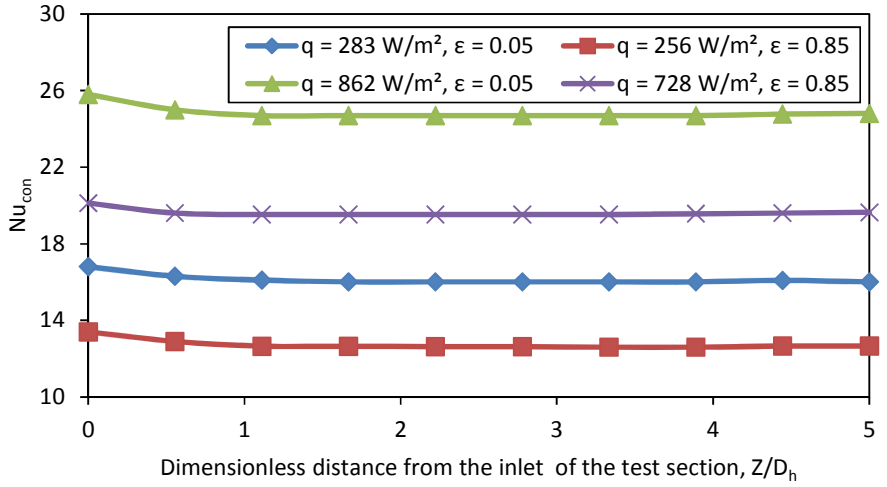

Figure 5.15 Effect of surface emissivity on the average convective Nusselt number at the heated wall (Re = 1788, AR =1).

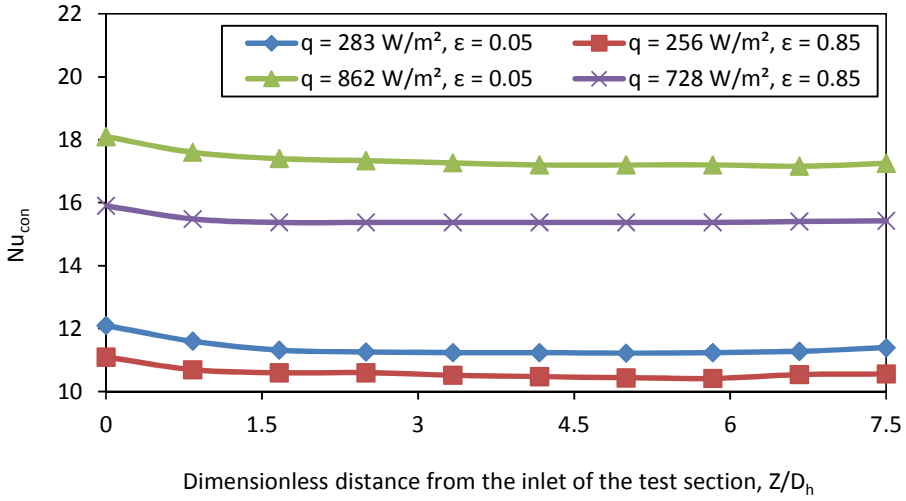

Figure 5.16 Effect of surface emissivity on the average convective Nusselt number at the heated wall (Re = 1788, AR = 0.5).

Figures 5.15 and 5.16 present the variation of average convective Nusselt number at the heated wall with different emissivity of low and high heat flux for Reynolds number (Re = 1788). The pattern of the graphs show that the Nusselt number values for both emissivity cases, 0.05 and 0.85, are of the same order. However the temperature difference between the hot walls range is higher for polished than black surface. Considering the effect of emissivity, the average convective Nusselt number

for square test section with high heat flux was found to be 24.9 and 19.6 for polished and black surface respectively. The average convective Nusselt number is 21.2 % higher for polished surface than black surface. For the rectangular test section, the average convective Nusselt number for the high heat flux case was found to be 17.4 and 15.4 for the case of polished and black surface respectively. The average convective Nusselt number is 11.5 % higher for polished surface than black surface.

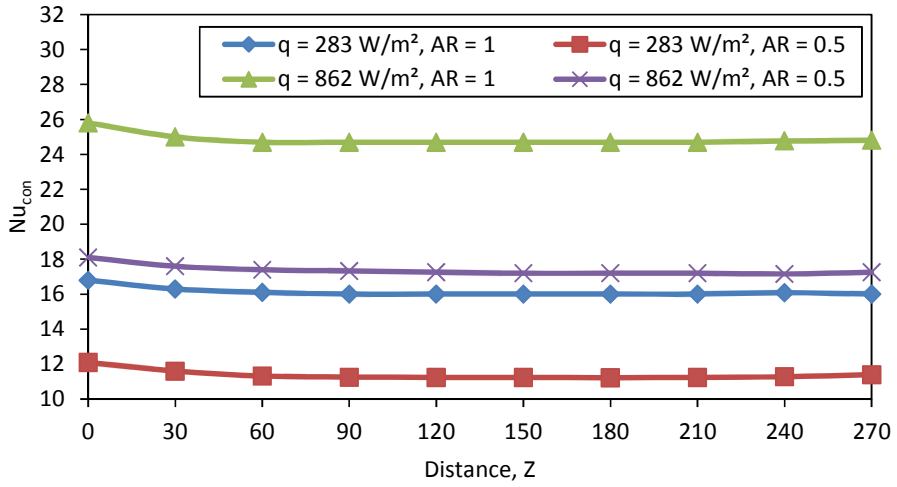

Figure 5.17 Effect of aspect ratio on the average convective Nusselt number at the heated wall (Re = 1788, ε = 0.05).

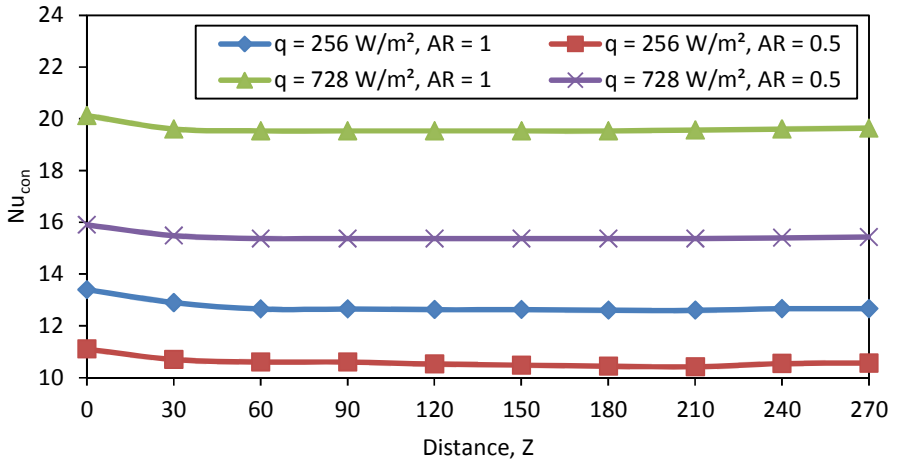

Figure 5.18 Effect of aspect ratio on the average convective Nusselt number at the heated wall (Re =1788, ε = 0.85).

Generally higher aspect ratio indicates long distance between two vertical walls and more volume of the air in the duct. In the present study, the height of the duct is fixed. The research included using four entrance sections with different lengths and the entrance sections maintaining the same aspect ratio of test section. Figure 5.17 and 5.18 show that the effect of aspect ratio on the convective Nusselt number at the heated wall for the case of square and rectangular test section with fixed Reynolds number. The Reynolds number was identically maintained for the two aspect ratios. When considering the effect of aspect ratio, the polished surface average convective Nusselt number for high heat flux was found to be 24.9 and 17.4 for the case of square and rectangular test section respectively. Similarly the black surface average convective Nusselt number for high heat flux was found to be 19.6 and 15.4 for the case of square and rectangular test section respectively. The above results show that the square and rectangular average convective Nusselt number between the polished and black surface differed by about 30.1 % and 21.4 %, respectively. It can be seen that for a given wall heat flux, the convective Nusselt number is higher for aspect ratio 1 compared with 0.5.

5.5 Radiation Heat Transfer

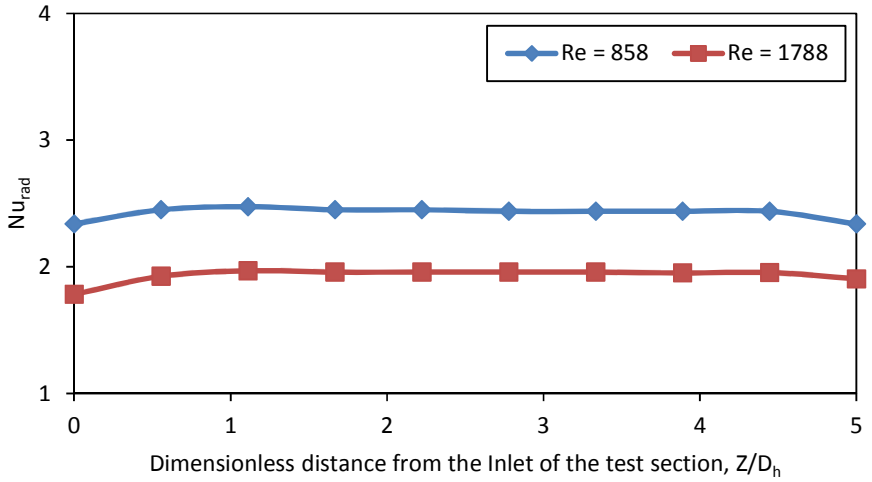

Figure 5.19 Effect of Reynolds number on the average radiative Nusselt number at the heated wall (q = 862 W/m², ε = 0.05, AR = 1).

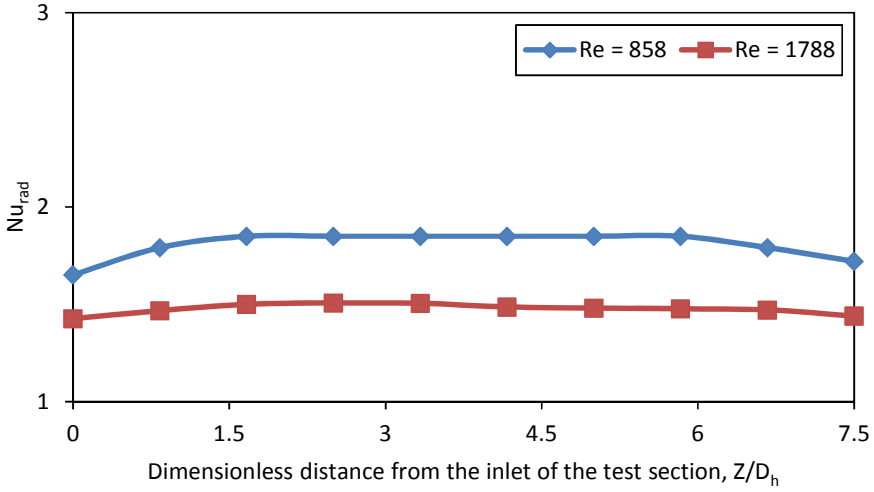

Figure 5.20 Effect of Reynolds number on the average radiative Nusselt number at the heated wall (q = 862 W/m², ε = 0.05, AR = 0.5).

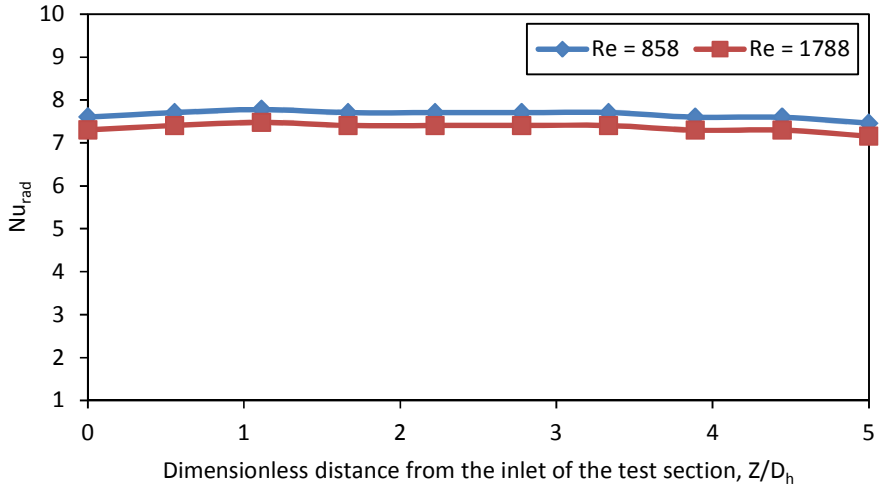

Figure 5.21 Effect of Reynolds number on the average radiative Nusselt number at the heated wall (q = 728 W/m², ε = 0.85, AR = 1).

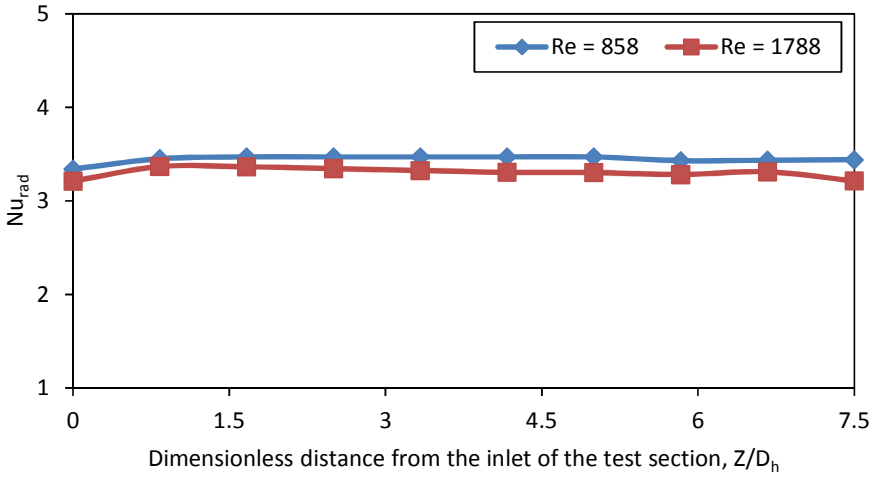

Figure 5.22 Effect of Reynolds number on the average radiative Nusselt number at the heated wall (q = 728 W/m², ε = 0.85, AR = 0.5).

The above graph shows the change in the heated wall average radiative Nusselt number along the test section from the inlet, for aspect ratio 1 and 0.5, respectively. The radiative heat flux is approximately constant for most part of the test section, except the inlet and outlet where some of the radiative energy is lost to the surrounding. The fully developed air flow extracts the heat uniformly from the heated wall, due to that the boundary layer is developed uniformly. The rate of

radiative Nusselt number rise near the inlet for all the cases were found to be in the range of 2.0 to 5.5 %.

Figures 5.19 and 5.20 show the effect of Reynolds number on the average radiative Nusselt number for polished surface (ε = 0.05) with heat flux q = 862 W/m². In this case the square test section average radiative Nusselt number was found to be 2.4 and 1.9 for the case of low (Re = 858) and high (Re = 1788) Reynolds numbers respectively. The average radiative Nusselt number is 20.8 % higher for low Reynolds number. Similarly the rectangular test section the average radiative Nusselt number is 16.6 % higher for low Reynolds number. Figures 5.21 and 5.22 show the effect of Reynolds number on the average radiative Nusselt number for black surface (ε = 0.85) with a heat flux q = 728 W/m². In this case the square test section average radiative Nusselt number is 3.8 % higher for low Reynolds number. Similarly the rectangular test section the average radiative Nusselt number is 5.8 % higher for low Reynolds number. For constant heat flux, the low Reynolds number average radiative Nusselt number values are always higher than the high Reynolds number average radiative Nusselt number.

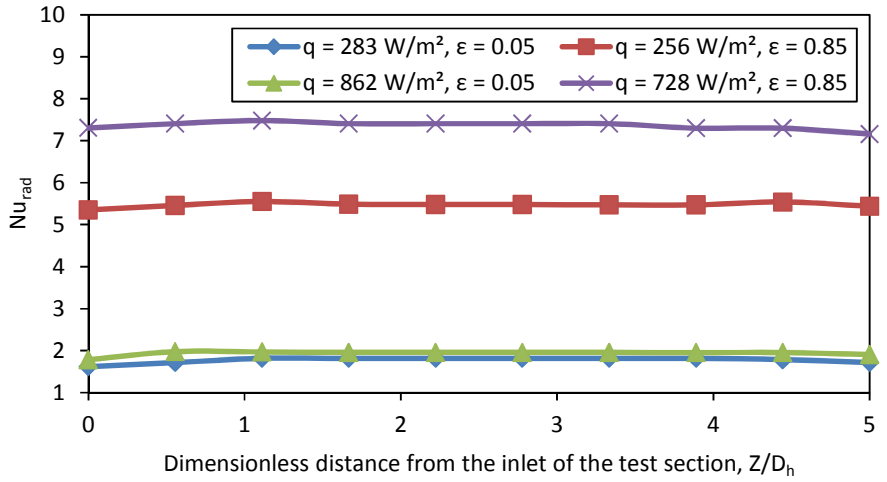

Figure 5.23 Effect of surface emissivity on the average radiative Nusselt number at the heated wall (Re = 1788, AR =1).

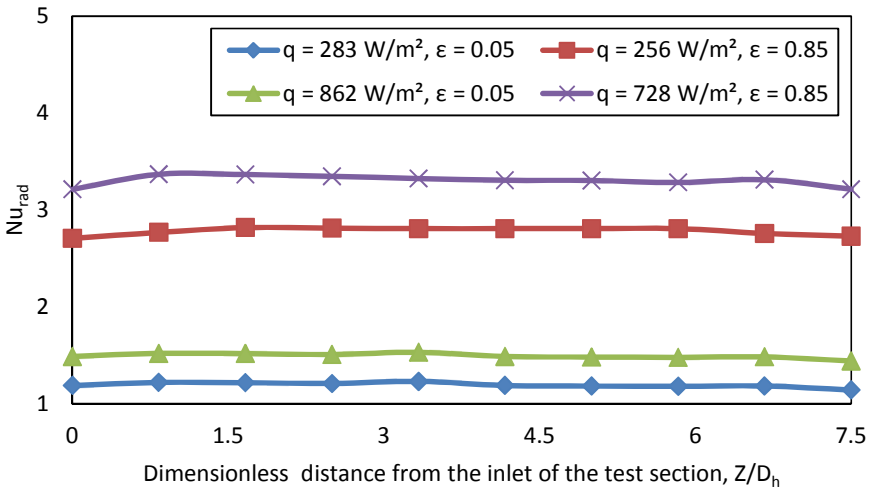

Figure 5.24 Effect of surface emissivity on the average radiative Nusselt number at the heated wall (Re = 1788, AR = 0.5).

Figures 5.23 and 5.24 present the effects of emissivity on the average radiative Nusselt number at the heated wall for low and high heat flux. For square test section the average radiative Nusselt number for high heat flux was found to be 1.9 and 7.4 for the case of polished and black surface respectively. In this case, the average radiative Nusselt number is 74.3 % higher for black surface than polished surface.

The average radiative Nusselt number for rectangular test section with high heat flux was found to be 1.5 and 3.2 for the case of polished and black surface respectively (Fig 5.24). In this case, the average radiative Nusselt number is 53.1 % higher for black surface than polished surface. It is observed that the average radiative Nusselt number is a very strong function of surface emissivity and the wall temperatures. The case of the duct having strong radiation and higher wall fluxes (and temperature) provides a higher value of the average radiative Nusselt number. For a given wall heat flux, the radiative Nusselt number is higher for black surface than highly polished surface.

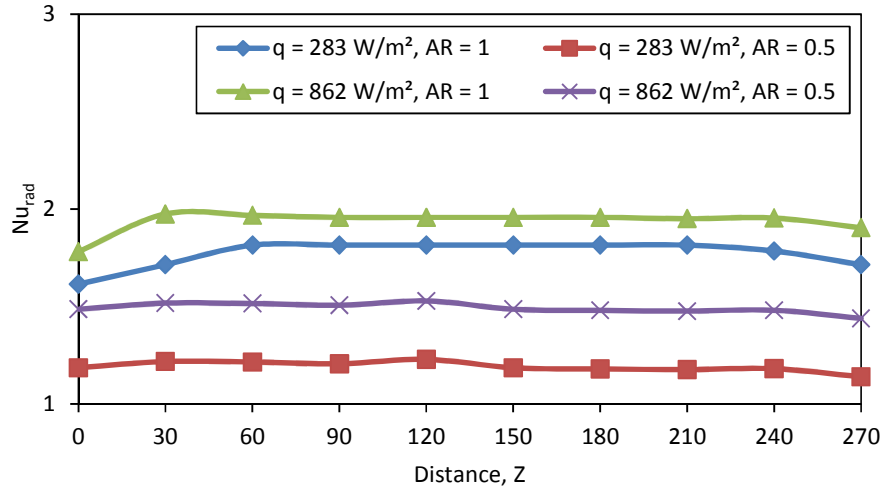

Figure 5.25 Effect of aspect ratio on the average radiative Nusselt number at the heated wall (Re = 1788, ε = 0.05).

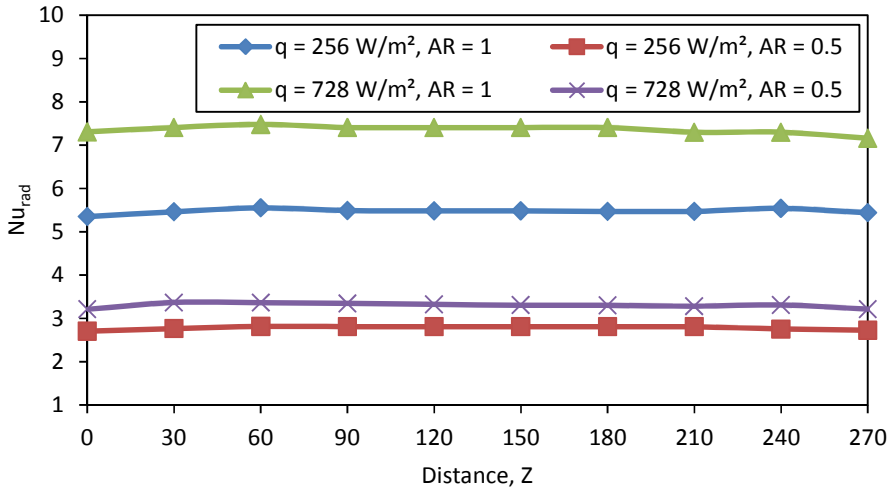

Figure 5.26 Effect of aspect ratio on the average radiative Nusselt number at the heated wall (Re = 1788, ε = 0.85).

In general, a higher aspect ratio duct has higher values of convective and radiative Nusselt number irrespective of the wall surface emissivity. Higher aspect ratio duct has more bottom wall area, and thus results in having more bottom wall effect. However, having larger distance between the hot and cold walls results in having less interaction of the wall heating effects caused by radiation heat exchange between the hot and cold walls, which delays the onset of thermal instability [35]. In this fully

developed condition the air flow is distributed uniformly all along the duct than the developed flow case and large volume of duct can help to improve higher heat transfer rate for higher aspect ratio cases.

Figure 5.25 shows the effect of aspect ratio on the average radiative Nusselt number for polished surface. In this case the average radiative Nusselt number for high heat flux was found to be 1.9 and 1.5 for the case of square and rectangular test section respectively. The average radiative Nusselt number is 21.0 % higher for square duct compared to the rectangular duct. Figure 5.26 shows the effect of aspect ratio on the average radiative Nusselt number for a black surface. In this case the average radiative Nusselt number for high heat flux was found to be 7.4 and 3.2 for the case of square and rectangular test section respectively. The average radiative Nusselt number is 56.7 % higher for square than rectangular duct. For a particular wall heat flux and fixed Reynolds number, the radiative Nusselt number values were found to be higher for aspect ratio 1 compared to aspect ratio 0.5.

5.6 Combined Convection and Radiation effect

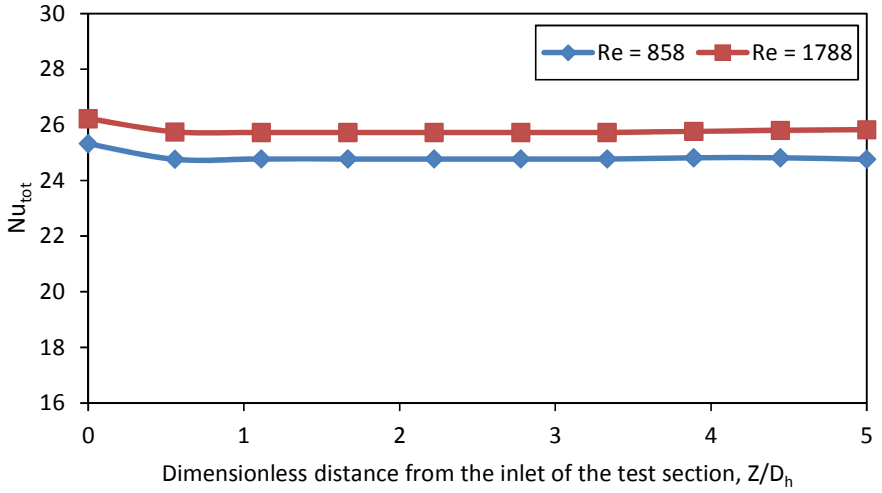

Figure 5.27 Effect of Reynolds number on the average total Nusselt number at the heated wall (q = 862 W/m², ε = 0.05, AR = 1).

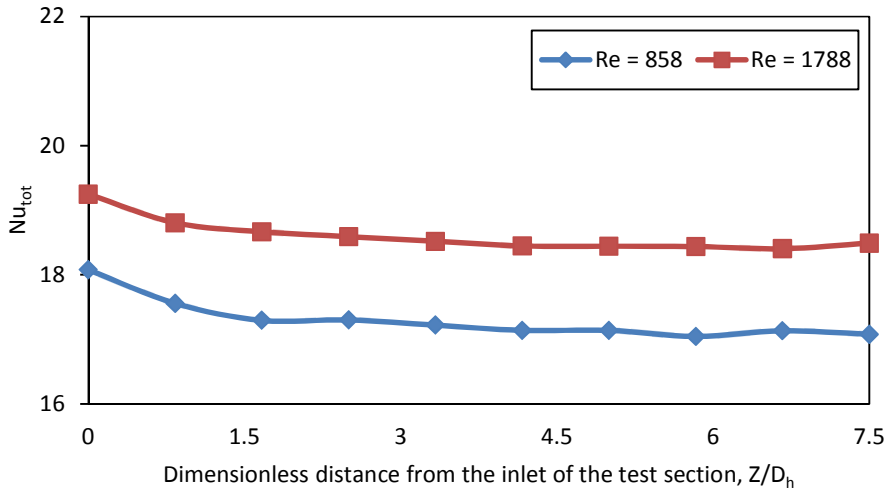

Figure 5.28 Effect of Reynolds number on the average total Nusselt number at the heated wall (q = 862 W/m², ε = 0.05, AR = 0.5).

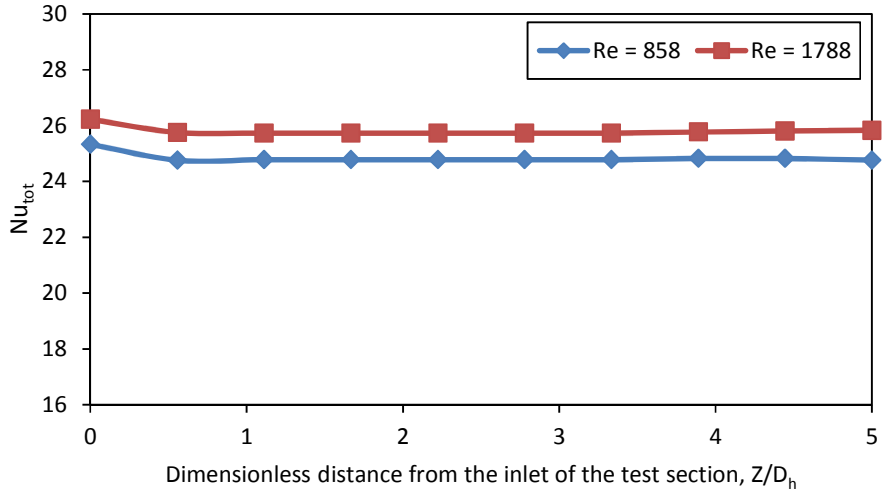

Figure 5.29 Effect of Reynolds number on the average total Nusselt number at the heated wall (q = 728 W/m², ε = 0.85, AR = 1).

Figure 5.27 and 5.28 show the effect of Reynolds number on the average total Nusselt number. For the polished surface (ε = 0.05) with heat flux q = 862 W/m² the average total Nusselt number was found to be 25.4 and 26.6 for the case of a square test section for low (Re = 858) and high (Re = 1788) Reynolds numbers. The average total Nusselt number is 4.5 % higher for high Reynolds number cases. Similarly the

rectangular test section average total Nusselt number was found to be 17.3 and 18.6 for the case of low (Re = 858) and high (Re = 1788) Reynolds number respectively. The average total Nusselt number is 6.9 % higher for the high Reynolds number case.

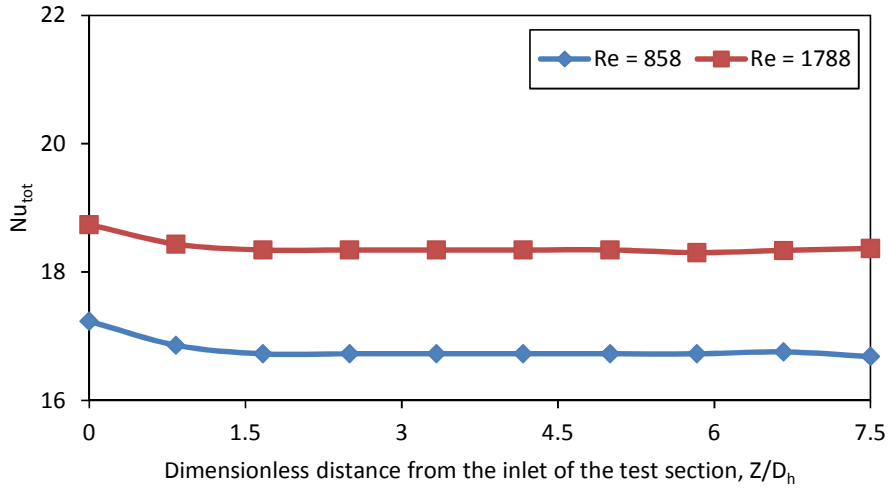

Figure 5.30 Effect of Reynolds number on the average total Nusselt number at the heated wall (q = 728 W/m², ε = 0.85, AR = 0.5).

Figures 5.29 and 5.30 show the effect of Reynolds number on the average total Nusselt number for black surface (ε = 0.85) with a heat flux q = 728 W/m². In this case the average total Nusselt number difference between the square and rectangular test section was found to be 3.8 % and 8.6 % for low (Re = 858) and high (Re = 1788) Reynolds number respectively.

The above results showed that the variation of percentage difference between low (Re = 858) and high (Re = 1788) Reynolds number for both cases to be identical. For constant heat flux and high Reynolds number, the average total Nusselt number is higher for square duct than that of the rectangular duct.

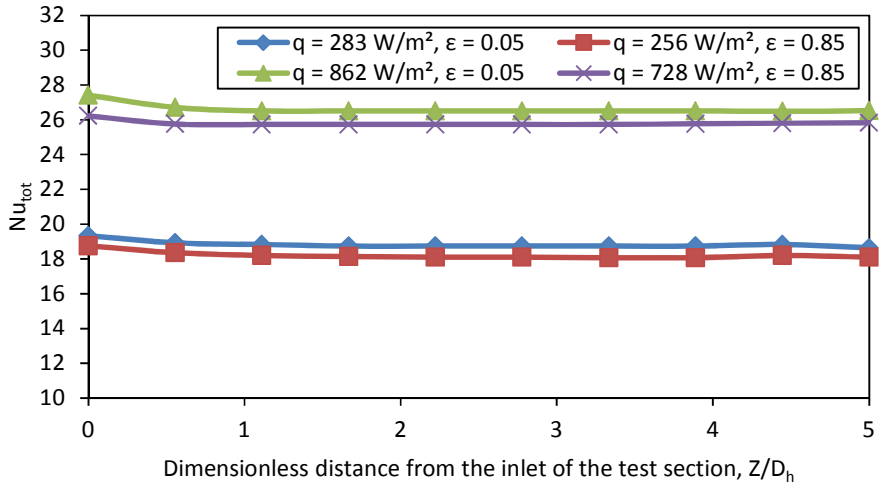

Figure 5.31 Effect of surface emissivity on the average total Nusselt number at the heated wall (Re = 1788, AR = 1).

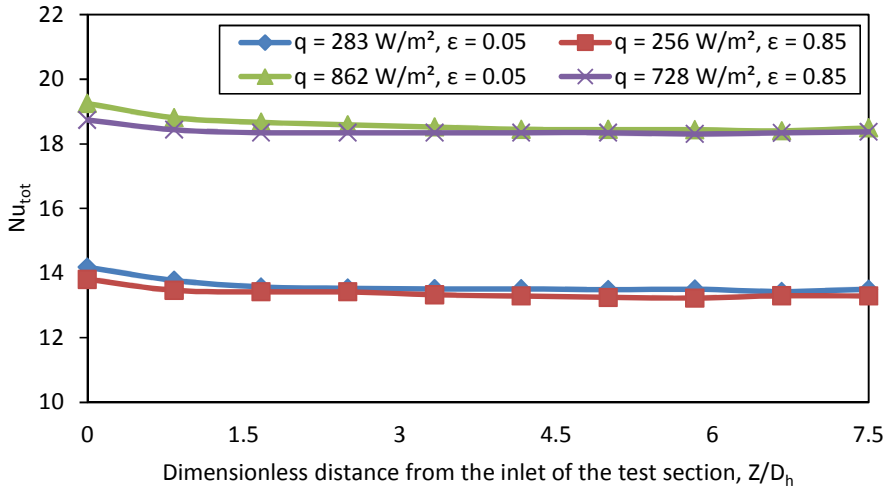

Figure 5.32 Effect of surface emissivity on the average total Nusselt number at the heated wall (Re = 1788, AR = 0.5).

Figures 5.31 and 5.32 show the effect of emissivity on the average total Nusselt number at the heated wall with Reynolds number Re = 1788 for the case of square and rectangular test section. The total heat transfer rate from the heated wall can be represented as the sum of the Nusselt numbers due to convection and radiation. The above graphs show the result of polished and black surface average total Nusselt

number almost equal for low and high heat flux respectively. The importance of surface emissivity is evident when convection and radiation effects are separately estimated. The detail was described in previous Section 5.4 and 5.5.

Figures 5.33 and 5.34 show that the effect of aspect ratio on the average total Nusselt number for the case of polished and black surfaces respectively. Considering the effect of aspect ratio, the polished surface average total Nusselt number for high heat flux was found to be 26.6 and 18.6 for the case of square and rectangular test section respectively. The average total Nusselt number rate is 30 % higher for a square duct. Similarly the black surface average total Nusselt number for high heat flux was found to be 18.8 and 13.6 for the case of square and rectangular test section respectively. The average total Nusselt number is 27.6 % higher for square duct. The same trend was observed for low heat flux and also noticed that for a given wall heat flux; the average total Nusselt number is higher for higher aspect ratio. A higher aspect ratio duct has higher values of convective and radiative Nusselt number irrespective of the wall surface emissivity.

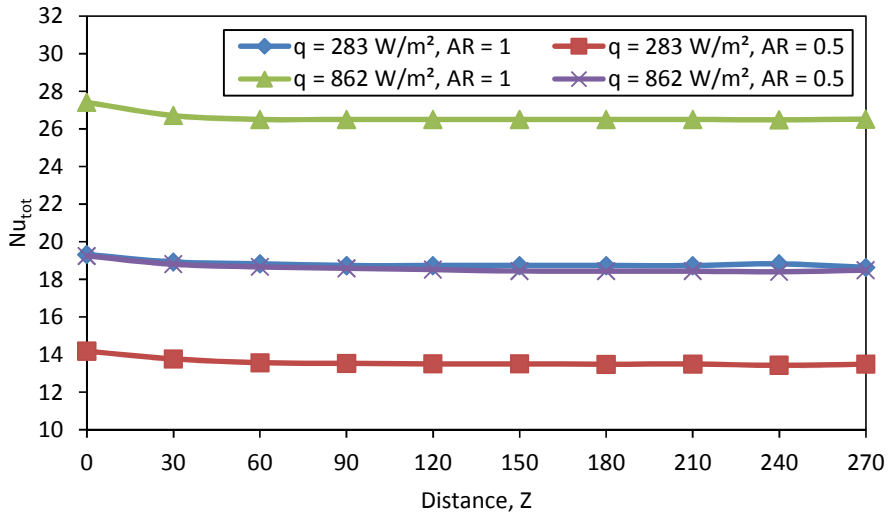

Figure 5.33 Effect of aspect ratio on the average total Nusselt number at the heated wall (Re = 1788, ε = 0.05).

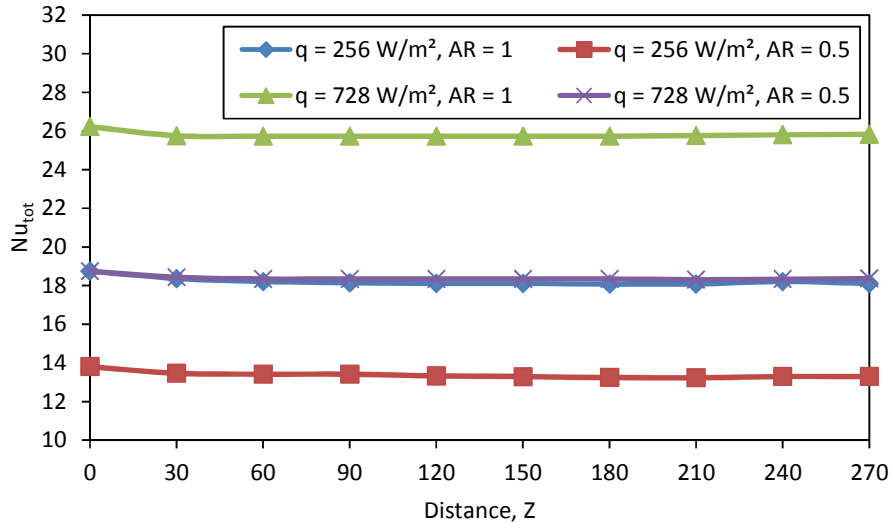

Figure 5.34 Effect of aspect ratio on the average total Nusselt number at the heated wall (Re = 1788, ε = 0.85).

5.7 Ratio of Convective and Radiative Nusselt Number to Total Nusselt Number

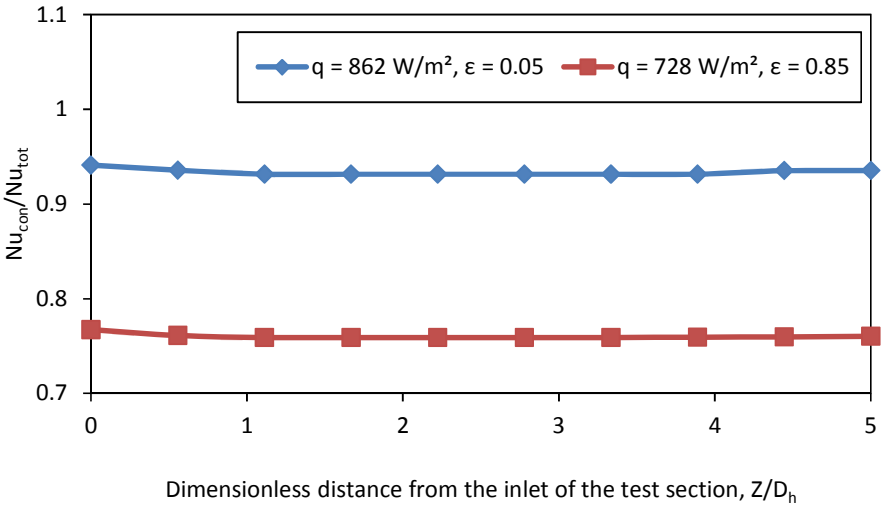

Figure 5.35 Ratio of convective to total Nusselt number (Re = 1788, AR = 1).

Figures 5.35 and 5.36 show the ratio of convective to the total Nusselt number for the case of aspect ratio 1 and 0.5. In this case, the percentage of square duct convective Nusselt value is higher for weak radiation (93 %) compared to strong radiation (76 %). Similarly the percentage of rectangular duct convective value is higher for weak

radiation (93 %) compare to strong radiation (84 %) conditions. It was found that weak radiation effects lead to higher values of convective Nusselt number irrespective of the aspect ratio of the cross section of the duct.

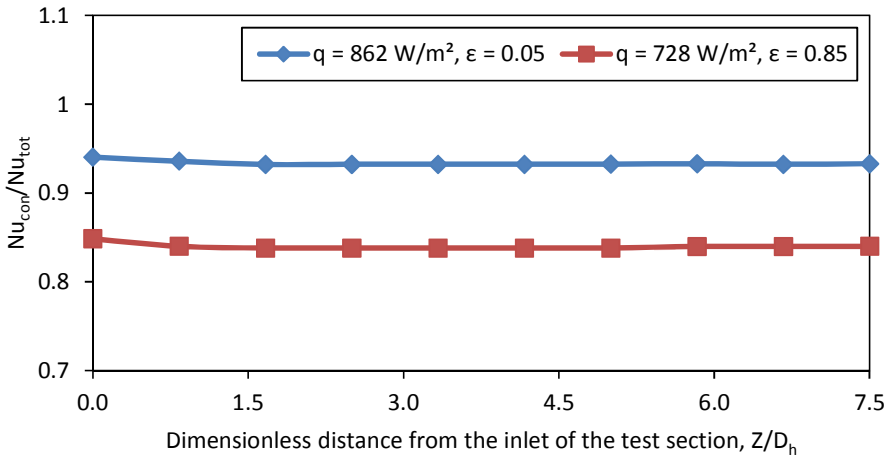

Figure 5.36 Ratio of convective to total Nusselt number (Re = 1788, AR = 0.5).

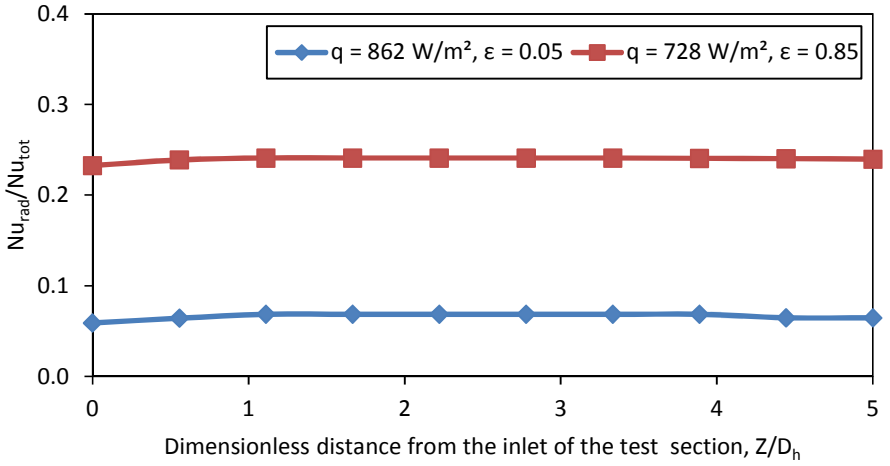

Figure 5.37 Ratio of radiative to total Nusselt number (Re = 1788, AR = 1).

Figures 5.37 and 5.38 show the ratio of radiative to the total Nusselt number for the case of aspect ratio 1 and 0.5. In this case the percentage of square duct radiative rate is higher for strong radiation (24 %) compared to weak radiation (7 %). Similarly the percentage of rectangualr duct radiative rate is higher for strong radiation (16 %) compared to weak radiation (7 %). The above results show that the percentage of

radiation is higher for strong radiation effects and the percentage of convection is higher for weak radiation effects within the duct.

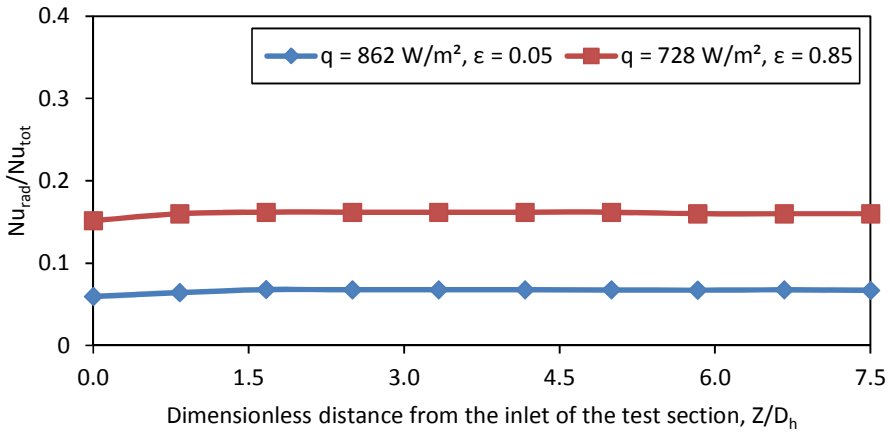

Figure 5.38 Ratio of radiative to total Nusselt number (Re = 1788, AR = 0.5).

5.8 Mixed Convection Flow Visualization

Figures 5.39 to 5.42 show mixed convection flow structure for hydrodynamically developed and thermally developing flow in a horizontal square and rectangular duct for the case of low and high heat flux. Figures 5.39 (a) and (b) show the mixed convection flow structure for the square duct with polished surface for low (q = 283 W/m²) and high (q = 862 W/m²) heat flux. The hot wall average temperature was maintained at 57.4 ^{o}C and 95.6 ^{o}C, respectively. It can be seen that the pattern of the flow is similar for both cases. Figures 5.40 (a) and (b) show the mixed convection flow structure for the square duct with black surface for low (q = 256 W/m²) and high (q = 728 W/m²) heat flux hot wall average temperature was maintained at 52.8 ^{o}C and 86.7 ^{o}C, respectively.

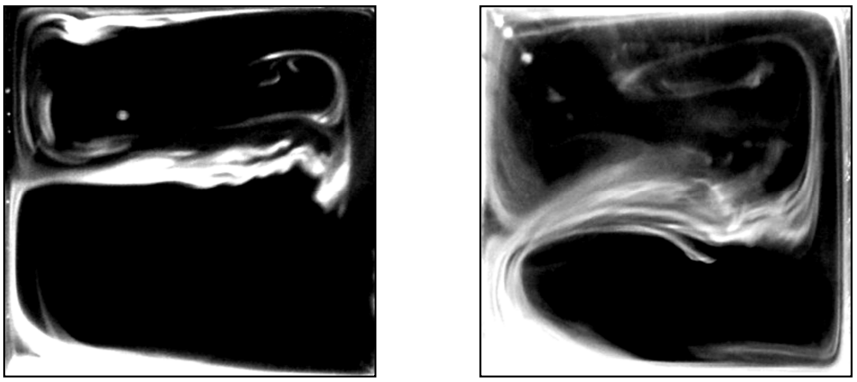

(a) (b)

Figure 5.39 Mixed convection flow structure within the square duct (Re = 858, ε = 0.05, AR = 1).

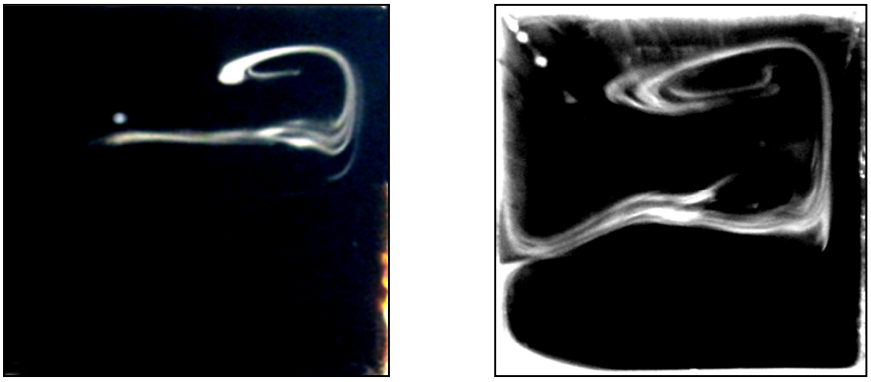

(a) (b)

Figure 5.40 Mixed convection flow structure within the square duct (Re = 858, ε = 0.85, AR = 1).

Figure 5.41 (a) and (b) provide the mixed convection flow structure for the rectangular duct with polished surface for low (q = 283 W/m²) and high (q = 862 W/m²) heat flux hot when the wall average temperature was maintained at 58.5 ^{o}C and 95.7 ^{o}C, respectively. Similarly the Figure 5.42 (a) and (b) provide the mixed convection flow structure for the rectangular duct with black surface for low (q = 256 W/m²) and high (q = 728 W/m²) heat flux when the hot wall average temperature was maintained at 53.9 ^{o}C and 86.9 ^{o}C, respectively.

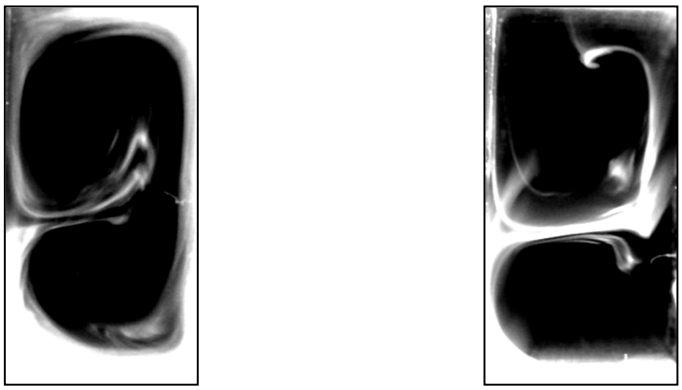

(a) (b)

Figure 5.41 Mixed convection flow structure within the square duct (Re = 858, ε = 0.05, AR = 0.5).

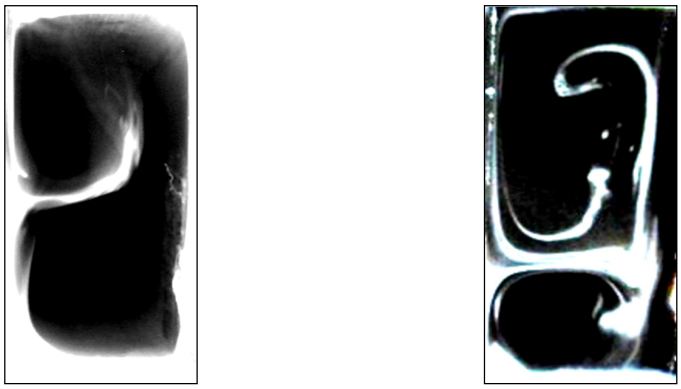

(a) (b)

Figure 5.42 Mixed convection flow structure within the rectangular duct (Re = 858, ε = 0.85, AR = 0.5).

The above result shows that the pattern of the flow almost same for all the cases. When comparing the wall surface temperature, the polished wall heated surface temperature is always higher than black surface. In this case the flow is induced by buoyancy, the heated air flow motion moves upward, accumulates near the top wall adjacent to the hot wall of the duct and continuously gets circulated to the cold wall on the opposite side. In middle of the cold wall, the flow turns to rotate and again gets joined with upward rotational motion. In this configuration, the hydrodynamically fully developed condition is achieved before the airflow enters the

test section, so the developed airflow helps to improve and extract the heat uniformly from the heated wall due to that the pattern of the flow appearing more stable. Similar trend is observed for all other cases of square and rectangular duct.

Table 5.1 Effect of Reynolds number on the average Nusselt number at heated wall for AR = 1

Description	Polished Surface (q = 862 W/m²)		Black Surface (q = 728 W/m²)	
	Re = 858	Re = 1788	Re = 858	Re = 1788
Convective Nusselt Number	23.8	24.9	19.1	19.6
Radiative Nusselt Number	2.4	1.9	7.7	7.4

Table 5.2 Average Nusselt number at heated wall for Re = 1788

Description	Polished Surface (q = 862 W/m²)		Black Surface (q = 728 W/m²)	
	Aspect Ratio (AR = 1)	Aspect ratio (AR = 0.5)	Aspect Ratio (AR = 1)	Aspect ratio (AR = 0.5)
Convective Nusselt Number	24.9	17.4	19.6	15.4
Radiative Nusselt Number	1.9	1.5	7.4	3.2

5.9 Summary

The result of mixed convection heat transfer for hydrodynamically developed and thermally developing flow in horizontal square and rectangular ducts with radiation effects are presented in this chapter. In this configuration airflow passes through the test section with a developing section (entrance section). The hydrodynamically fully developed condition is achieved, before the air flow enters the test section. The effects of mixed convection, Reynolds number, radiation heat transfer and aspect ratio have been thoroughly discussed.

Table 5.1 presents the effect of Reynolds number on the average convective and radiative Nusselt number for square test section (AR = 1).It was found that the convective Nusselt values along the duct are higher for high Reynolds number and the radiative Nusselt values give lower results. For the polished surface, the Radiative Nusselt number (2.4) higher for low Reynolds number and the Radiative Nusselt number (1.9) lower for high Reynolds number is presented in the table 5.1. It is observed that forced convection domination is higher for high Reynolds number and the natural convection domination is higher for low Reynolds number. Similar trend was observed for the rectangular duct. The effect of emissivity and aspect ratios on the average convective and radiative Nusselt numbers for a fixed Reynolds number (Re = 1788) is presented in Table 5.2. The convective Nusselt number was found to be higher for highly polished surface and higher aspect ratio, the radiative Nusselt number was higher for black surface. When considering the heat transfer conditions, in general the higher aspect ratio generally has higher overall convective Nusselt number and radiative Nusselt number irrespective of the wall surface emissivity. The same trend is observed for the Reynolds number of 858.

It was observed that the total heat transfer from the hot wall to the cold wall depends on the developed flow condition, mixed convection, and also on the surface radiation heat transfer. The result also shows that flow condition and radiation significantly affect the total Nusselt number and tends to reduce the thermal buoyancy effects.

The results obtained from this chapter will be used to compare with the case of thermally developing flow in horizontal ducts. In the next chapter, the results obtained from mixed convection heat transfer for thermally developing flow in vertical ducts will be presented and discussed.

CHAPTER 6

RESULTS AND DISCUSSION

CASE STUDY 3: THERMALLY DEVELOPING FLOW IN VERTICAL DUCTS (CS3)

6.1 Introduction

In the previous chapter, the results from the experiment work on mixed convection heat transfer for hydrodynamically developed and thermally developing flow in horizontal ducts with radiation effects was presented. In this chapter, the results for experiments performed to investigate radiation effects on mixed convection heat transfer for thermally developing airflow in a vertical duct is presented. The investigation covers the Reynolds number range from Re = 800 to 2900, heat flux from 256 W/m^2 to 863 W/m^2, hot wall temperature from 27 ^{o}C to 100 ^{o}C, aspect ratios 1 & 0.5 and the emissivity of internal walls: 0.05 and 0.85. Flow visualization was conducted to observe the flow patterns within the ducts and the effect of surface temperature along the walls studied to investigate the local Nusselt number variation. The results show that flow condition and radiation significantly affect the total Nusselt number.

6.2 Thermally Developing Flow in Vertical Ducts

Figures 6.1 and 6.2 show the schematic diagram of a vertical duct with square (AR = 1) and rectangular (AR = 0.5) test sections that were considered for the analysis of a thermally developing flow. The test section is made of two isothermal hot walls and two adiabatic walls, fixed vertically.

In this vertical orientation, the adiabatic walls were named side A and side B instead of top and bottom walls as was done in the horizontal orientation of the test section discussed earlier. The isothermal hot wall incorporates an electrical heater and isothermal cold wall is a milled-channel for circulating constant temperature water.

The detailed description of test section was described in Chapter 3 and the range of parameters used in this experiment was given in Table 3.3.

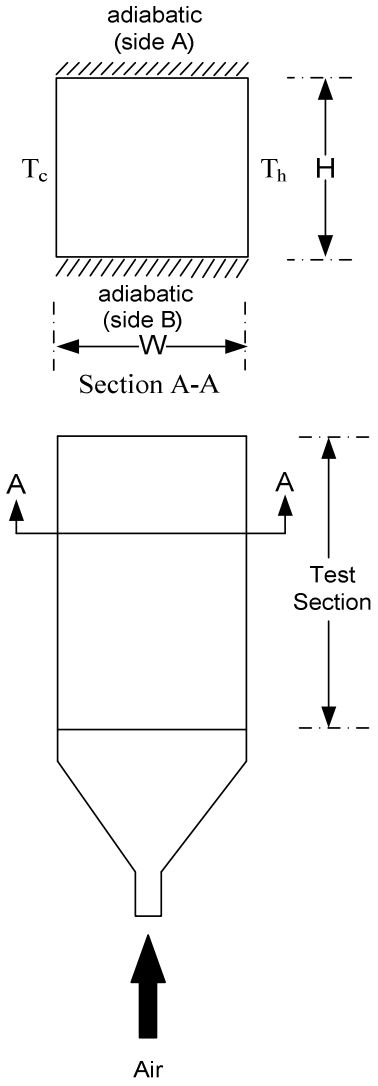

Figure 6.1 Schematic of the vertical square test section.

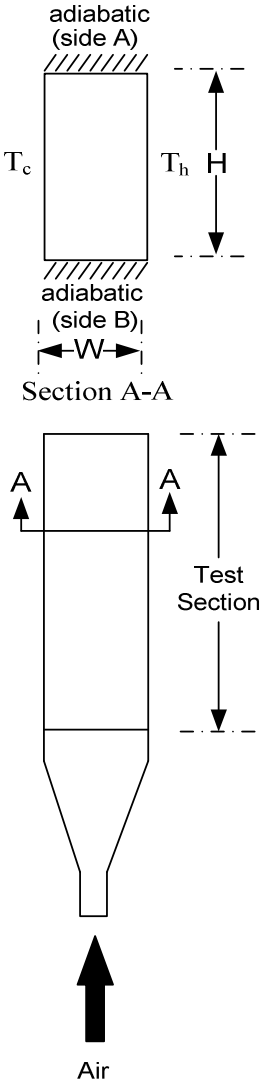

Figure 6.2 Schematic of the vertical rectangular test section.

6.3 Surface Temperature Distribution along the Duct Walls

6.3.1 Surface Temperature Distribution on the Heated Wall

Figures 6.3 and 6.4 show the variation of surface temperature on the wall as a function of the vertical distance from the inlet of the test section to the exit of the test

section for different wall heat flux values with a fixed Reynolds number of 1788. The temperature variation along the heated wall surface is very marginal in the vertical orientation owing to the shorter length of test section.

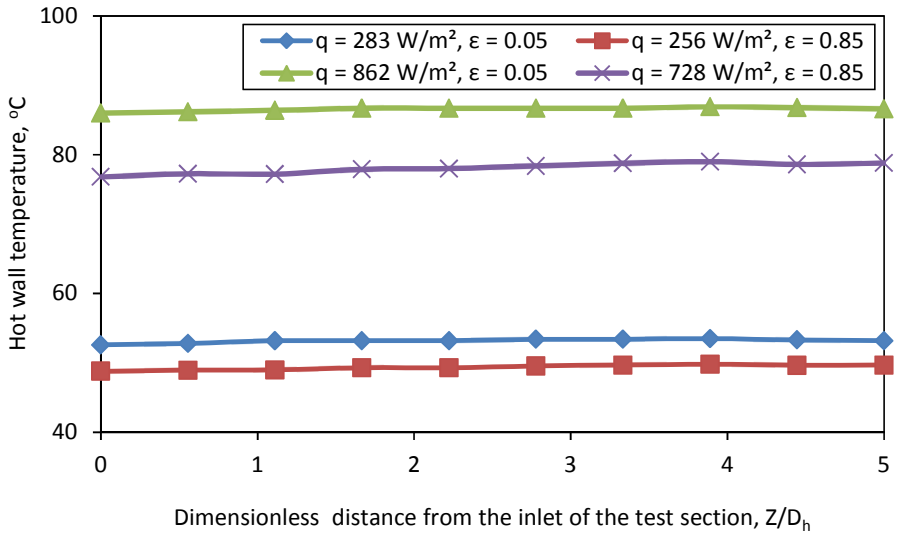

Figure 6.3 Variation of the surface temperature on the heated wall (Re = 1788, AR = 1).

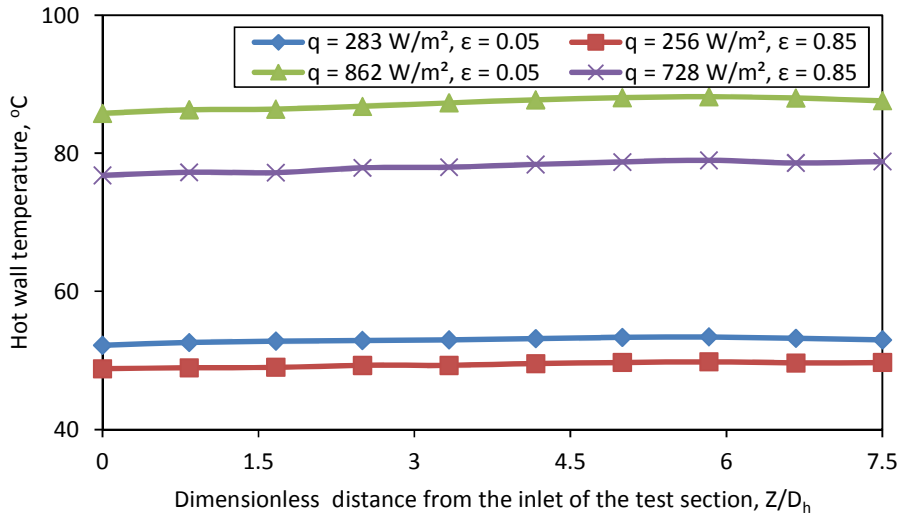

Figure 6.4 Variation of the surface temperature on the heated wall (Re = 1788, AR = 0.5).

The above graph shows that the square (AR = 1) test section had the highest heated wall average surface temperature of 86.6 ^{o}C (Fig 6.3) for highly polished walls (ε = 0.05) with high heat flux q = 862 W/m², whereas for the duct with black surface (ε = 0.85) the surface temperature is 78.1 ^{o}C with high heat flux q = 728 W/m². The average temperature between the two surfaces differed by about 8.5 ^{o}C. Figure 6.4 shows the rectangular test section highest heated wall average surface temperature of 87.2 ^{o}C obtained for the case of a duct having highly polished walls (ε = 0.05) with high heat flux q = 862 W/m² and 78.4 ^{o}C is obtained for the case of a duct having black surface walls (ε = 0. 85) with high heat flux q = 728 W/m². The average temperature between the two surface differed by about 8.8 ^{o}C. It can be observed that the polished heated wall surface temperature is 9.8 % and 10.0 % higher for the case of square and rectangular duct respectively. Figure 6.3 and 6.4 show that the hot wall temperature increases gradually towards the exit and it is significant for high heat flux, the difference is more for heat flux q = 728 W/m^2. For black body (q = 728 W/m^2) the accumulated temperature towards the exit higher due to strong black body absorption effect.

6.3.2 Surface Temperature Distribution on the Cold Wall

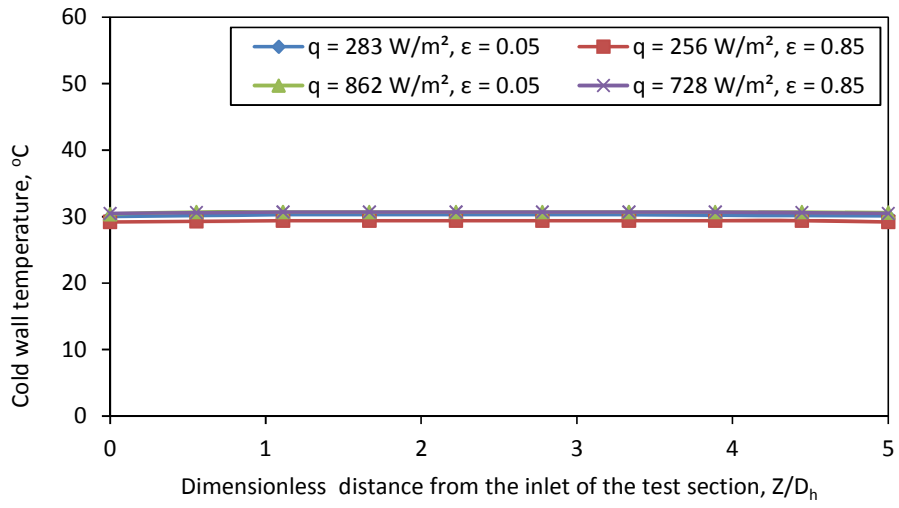

Figure 6.5 Variation of the surface temperature on the cold wall (Re = 1788, AR = 1).

Figures 6.5 and 6.6 show that the variation of the surface temperature on the cold wall. The temperature of the cold wall is always maintained at the inlet air temperature for all cases.

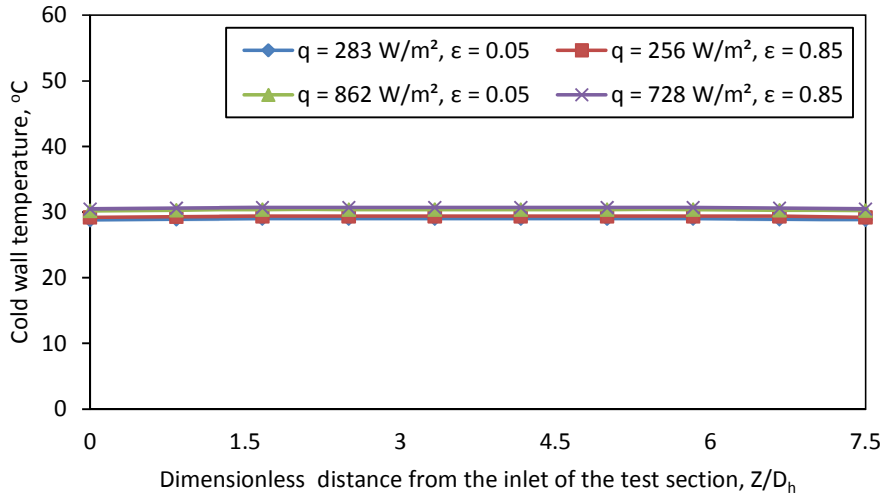

Figure 6.6 Variation of the surface temperature on the cold wall (Re = 1788, AR =0.5).

6.3.3 Surface Temperature Distribution on the Side Walls

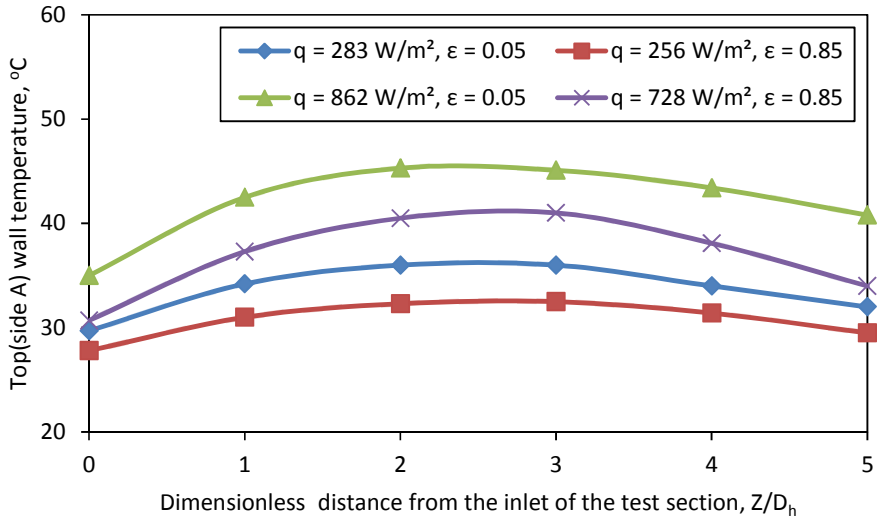

Figure 6.7 Variation of the surface temperature on the adiabatic (side A) wall (Re = 1788, AR =1).

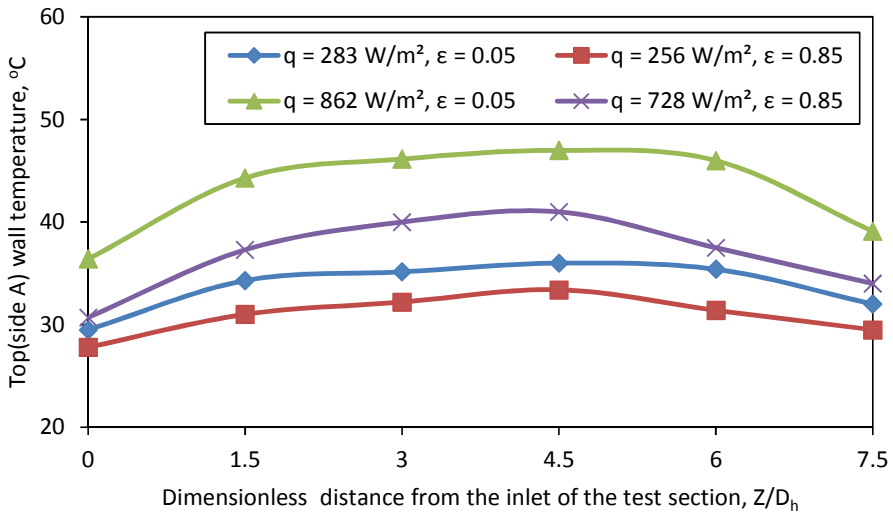

Figure 6.8 Variation of the surface temperature on the adiabatic (side A) wall (Re = 1788, AR =0.5).

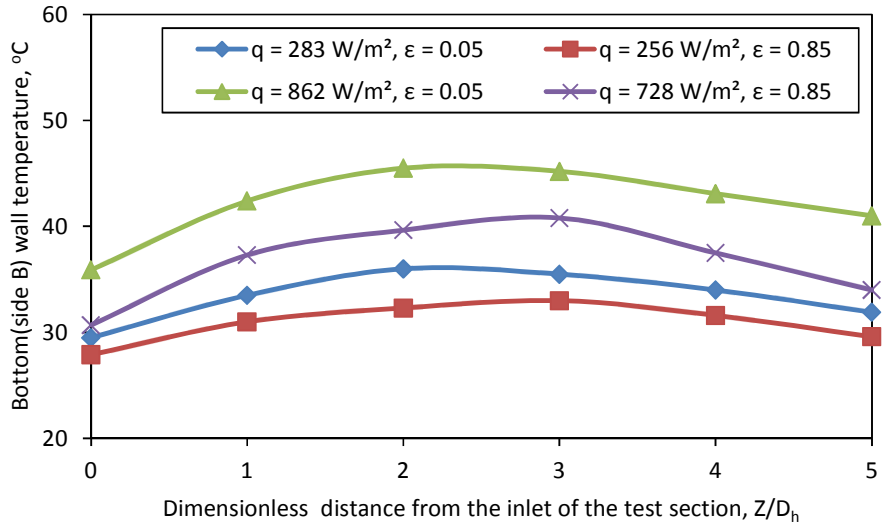

Figure 6.9 Variation of the surface temperature on the adiabatic (side B) wall (Re = 1788, AR =1).

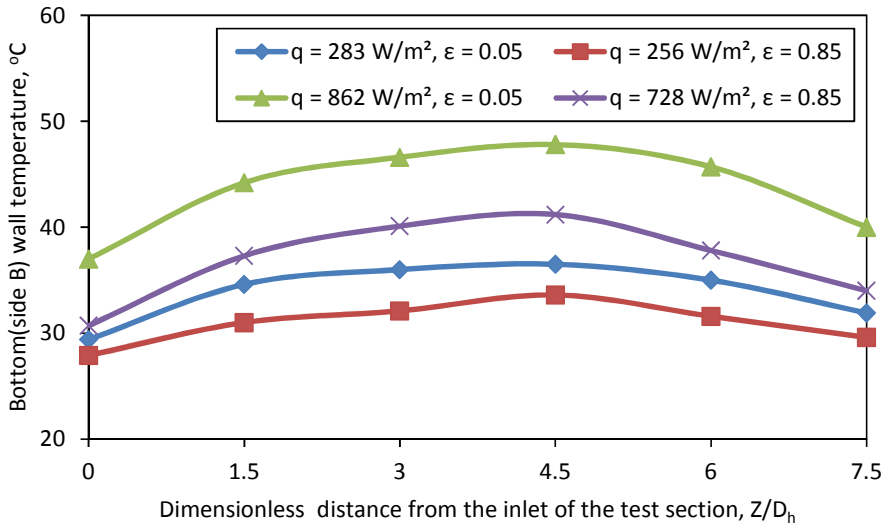

Figure 6.10 Variation of the surface temperature on the adiabatic (side B) wall (Re = 1788, AR =0.5).

Table 6.1 Surface temperature comparison of side wall A and B for Reynolds number for 1788

Description	Polished Surface (q = 862 W/m²)		Black Surface (q = 728 W/m²)	
	Aspect Ratio (AR = 1)	Aspect ratio (AR = 0.5)	Aspect Ratio (AR = 1)	Aspect ratio (AR = 0.5)
Adiabatic (Side A) Wall	42.0	43.2	36.5	36.9
Adiabatic (Side B) Wall	42.2	43.6	36.7	36.8

Figures 6.7 to 6.10 show the variation of side walls temperature as a function of the horizontal distance. Table 6.1 presents the variation of the average temperature of side wall A and B for a duct of square and rectangle cross section (A R = 1 & 0.5) with high heat flux. It can be clearly seen that the side wall average temperature was higher for polished surface compared to the black surface. When considering the aspect ratio, the rectangular test section side walls temperature was higher compared to the square test section.

6.4 Combined Forced and Natural Convection Heat Transfer

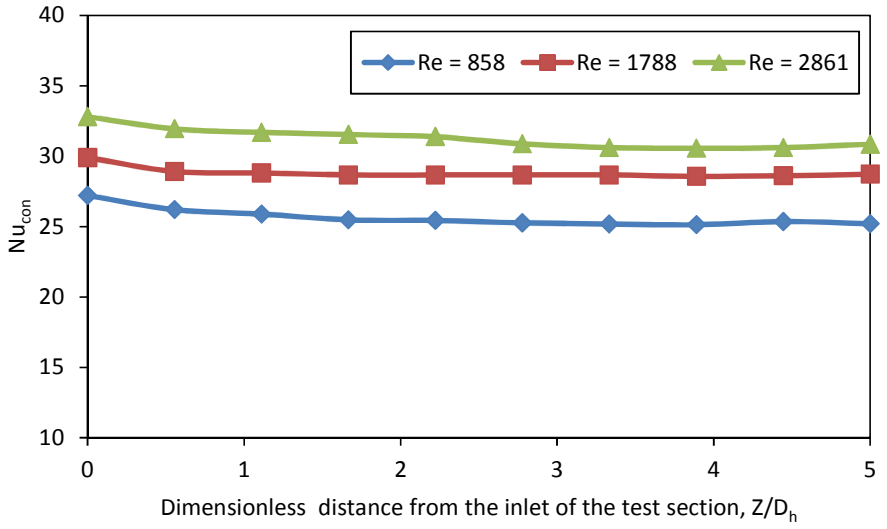

Figure 6.11 Effect of Reynolds number on the average convective Nusselt numberat the heated wall (q = 862 W/m², AR = 1, ε = 0.05).

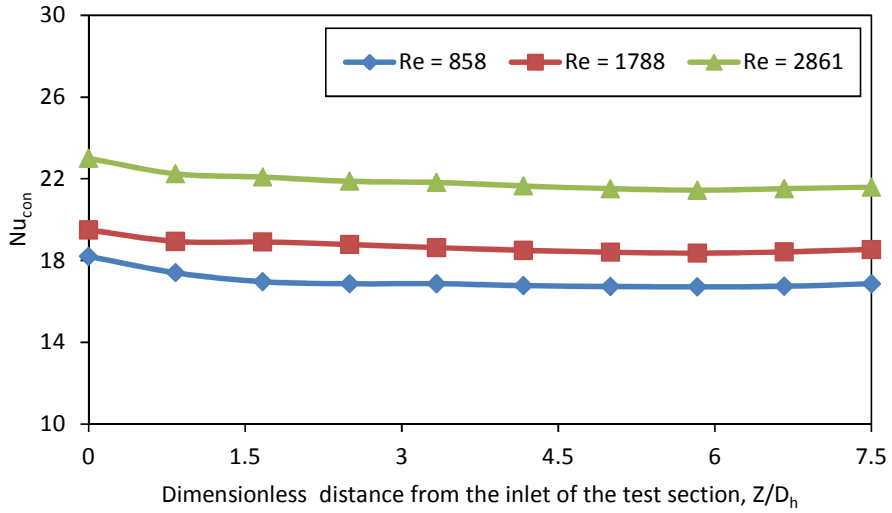

Figure 6.12 Effect of Reynolds number on the average convective Nusselt number at the heated wall (q = 862 W/m², AR = 0.5, ε = 0.05).

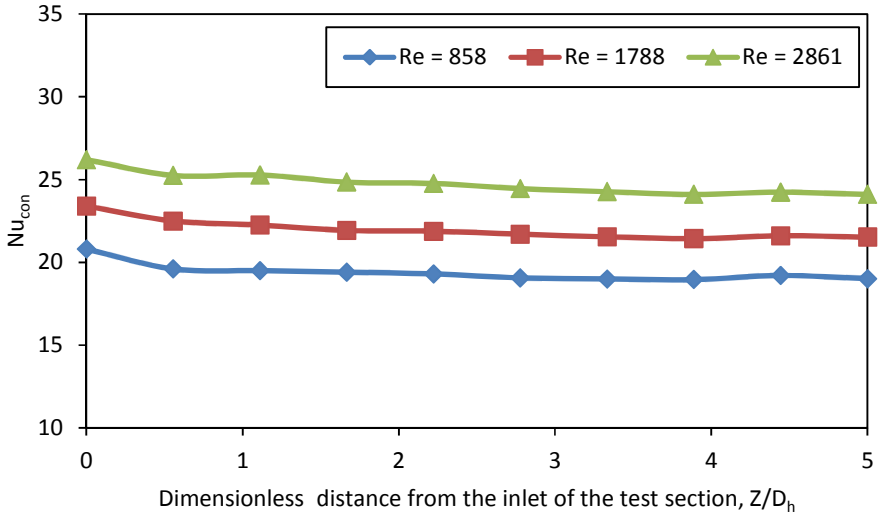

Figure 6.13 Effect of Reynolds number on the average convective Nusselt number at the heated wall (q = 728 W/m², AR = 1, ε = 0.85).

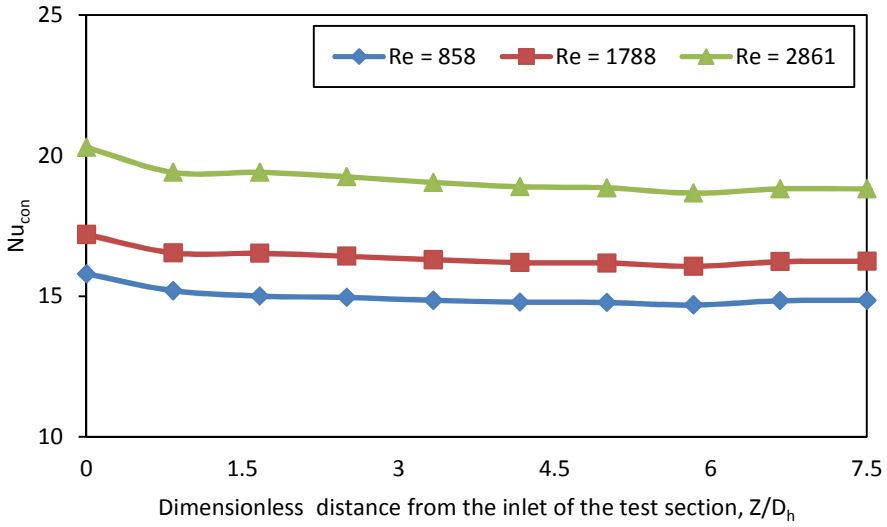

Figure 6.14 Effect of Reynolds number on the average convective Nusselt number at the heated wall (q = 728 W/m², AR = 0.5, ε = 0.85).

The effect of Reynolds Number on the local average convective Nusselt number with horizontal distance from the inlet of the test section to the exit is shown for selected runs in figures 6.11 to 6.14. The result shows that the Nusselt number value is high for higher Reynolds number than for the low Reynolds number. The Nusselt number value is high near the inlet of the test section, then gradually decreases towards the

exit of the duct. The rate of Nusselt number drop near the inlet for all the cases were found to be in the range of 1 to 2 %.

Figures 6.11 and 6.12 show the Nusselt number for polished (ε = 0.05) surface with heat flux q = 862 W/m². In this case the square test section average convective Nusselt number was found to be 25.6 and 31.3 for the case of low (Re = 858) and high (Re = 2861) Reynolds number. The average convective Nusselt number is 18.2 % higher for higher Reynolds number. The rectangular test section average convective Nusselt number was found to be 17 and 21.9 for the case of low (Re = 858) and high (Re = 2861) Reynolds number respectively. The average convective Nusselt number is 22.3 % higher for higher Reynolds numbers. Similarly Figures 6.13 and 6.14 show the effect of Reynolds number on the Nusselt number for black (ε = 0.85) surface with heat flux q = 728 W/m². The average convective Nusselt number is 22.3 % and 21.4 % higher for higher Reynolds numbers for the case of aspect ratio 1 and 0.5, respectively.

Normally, parts of the fluid having higher temperatures move upward due to the density gradient caused by natural convection effect. The buoyant flow and airflow move together in an upward direction to give significant effect of heat transfer rate. Due to this, the accumulation of heat flow on the side walls is very less compared to horizontal duct. For constant heat flux and high Reynolds number, the average convective Nusselt values are higher for a shorter test section (small height). The forced convection domination on the heat transfer process has little effect of buoyancy force for high Reynolds number. However, for the same heat flux, the natural convection effects are found to dominate the heat transfer process with large effect of buoyancy force for low Reynolds number flows.

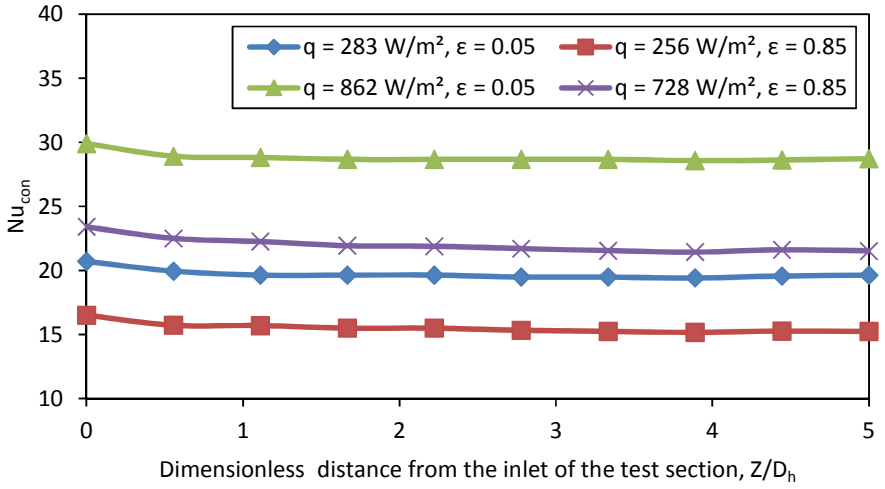

Figure 6.15 Effect of surface emissivity on the average convective Nusselt number at the heated wall (Re = 1788, AR =1).

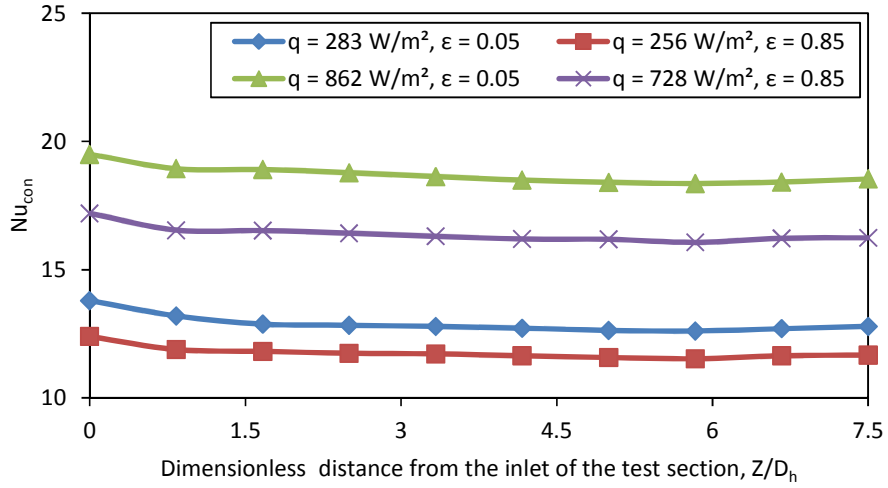

Figure 6.16 Effect of surface emissivity on the average convective Nusselt number at the heated wall (Re = 1788, AR =0.5).

Figures 6.15 and 6.16 show the effect of emissivity on the average convective Nusselt number at the heated wall for a duct of square and rectangle cross section with different wall emissivities for low and high heat flux applied to one of the vertical walls. Considering the effect of emissivity, the average convective Nusselt number for the square test section with high heat flux was found to be 28.8 and 22.0 for polished and black surface respectively. The average convective Nusselt number

between the polished and black surface differed by about 23.6 %.Similarly for the rectangular test section, the average convective Nusselt number for high heat flux was found to be 18.7 and 16.4 for the case of polished and black surfaces respectively. The average convective Nusselt number between the polished and black surface differed by about 12.3 %. It is found that the convective Nusselt number is higher for highly polished surface wall surface than a black surface; the same trend was observed for low heat flux cases also. It can be observed that generally the convective Nusselt number is higher for weak radiation (polished surface) than strong radiation (black surface). The above trend also indicates that the effects due to surface emissivity is independent from the flow, as air is a non-participating medium as far as radiation is concerned.

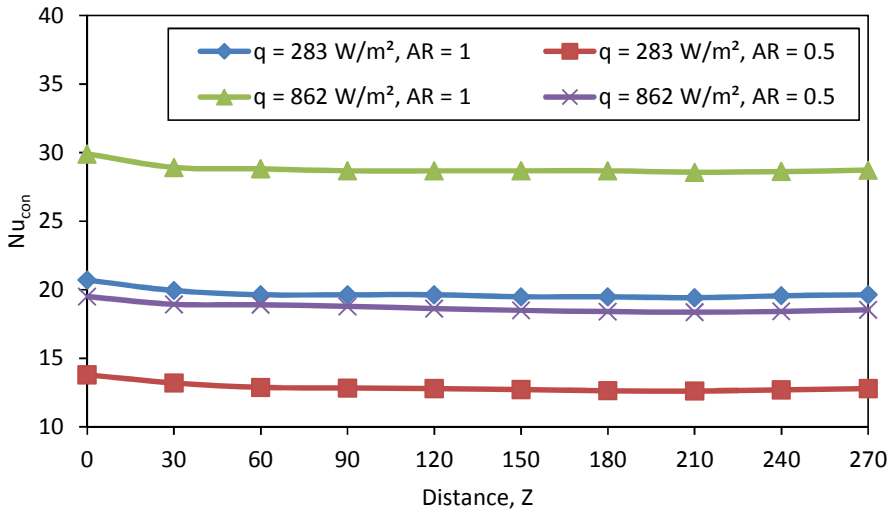

Figure 6.17 Effect of aspect ratio on the average convective Nusselt number at the heated wall (Re = 1788, ε = 0.05).

Figures 6.17 and 6.18 show the effect of aspect ratio on the convective Nusselt number at the heated wall for aspect ratios 1 and 0.5. The width between the two adiabatic side walls is fixed for both aspect ratios; the higher aspect ratio shows larger distance between the hot and cold walls. Higher aspect ratio provides more duct volume and allows more air inside the duct. Hence, the fluid with higher

temperature moves vertically upward due to the density gradient caused by natural convection effect, both conditions help to improve the convection and significantly enhance heat transfer. For the lower aspect ratio, as the walls are closer to the hot wall, the heat transfer rate is low compared to the higher aspect ratio duct.

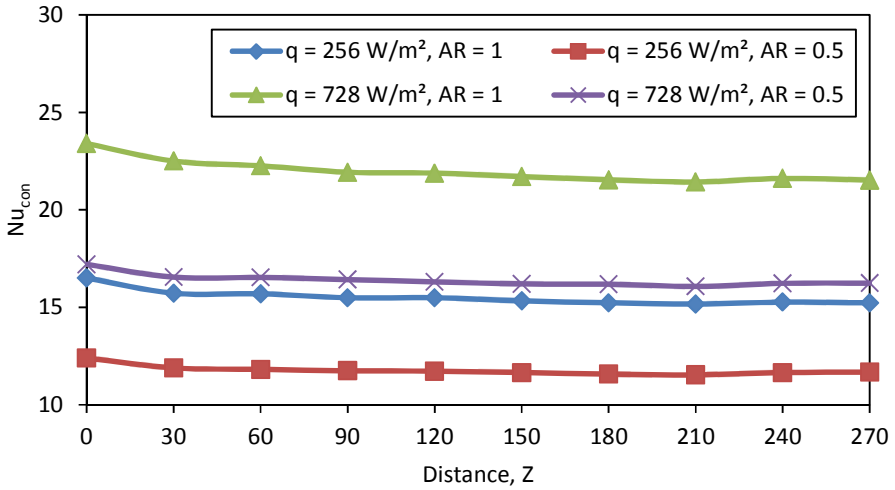

Figure 6.18 Effect of aspect ratio on the average convective Nusselt number at the heated wall (Re =1788, ε = 0.85).

Considering the effect of aspect ratio, the polished wall surface average convective Nusselt number is 35.1 % higher for aspect ratio 1. Similarly the black surface average convective Nusselt number is 25.4 % higher for aspect ratio 1. It was found that the aspect ratio of 1 has a higher convective Nusselt number compared to aspect ratio 0.5, but the phenomena of heat removal rate is the same for all aspect ratios.

6.5 Radiation Heat Transfer

Figures 6.19 to 6.22 and Table 6.2 show the effect of Reynolds number on the average radiative Nusselt number for the case of low and high emissive wall for aspect ratio 1 and 0.5, respectively. It can be seen that the patterns of Nusselt number for different Reynolds numbers are comparable to the case of low and high surface emissivity. The surface radiation heat transfer has no direct interaction with the convective flow. The side walls are heated by radiation heat transfer from the heated

wall. In this case the heated air starts to move upwards from the entrance of the test section, then continuously moves upward in the vertical direction, due to that radiation heat transfer to the side walls is very less.

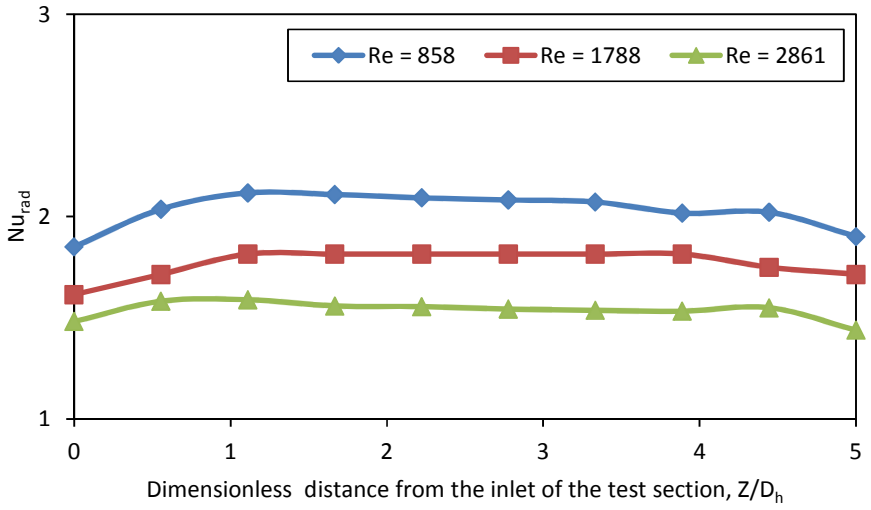

Figure 6.19 Effect of Reynolds number on the average radiative Nusselt number at the heated wall (q = 862 W/m², ε = 0.05, AR = 1).

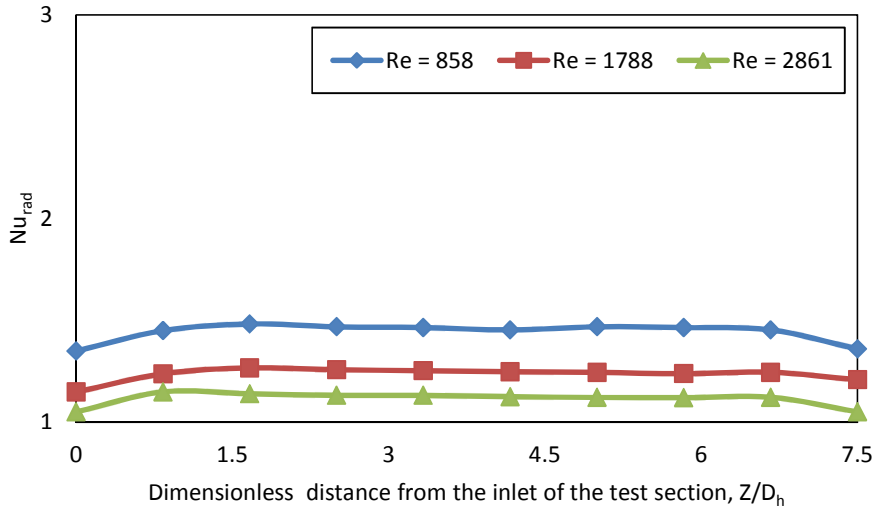

Figure 6.20 Effect of Reynolds number on the average radiative Nusselt number at the heated wall (q = 862 W/m², ε = 0.05, AR = 0.5).

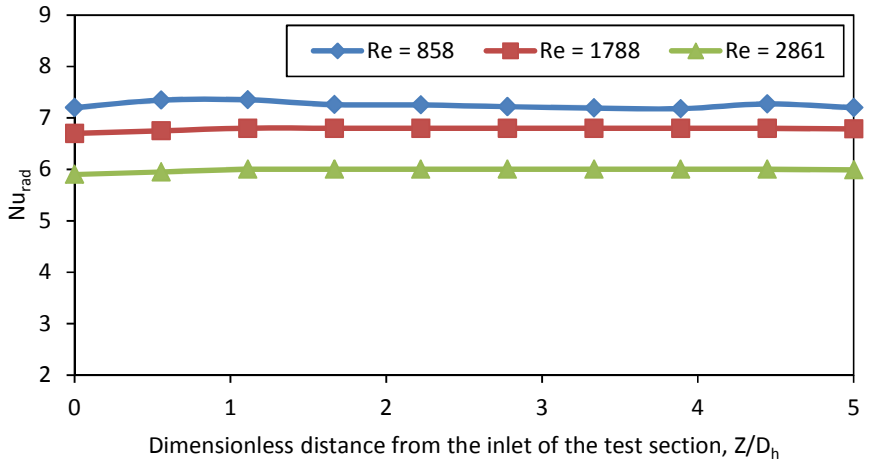

Figure 6.21 Effect of Reynolds number on the average radiative Nusselt number at the heated wall (q = 728 W/m², ε = 0.85, AR = 1).

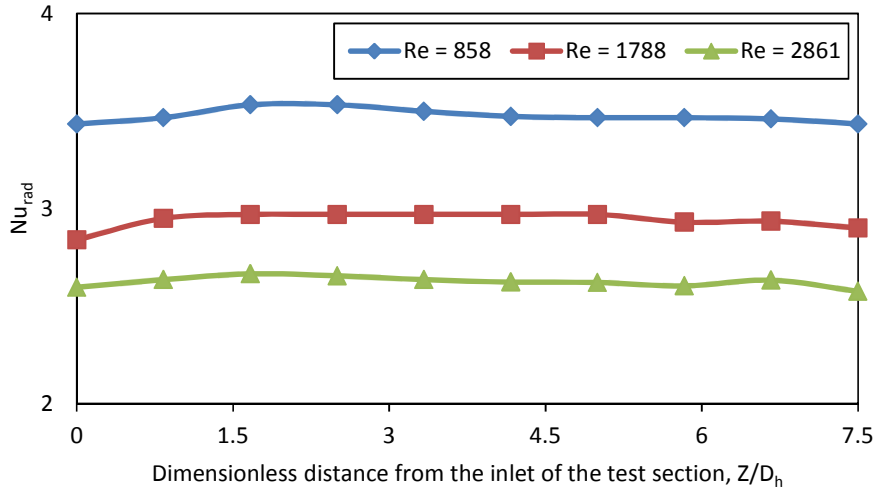

Figure 6.22 Effect of Reynolds number on the average radiative Nusselt number at the heated wall (q = 728 W/m², ε = 0.85, AR = 0.5).

Figures 6.19 and 6.20 show the effect of Reynolds number on the average radiative Nusselt number for polished surface (ε = 0.05) with heat flux q = 862 W/m². In this case the square duct average radiative Nusselt number between the low (Re = 858) and high (Re = 2861) Reynolds number differed by about 25.0 %. Similarly the rectangular duct average radiative Nusselt number between the low (Re = 858) and high (Re = 2861) Reynolds number differed by about 21.4 %. Figures 6.21 and 6.22 show the effect of Reynolds number on the average radiative Nusselt number for

black surface (ε = 0.85) with a heat flux q = 728 W/m². In this case, the average radiative Nusselt number difference between the square and rectangular test section was found to be 16.6 % and 25.7 % for low (Re = 858) and high (Re = 2861) Reynolds number respectively.

Table 6.2 Effect of Reynolds number on the average radiative Nusselt number at heated wall

Description	Polished Surface (q = 862 W/m²)			Black Surface (q = 728 W/m²)		
	Reynolds Number			Reynolds Number		
	858	1788	2861	858	1788	2861
Aspect Ratio 1	2.0	1.7	1.5	7.2	6.8	6.0
Aspect Ratio 0.5	1.4	1.2	1.1	3.5	2.9	2.6

For constant heat flux, the low Reynolds number average radiative Nusselt numbers are always higher than the high Reynolds number average radiative Nusselt numbers. The radiative heat flux remains constant for most of the part of the test section, except at the inlet and outlet where some of the radiative energy is lost to the surroundings.

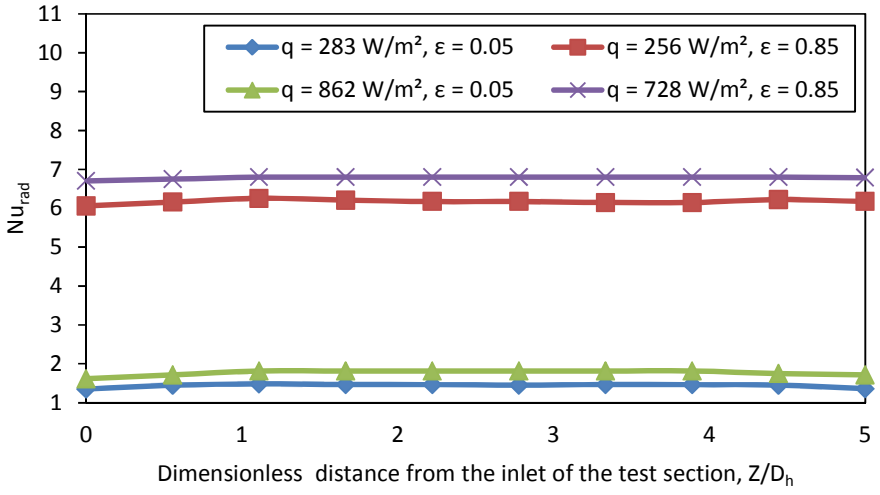

Figure 6.23 Effect of surface emissivity on the average radiative Nusselt number at the heated wall (Re = 1788, AR =1).

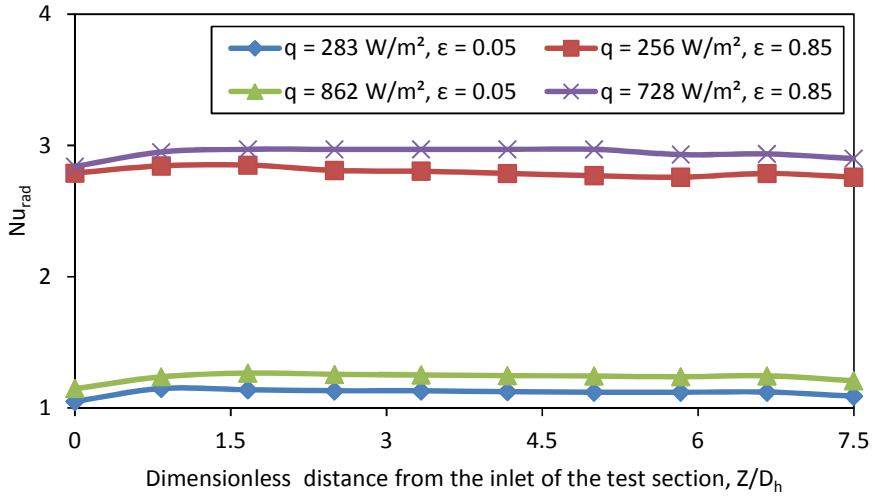

Figure 6.24 Effect of surface emissivity on the average radiative Nusselt number at the heated wall (Re = 1788, AR = 0.5).

The effect of surface emissivity on the average radiative Nusselt number at the heated wall for a duct of square and rectangle cross section (AR = 1 & 0.5) with different emissivity of low and high heat flux are shown in figure 6.23 and 6.24. The effect of emissivity, the square test section the average radiative Nusselt number for high heat flux was found to be 1.7 and 6.8 for the case of polished and black surface respectively (Fig 6.23). The black surface average radiative Nusselt number increases by 75 %. The average radiative Nusselt number for rectangular test section with high heat flux was found to be 1.2 and 2.9 for the case of polished and black surface respectively (Fig 6.24). For high heat flux, the average radiative Nusselt number between the black and polished surface differed by about 58.6 %.It is found that for a given wall heat flux, the radiative Nusselt number is higher for strong radiation than weak radiation; the same trend is observed for both cases of square and rectangular duct.

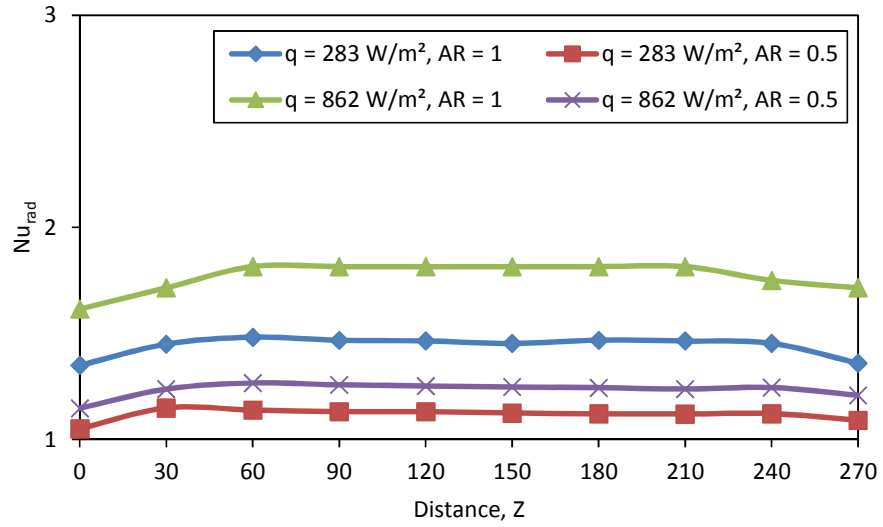

Figure 6.25 Effect of aspect ratio on the average radiative Nusselt number at the heated wall (Re = 1788, ε = 0.05).

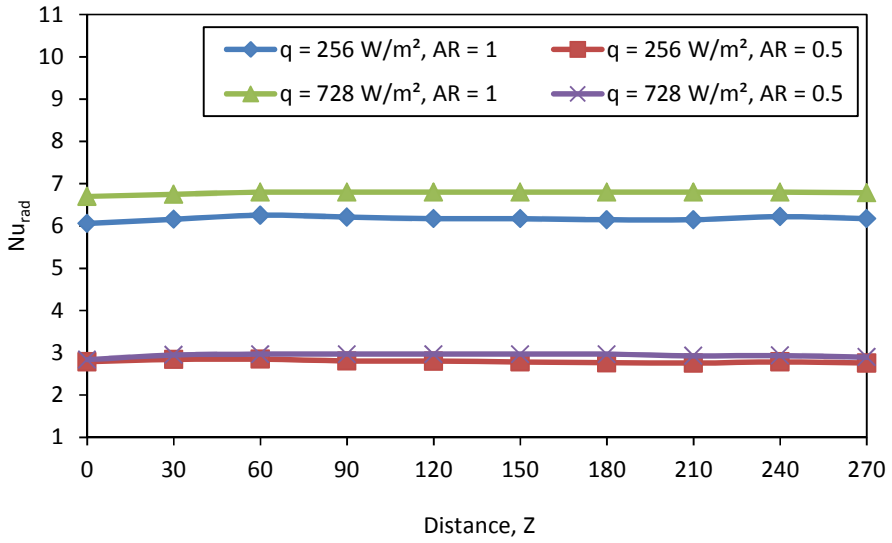

Figure 6.26 Effect of aspect ratio on the average radiative Nusselt number at the heated wall (Re = 1788, ε = 0.85).

In this case, the amount of heat that is transferred from the side walls to air depends on the radiative energy from heated wall. The lower aspect ratio with a higher wall temperature contributes significantly to radiation heat transfer. This is because of the cavity effect that dominates as the aspect ratio decreases.

Figure 6.25 shows the average radiative Nusselt number for high heat flux (ε = 0.05) as 1.7 and 1.2 for the case of square and rectangular test section respectively. The average radiative Nusselt number between the square and rectangular test section differed by about 29.4 %. Similarly, Figure 6.26 shows that the average radiative Nusselt number for high heat flux (ε = 0.85) as 6.8 and 2.9 for the case of square and rectangular test section respectively. The average radiative Nusselt number between the square and rectangular test section differed by about 57.3 %. The specific heat flux and fixed Reynolds number (Re = 1788), radiative Nusselt number values of aspect ratio of 1 is found to be higher than those of aspect ratio of 0.5 for most part of the duct.

6.6 Combined Convection and Radiation Effect

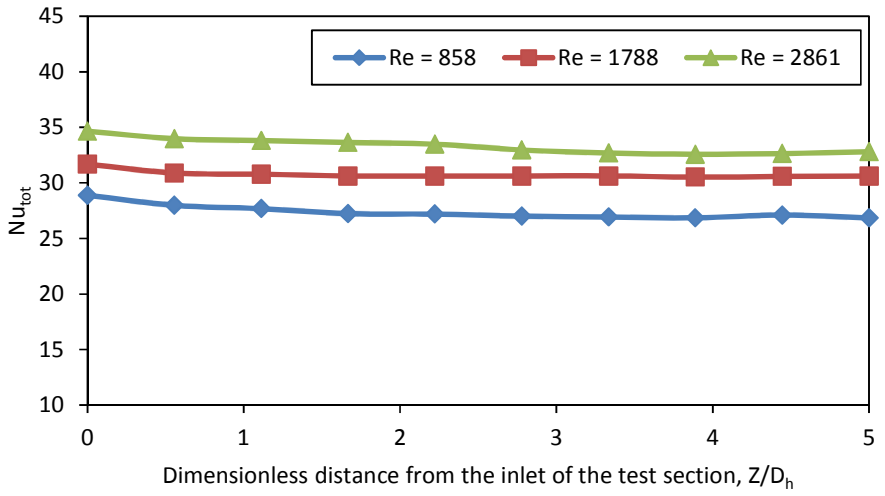

Figure 6.27 Effect of Reynolds number on the average total Nusselt number at the heated wall (q = 862 W/m², ε = 0.05, AR = 1).

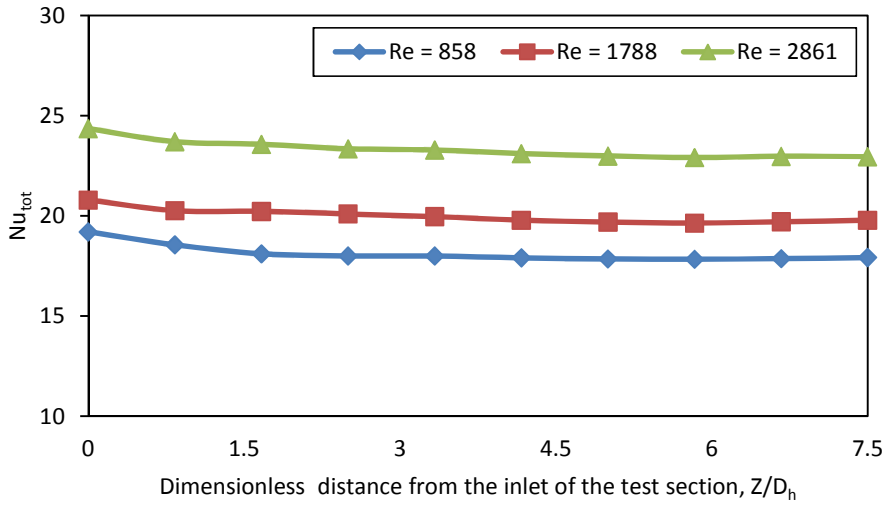

Figure 6.28 Effect of Reynolds number on the average total Nusselt number at the heated wall (q = 862 W/m², ε = 0.05, AR = 0.5).

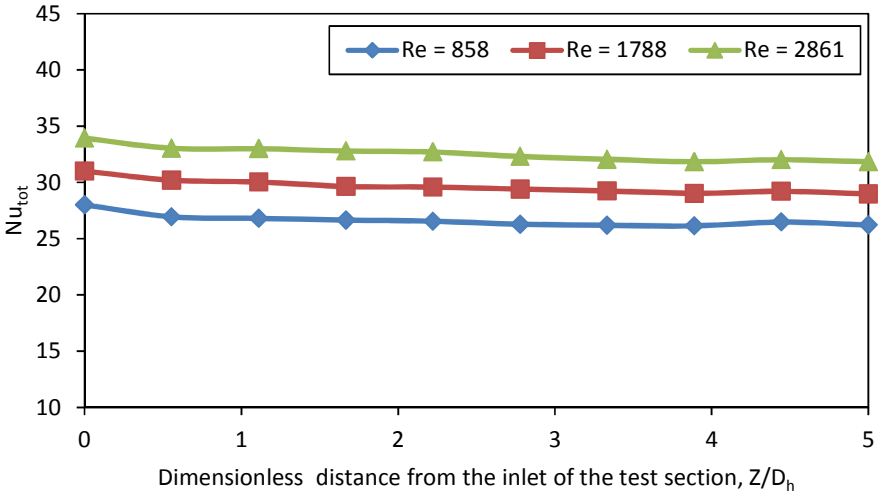

Figure 6.29 Effect of Reynolds number on the average total Nusselt number at the heated wall (q = 728 W/m², ε = 0.85, AR = 1).

Figures 6.27 to 6.30 and Table 6.3 present the effect of Reynolds number on the average total Nusselt number for the case of low and high emissive wall for aspect ratio 1 and 0.5, respectively. It can be observed that the increase in Nusselt number is only marginal considering about twofold increase in Reynolds number. It can also be seen that Nusselt number is of the same order of magnitude for both the polished and black surfaces.

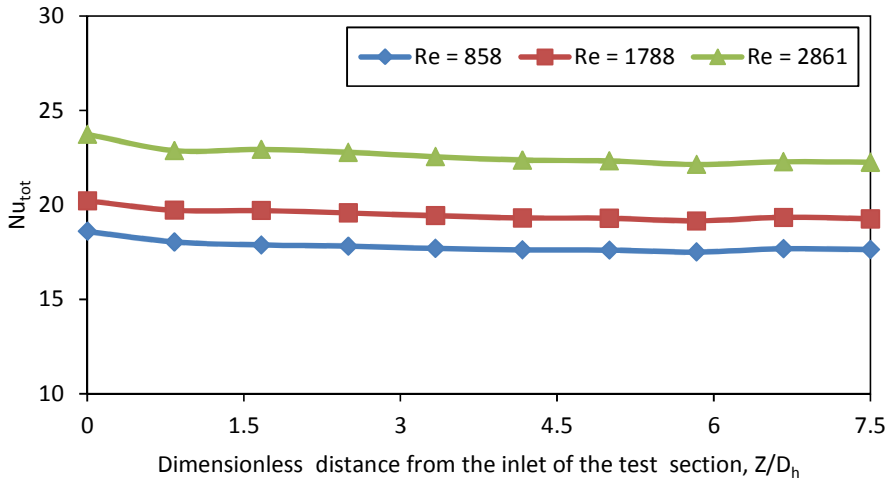

Figure 6.30 Effect of Reynolds number on the average total Nusselt number at the heated wall (q = 728 W/m², ε = 0.85, AR = 0.5).

Table 6.3 Effect of Reynolds on the average total Nusselt number at heated wall

Description	Polished Surface (q = 862 W/m²)			Black Surface (q = 728 W/m²)		
	Reynolds Number			Reynolds Number		
	858	1788	2861	858	1788	2861
Aspect Ratio 1	27.4	30.8	33.3	26.6	29.6	32.6
Aspect Ratio 0.5	18.5	20.2	23.7	18.1	20.0	23.3

Figures 6.27 and 6.28 show that the effect of Reynolds number on the average total Nusselt number for polished surface (ε = 0.05) with heat flux q = 862 W/m^2. In this case, the effect of high Reynolds number (Re = 2861) on the average total Nusselt number rates are increases 17.8 % and 18.4 % for square and rectangular test section respectively. Figures 6.29 and 6.30 show the effect of Reynolds number on the average total Nusselt number for black surface (ε = 0.85) with a heat flux q = 728 W/m². The average total Nusselt number for the highest Reynolds number (Re = 2861) increases by 21.9 % and 22.3 % for square and rectangular test section respectively. For constant heat flux and high Reynolds number with higher aspect ratio the average total Nusselt numbers are higher. This was explained earlier in Section 6.4.

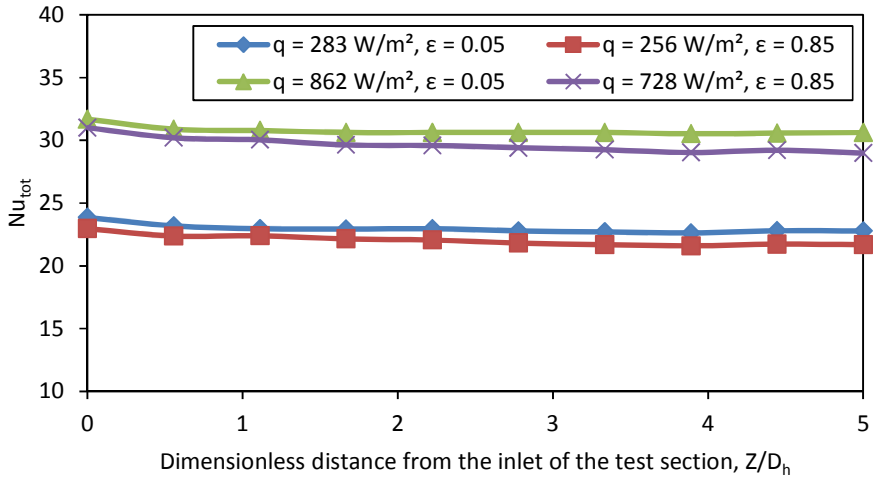

Figure 6.31 Effect of surface emissivity on the average total Nusselt number at the heated wall (Re = 1788, AR =1).

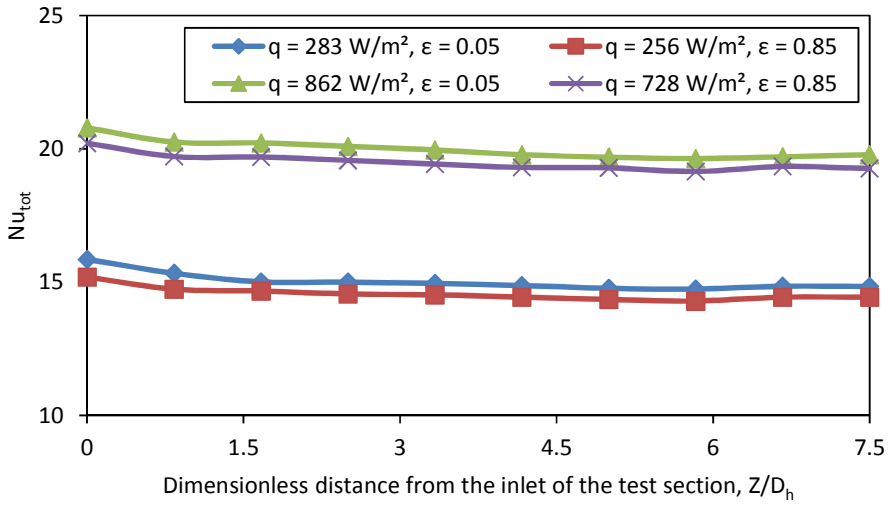

Figure 6.32 Effect of surface emissivity on the average total Nusselt number at the heated wall (Re = 1788, AR = 0.5).

Figures 6.31 and 6.32 show the effect of emissivity on the average total Nusselt number at heated wall with Reynolds number Re = 1788 for the case of square and rectangular test section. The above graphs show that the results for polished and black surface average total Nusselt number to be equal for low and high heat flux cases. The same trend was observed as in previous Chapters 4 and 5. The

contribution of convection and the radiation can be clearly seen when analyzing the heat transfer modes separately. In this vertical orientation, the contribution of convection heat transfer significantly affects the overall heat transfer enhancement.

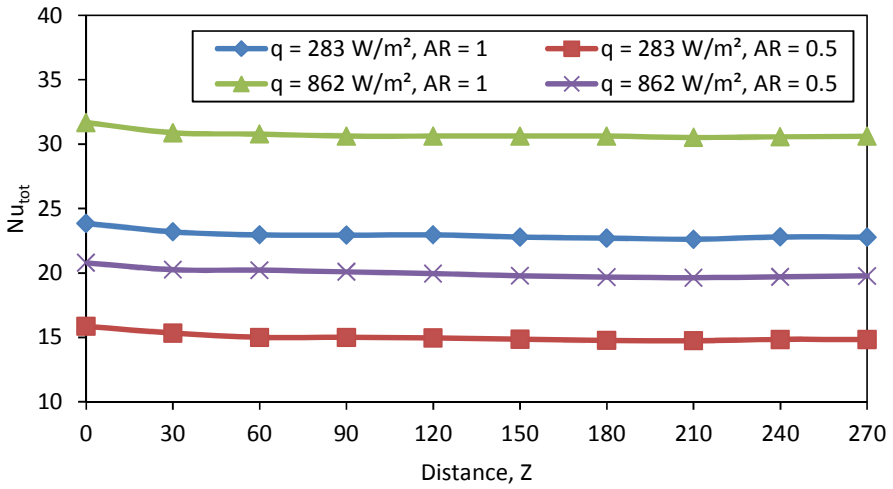

Figure 6.33 Effect of aspect ratio on the average total Nusselt number at the heated wall (Re = 1788, ε = 0.05).

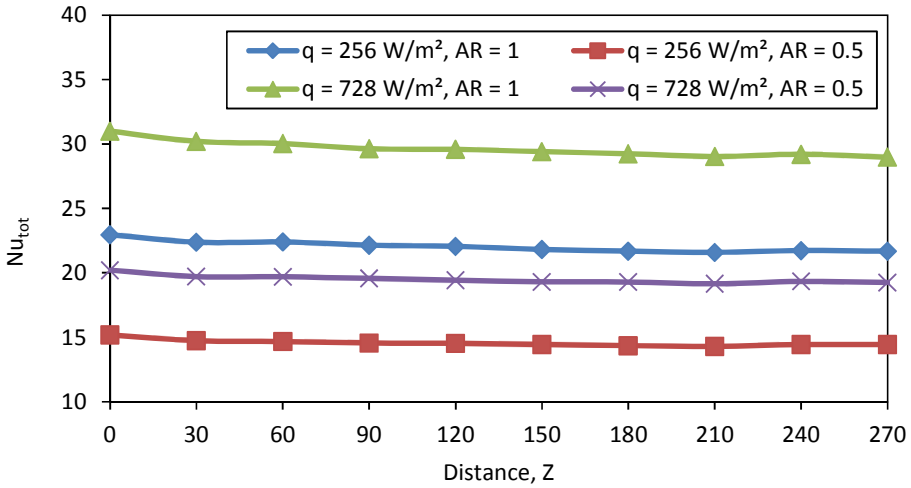

Figure 6.34 Effect of aspect ratio on the average total Nusselt number at the heated wall (Re = 1788, ε = 0.85).

In the present study, it was observed that the higher aspect ratio has higher values of total Nusselt number irrespective of the wall surface emissivity. This was described

in Section 6.4. Figure 6.33 shows that the effect of aspect ratio on the polished surface average total Nusselt number for high heat flux was found to be 28.8 and 18.7 for the case of square and rectangular test section respectively. The average total Nusselt number is 35.0 % higher for a square duct. Similarly, Figure 6.34 shows that the black surface average total Nusselt number for high heat flux to be 22.0 and 16.4 for the case of square and rectangular test section respectively. The average total Nusselt number rate is 25.4 % higher for square duct. The above trend was observed for the low heat flux heating for the vertical wall.

6.7 Ratio of Convective and Radiative Nusselt Number to Total Nusselt Number

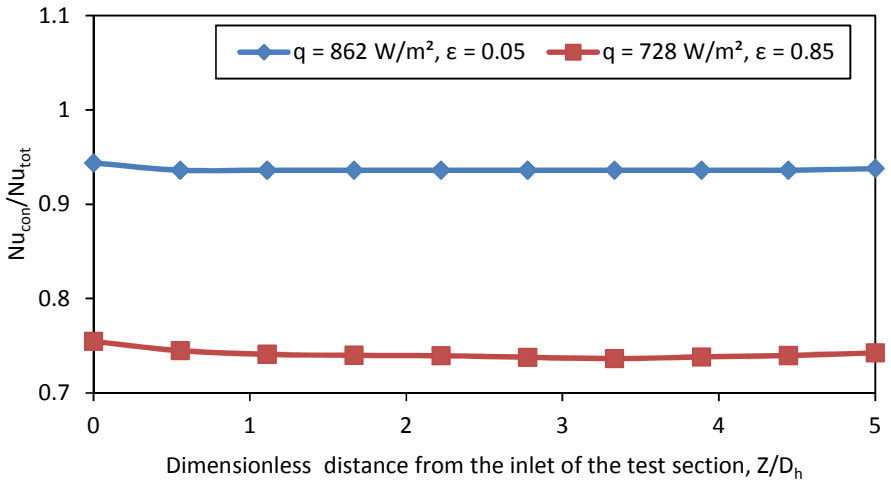

Figure 6.35 Ratio of convective to total Nusselt number (Re = 1788, AR = 1).

Considering the ratio of convective and radiative Nusselt numbers to the total Nusslet number, it can be observed that the convective ratio is higher than radiative ratio for the all the cases. However, the ratio also depends on the surface emissivity of the wall surfaces.

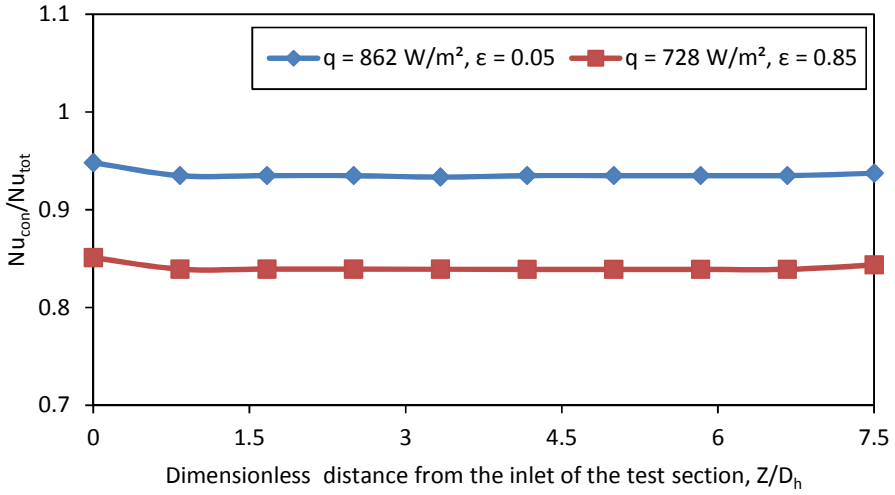

Figure 6.36 Ratio of convective to total Nusselt number (Re = 1788, AR = 0.5).

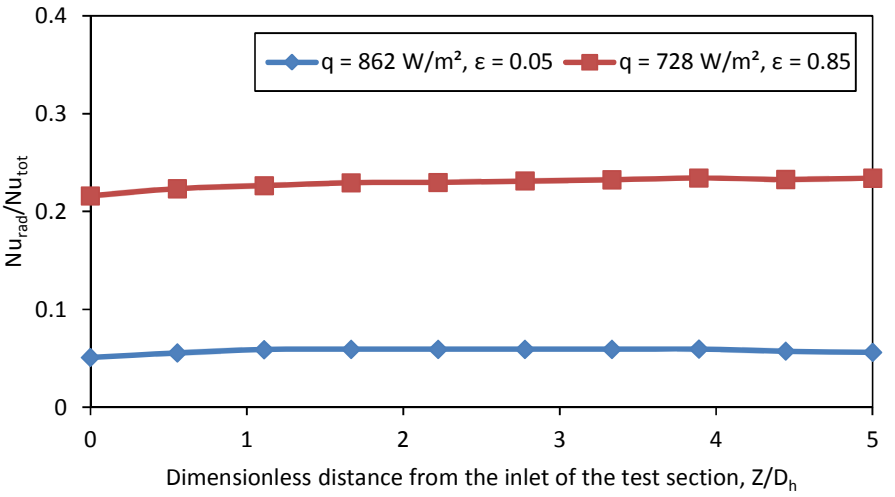

Figure 6.37 Ratio of radiative to total Nusselt number (Re = 1788, AR = 1).

Figures 6.35 and 6.36 show the ratio of convective to the total Nusselt number for the case of aspect ratio 1 and 0.5. In this case the percentage of square duct convective Nusselt value is higher for weak radiation (94 %) compared to strong radiation (74 %). Similarly the percentage of rectangular duct convective value is higher for weak radiation (94 %) compared to strong radiation (84 %). It can be observed that the weak radiation has higher values of convective Nusselt number irrespective of aspect ratio. Figures 6.37 and 6.38 show the ratio of radiative to the total Nusselt number for

the case of aspect ratio 1 and 0.5. In this case the percentage of square duct radiative Nusselt number is higher for strong radiation (25%) compared to weak radiation (6 %). Similarly the percentage of rectangular duct radiative Nusselt number is higher for strong radiation (15 %) compare to weak radiation (6 %). These experimentally obtained results show that the percentage of convection is higher for weak radiation and the percentage of radiation is higher for strong radiation.

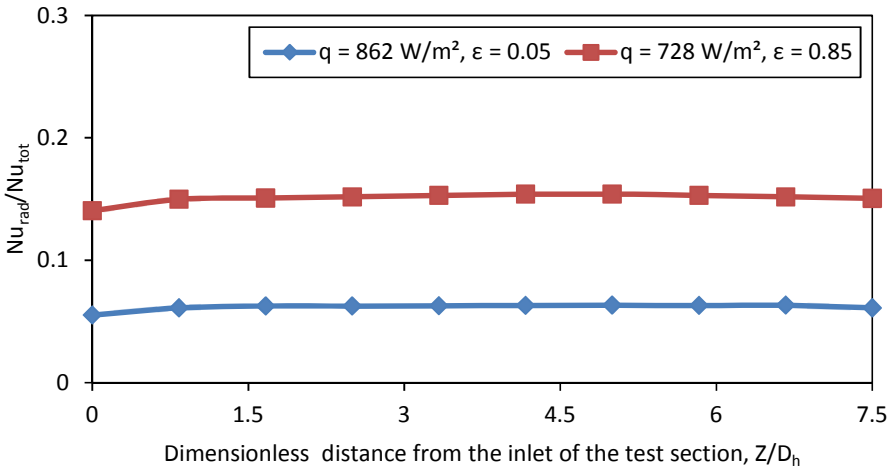

Figure 6.38 Ratio of radiative to total Nusselt number (Re = 1788, AR = 0.5).

Finally analyzing the convective and radiative heat transfer, the percentage of convection is higher for weak radiation compared to strong radiation and the percentage of radiation is higher for strong radiation compared to weak radiation conditions. When analyzing the heat flux separately with aspect ratio 1 and 0.5, the ratio of convective and radiative to the total Nusselt numbers for both cases are found to be the same.

6.8 Natural Convection Flow Visualization

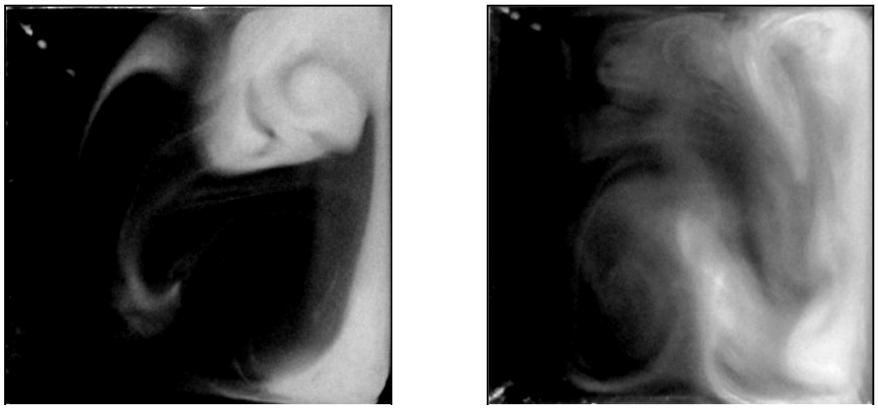

(a) (b)

Figure 6.39 Natural convection flow structure within the square ducts.

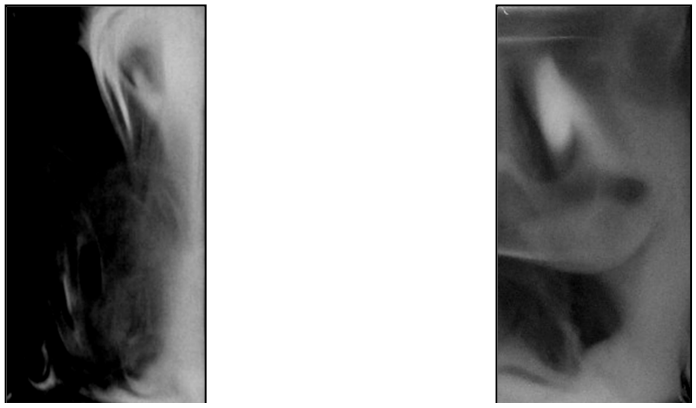

(a) (b)

Figure 6.40 Natural convection flow structure within the rectangular ducts.

Figures 6.39 (a) and (b) shows the flow visualization photographs for natural convection flow structure for the square duct with polished (q = 862 w/m², ε = 0.05) and black (q = 728 w/m², ε = 0.85) surface respectively. Similarly, figures 6.40 (a) and (b) show the natural convection flow structure for the rectangular duct with polished (q = 862 w/m², ε = 0.05) and black (q = 728 w/m², ε = 0.85) surfaces respectively. Due to the effect of buoyancy force, flow moves upward to the vertical direction from the inlet of the test section to the exit. In this case, the lighter density

warmer fluid moves in the upward direction. It was observed that, the buoyant flow is faster for higher heat flux than lower heat flux.

6.9 Mixed Convection Flow Visualization

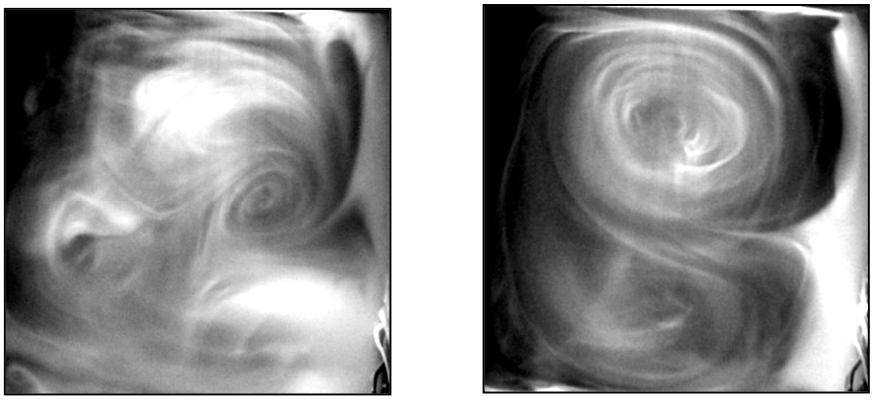

(a) (b)

Figure 6.41 Mixed convection flow structure within the square duct (Re = 858, ε = 0.05, AR = 1).

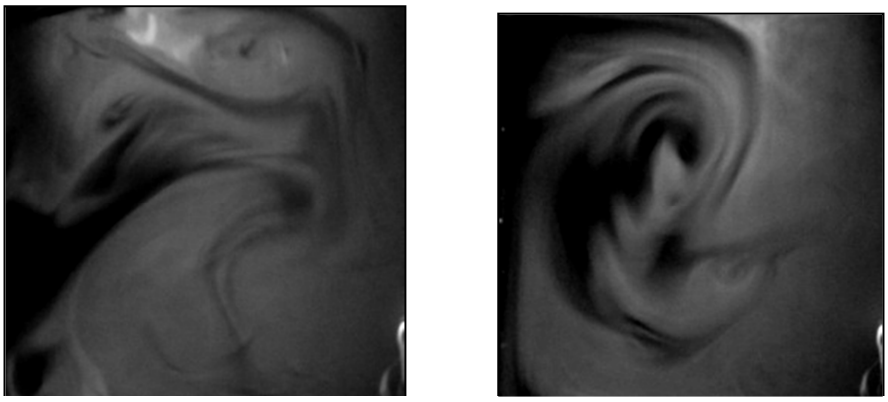

(a) (b)

Figure 6.42 Mixed convection flow structure within the square duct (Re = 858, ε = 0.85, AR = 1).

Figures 6.41 to 6.44 show mixed convection flow structure for thermally developing flow in a vertical square and rectangular duct for the case of low and high heat flux. Normally the flow is induced by buoyancy and the heated flow moves upward

direction. Due to the effect of buoyancy force, in the vertical duct, the heated airflow accumulates near the heated wall then, the accumulated flow motion continuously circulates and moves upward from the inlet of the test section to the exit. In this case the stream-wise velocity of the accumulated flow and the mainstream velocity move together in the vertical direction. The stream-wise velocity of the accumulated flow is lower than the mainstream. Similar trend is observed for all other cases of square and rectangular duct. The pattern of flow is not uniform when compared to a similar flow and heat transfer condition in the case of a horizontal duct.

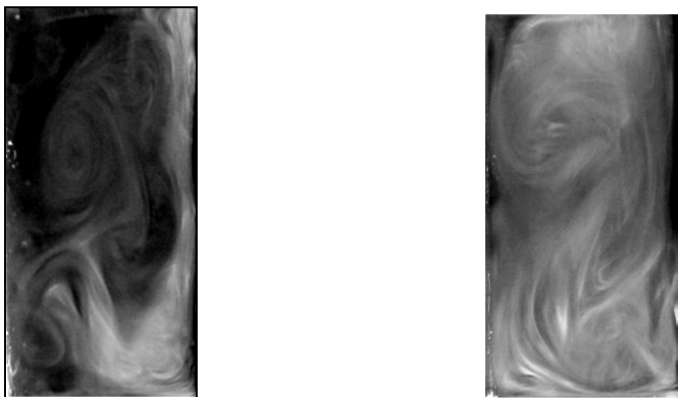

(a) (b)

Figure 6.43 Mixed convection flow structure within the square duct (Re = 858, ε = 0.05, AR = 0.5).

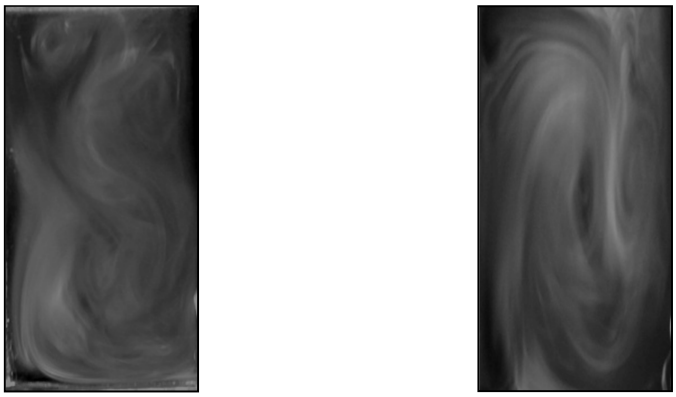

(a) (b)

Figure 6.44 Mixed convection flow structure within the rectangular duct (Re = 858, ε = 0.85, AR = 0.5).

Figures 6.41 (a) and (b) show the mixed convection flow structure for the square duct with polished surface. In this case the low (q = 283 W/m²) and high (q = 862 W/m²) heat flux hot wall average temperature was maintained as 56.4 ^{o}C and 94.2 ^{o}C, respectively. Due to high heat flux and buoyancy effect, the flow starts to circulate and simultaneously move upward from the inlet to the exit of the test section. Similarly Figure 6.42 (a) and (b) show the mixed convection flow structure for the square duct with black surface. In this case the low (q = 256 W/m²) heat flux the hot wall average temperature was maintained at 52.0 ^{o}C and the high (q = 728 W/m²) heat flux the hot wall temperature was maintained at 85.6 ^{o}C.

Figure 6.43 (a) and (b) provide the mixed convection flow structure for the rectangular duct with polished surface. In this case the low (q = 283 W/m²) heat flux the hot wall average temperature was maintained at 56.6 ^{o}C and the high (q = 862 W/m²) heat flux the hot wall temperature was maintained at 94.7 ^{o}C. Similarly Figures 6.44 (a) and (b) provide the mixed convection flow structure for the rectangular duct with black surface. In this case the low (q = 256 W/m²) heat flux the hot wall average temperature was maintained at 52.6 °C and the high (q = 728 W/m²) heat flux the hot wall temperature was maintained at 85.8 °C. For all the cases, due to high heat flux and buoyancy effect, the flow starts to circulate and simultaneously and move upward from the inlet to the exit of the test section. Similar trend is observed with both square and rectangular ducts.

Table 6.4 Effect of Reynolds number on the average Nusselt number at heated wall for AR = 1

Description	Polished Surface (q = 862 W/m²)			Black Surface (q = 728 W/m²)		
	Reynolds Number			Reynolds Number		
	858	1788	2861	858	1788	2861
Convective Nusselt Number	25.6	28.8	31.3	19.8	22.0	24.8
Radiative Nusselt Number	2.0	1.7	1.5	7.2	6.8	6.0

Table 6.5 Average Nusselt number at heated wall for Re = 1788

Description	Polished Surface (q = 862 W/m²)		Black Surface (q = 728 W/m²)	
	Aspect Ratio (AR = 1)	Aspect ratio (AR = 0.5)	Aspect Ratio (AR = 1)	Aspect ratio (AR = 0.5)
Convective Nusselt Number	28.8	18.7	22.0	16.4
Radiative Nusselt Number	1.7	1.2	6.8	2.9

6.10 Summary

In this chapter, the results and discussion of mixed convection heat transfer for thermally developing flow in vertical square and rectangular ducts with radiation effects have been presented. The duct walls are maintained at a uniform temperature on one vertical wall, and cooled by uniform temperature on the opposite wall. The discussion included the effect of mixed convection, the effect of Reynolds number, and the effect of surface radiation interaction on the heat transfer in vertical duct flow, and also the influence of duct aspect ratio.

Table 6.4 presents the effects of Reynolds number on the average convective and radiative Nusselt for square test section (AR = 1). It can be observed that forced convection dominates for high Reynolds number and natural convection dominates for low Reynolds number. The results show that the convective Nusselt number along the duct would be higher for high Reynolds number and the radiative Nusselt number give lower results. The same trend is observed for rectangular duct. The effect of emissivity and aspect ratios on the average convective and radiative Nusselt for a fixed Reynolds number is presented in Table 6.5. It is observed that the results follow the same trend as in the previous Chapters 4 and 5. The results obtained from this chapter will be used for comparison with other cases considered in this study. The comparison is presented in the next Chapter.

CHAPTER 7
RESULTS AND DISCUSSION
COMPARISON OF CASES CONSIDERED IN THE PRESENT RESEARCH: CS1, CS2 AND CS3

7.1 Introduction

In the previous chapter, the results from the experimental work on mixed convection heat transfer for thermally developing flow in a vertical duct with surface radiation effects was presented. In this chapter, the results of the three case studies: CS1, CS2, and CS3 are compared and discussed. CS1 and CS2 configurations were compared based on the hydrodynamically developing and hydrodynamically developed flow conditions. CS1 and CS3 configurations were compared based on the horizontal and vertical orientation of the duct. The comparison is presented in terms of the convective Nusselt number, the radiative Nusselt number, and flow features obtained from flow visualization. Since mixed convection with radiation effects is the main mechanism that enhances heat transfer in this series of case studies, it is meaningful and significant to compare convective and radiative heat transfer characteristics among the different cases considered (CS1, CS2, and CS3).

7.2 Comparison of CS1 and CS2

For convenience, the schematic diagram of CS1 and CS2 configurations are shown in Figures 7.1 and 7.2 respectively. Figure 7.1 represents the case of thermally developing flow in a horizontal duct (CS1), and Figure 7.2 represents the case of hydrodynamically developed and thermally developing flow in a horizontal duct (CS2). In the CS1 configuration, airflow passes through the test section without a developing section, whereas in the CS2 configuration, the flow travels through a developing section (entrance section). Hydrodynamically fully-developed condition was achieved by using an entrance section having the similar cross section as the test

section. The length of this section was varied from 1.5 m to 4.8 m depending on the Reynolds number. It should be noted that, identical values of heat flux, cold wall temperature, and inlet air velocity were used for both the cases so as to enable a meaningful comparison.

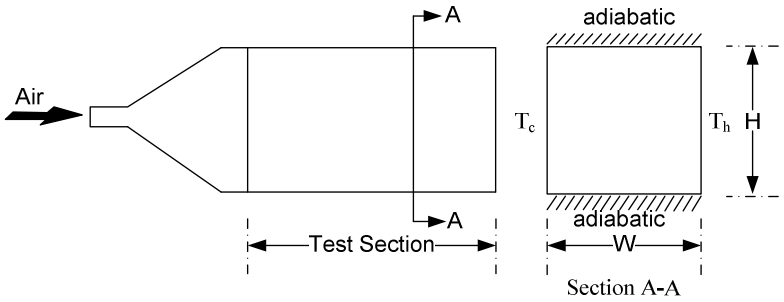

Figure 7.1 Schematic of case CS1.

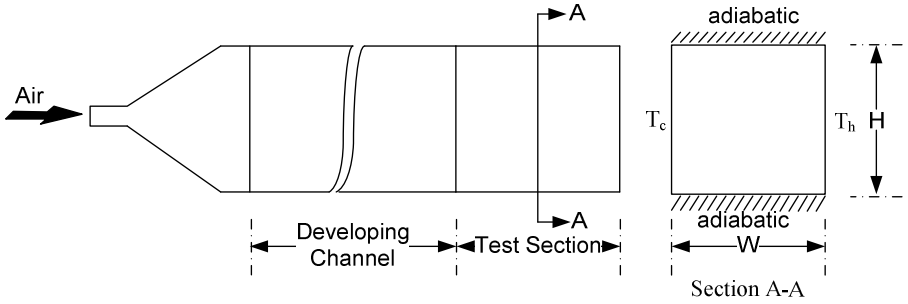

Figure 7.2 Schematic of case CS2.

7.2.1 Combined Forced and Natural Convection Heat Transfer

Figure 7.3 shows the average convective Nusselt number for the polished wall surface to be 27.3 and 24.9 for the case of CS1 and CS2 configurations respectively. In this case, the average convective Nusselt number between the case of CS1 and CS2 differed by about 8.8 %. A similar observation can be made for the duct having highly emissive surfaces (Figure 7.4). In both the cases, the convective Nusselt number near the inlet of the test section is slightly higher and decreases as the thermal boundary layer develops. The rate of convective Nusselt number drop near the inlet for CS1 was found to be 2.5 % and CS2 was found to be 2.3 %. When

comparing the patterns of local average convective Nusselt number, CS1 shows a slightly wavy trend compared to CS2. In the CS2 configuration, airflow is hydrodynamically fully developed before entering the test section. When the air flow is fully developed, its helps to extract heat uniformly from the heated wall, and due to this, the convective Nusselt number is more uniform for CS2. However, CS1 has generally higher Nusselt number values compared to CS2and this can be attributed to the higher velocity gradients in the case of CS1.

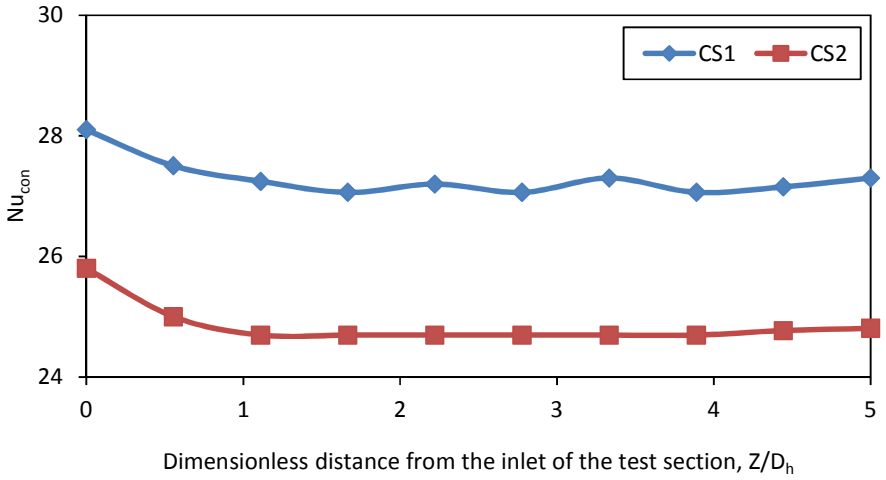

Figure 7.3 Comparison of average convective Nusselt number at the heated wall between CS1 and CS2 (Re = 1788, q = 862 W/m², AR = 1, ε = 0.05).

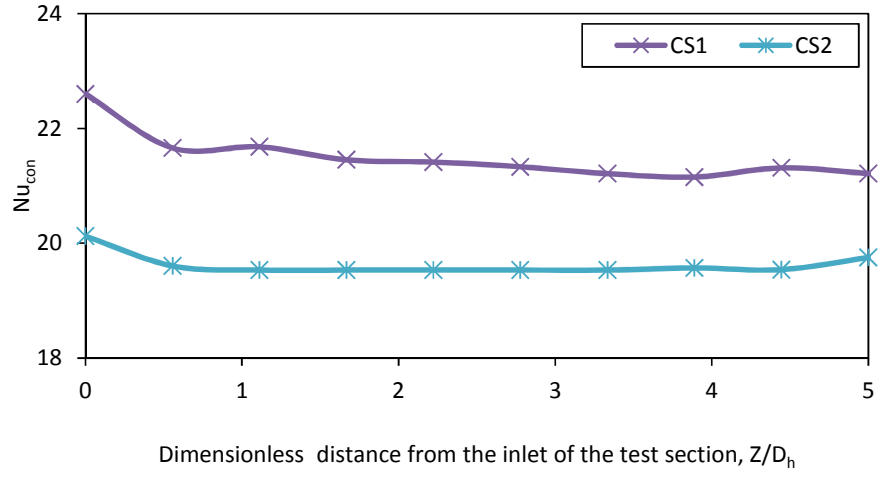

Figure 7.4 Comparison of average convective Nusselt number at the heated wall between CS1 and CS2 (Re = 1788, q = 728 W/m², AR = 1, ε = 0.85).

7.2.2 Radiation Heat Transfer

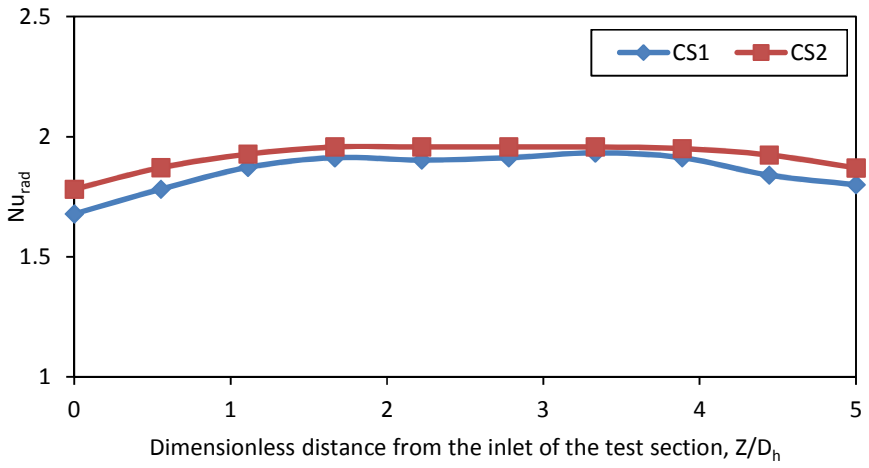

Figure 7.5 Comparison of average radiative Nusselt number at the heated wall between CS1 and CS2 (Re = 1788, q = 862 W/m², AR = 1, ε = 0.05).

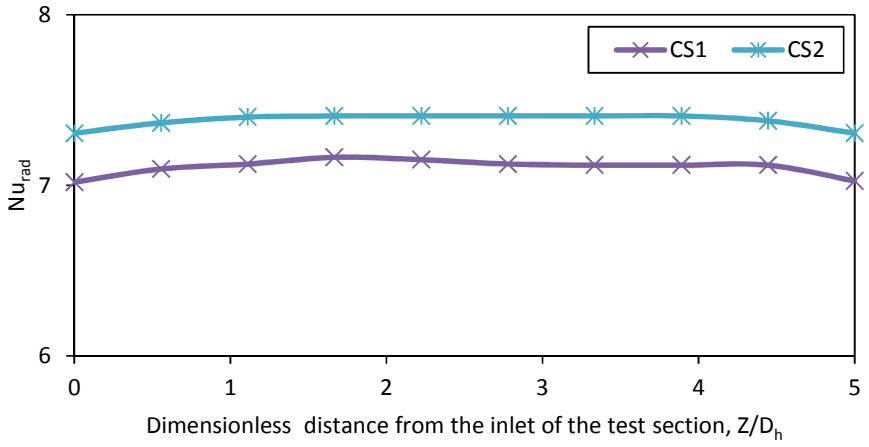

Figure 7.6 Comparison of average radiative Nusselt number at the heated wall between CS1 and CS2 (Re = 1788, q = 728 W/m², AR = 1, ε = 0.85).

In this section, the comparison of average radiative Nusselt number at heated wall for CS1 and CS2 configurations is presented. Figure 7.5 shows the average radiative Nusselt number for polished surface to be 1.8 and 1.9 for the case of CS1 and CS2 configurations respectively. The average radiative Nusselt number between CS1 and CS2 differed by about 3.6 %. Similarly figure 7.6 shows the average radiative

Nusselt number for a highly emissive surface to be 7.1 and 7.3 and the difference to be about 3.8 %. In case CS2, the hydrodynamically developed airflow helps to improve radiative Nusselt number to become more stable. This was described in the previous chapter (Section 7.2.1). Case CS2 provided generally higher radiative Nusselt numbers than CS1. However, the convective heat transfer is higher for CS1 configuration. It can be observed that wherever the value of convection Nusselt number increases, the value of radiative Nusselt number decreases. As the Reynolds number is increased, the buoyancy effect is expected to be not that significant. It was observed that the forced convection domination on the heat transfer process with little effect of buoyancy force is highly affecting the radiative Nusselt number rate in CS1.

For a polished wall surface, the rate of radiative Nusselt number increase near the inlet for CS1 was found to be 5.6 % and 4.6 % for CS2. Similarly for a black surface, rate of radiative Nusselt number increase near the inlet for CS1 was found to be 1.1 % and 0.9 % for CS2. The percentage increase in the radiative Nusselt numbers near the inlet is very high for CS1 than CS2; in this case the low average radiative Nusselt number shows higher percentage difference.

7.2.3 Mixed Convection Flow Visualization

Figure 7.7 shows the mixed convection flow structure for thermally developing flow in horizontal square ducts. Figure 7.8 shows mixed convection flow structure for hydrodynamically developed and thermally developing flow in a horizontal square duct. In both cases, the flow is induced by buoyancy, the heated airflow moves upward and accumulates near the top wall adjacent to the hot wall of the duct, and travels to the cold wall on the opposite side. This was explained earlier in Chapter 4 and 5. For the CS2 configuration, the hydrodynamically fully developed condition is achieved before the airflow enters the test section, so the developed airflow helps to improve and extract the heat uniformly from the heated wall; due to this flow appears more uniform. In CS1 configuration, without achieving the fully developed condition

(without the developing section part), the airflow straightaway enters the test section, because of which the flow is not uniform compared to CS2.

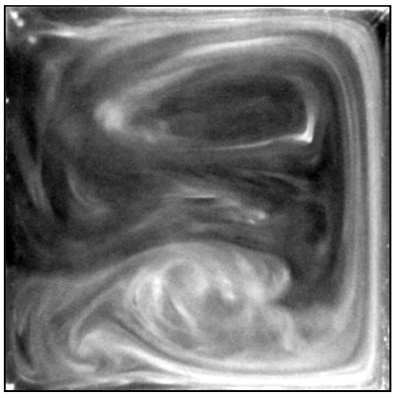

Figure 7.7 Mixed convection flow structure for thermally developing flow in horizontal square ducts (CS1).

Figure 7.8 Mixed convection flow structure for hydrodynamically developed, thermally developing flow in horizontal square ducts (CS2).

7.3 Comparison of CS1 and CS3

The schematic diagram of CS3 configuration is shown in Figure 7.9, in which the flow is thermally developing in vertical ducts. In this section CS1 and CS3 configurations were compared based on the horizontal and vertical orientation of the test section with a fixed Reynolds number at 1788 for the case of highly reflecting (polished) and highly emissive (black surface) respectively. In both cases, the airflow passes through the test section without a developing section; it is worth mentioning that identical values of heat flux, cold wall temperature, and inlet air velocity was used for both cases.

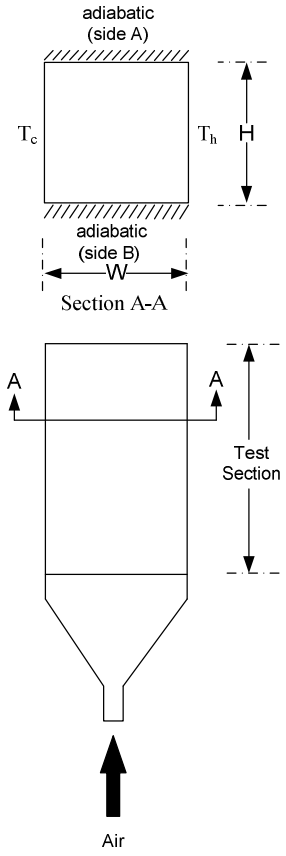

Figure 7.9 Schematic of case CS3.

7.3.1 Combined Forced and Natural Convection Heat Transfer

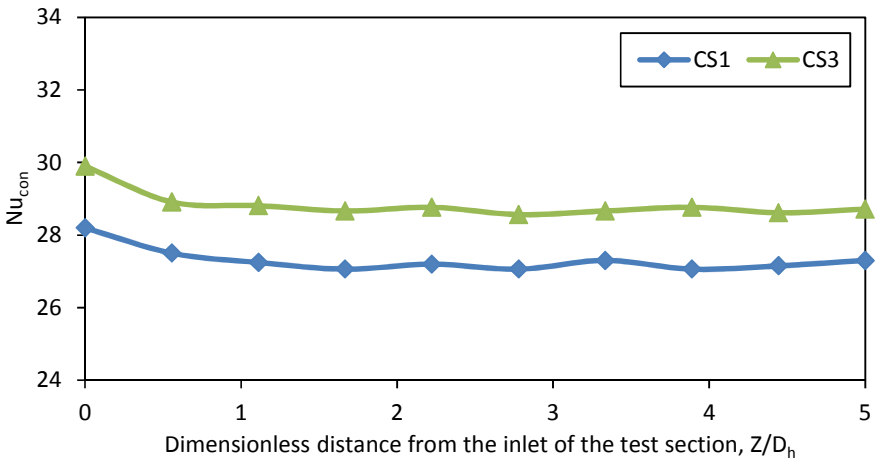

Figure 7.10 Comparison of convective Nusselt number at the heated wall between CS1 and CS3 (q = 862 W/m², AR = 1, ε = 0.05).

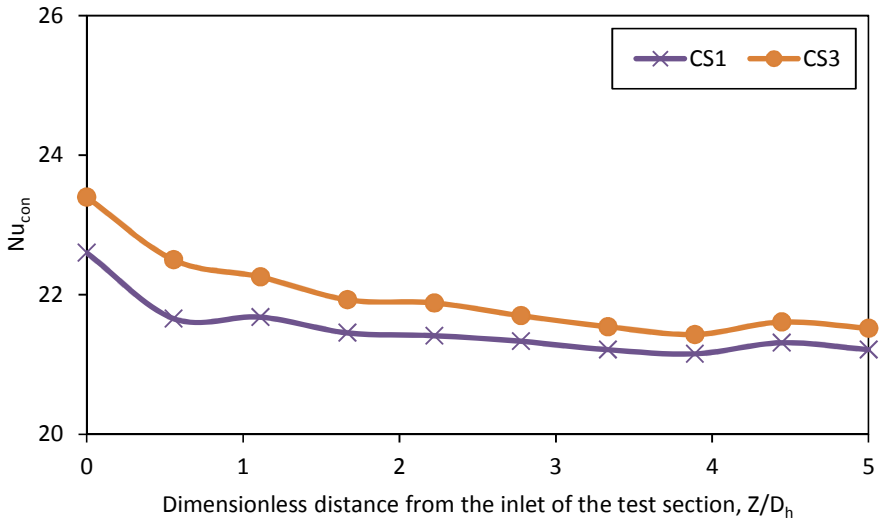

Figure 7.11 Comparison of convective Nusselt number at the heated wall between CS1 and CS3 (q = 728 W/m², AR = 1, ε = 0.85).

It can be observed that the average convective Nusselt number for polished wall surface to be 27.3 and 28.8 for the case of CS1 and CS3 respectively (Fig. 7.10). The average convective Nusselt number differed by about 5.2 %. Similarly Figure 7.11 shows the average convective Nusselt number for a highly emissive surface to be 21.5 and 22.0 for the case of CS1 and CS3 configuration. The average convective Nusselt number between CS1 and CS3 differed by about 2.3 %.

The fluid having a higher temperature moves upward due to the density gradient caused by natural convection effect. In this vertical orientation, the airflow passes through the test section from bottom to upward direction and fluid with higher temperature moves upward; thus both conditions aid in improving heat transfer and reducing the buoyancy effect in CS3. In the horizontal orientation, the air flow moves horizontally from the inlet of the test section to the exit. When the airflow moves horizontally, due to the buoyancy force the heated flow moves upward and accumulates near the top wall adjacent to the hot wall, and causes higher average top wall temperatures in CS1. Finally the above graphs clearly indicate that the vertical orientation (CS3) shows higher convective Nusselt number compared to horizontal

orientation (CS1). In this case, the rate of Nusselt number drop nearer to the inlet for both cases was found to be 2 to 4 %.

7.3.2 Radiation Heat Transfer

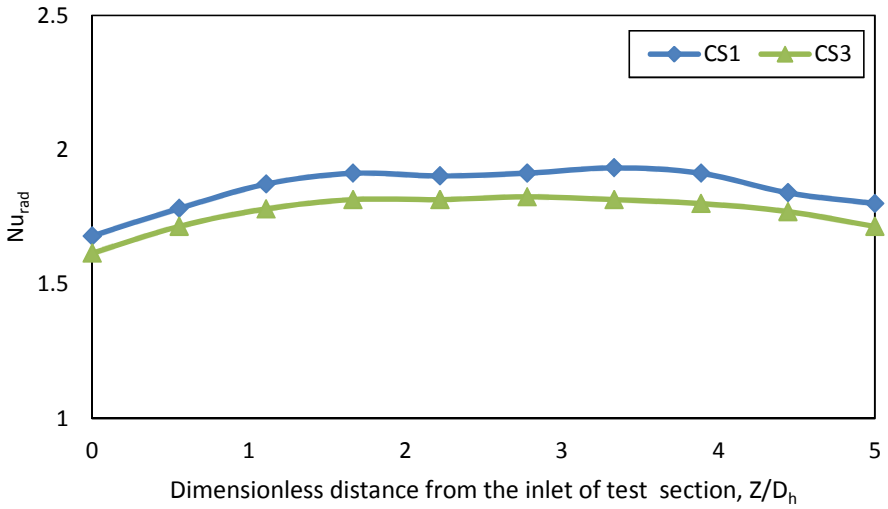

Figure 7.12 Comparison of average radiative Nusselt number at the heated wall between CS1 and CS3 (q = 862 W/m², AR = 1, ε = 0.05).

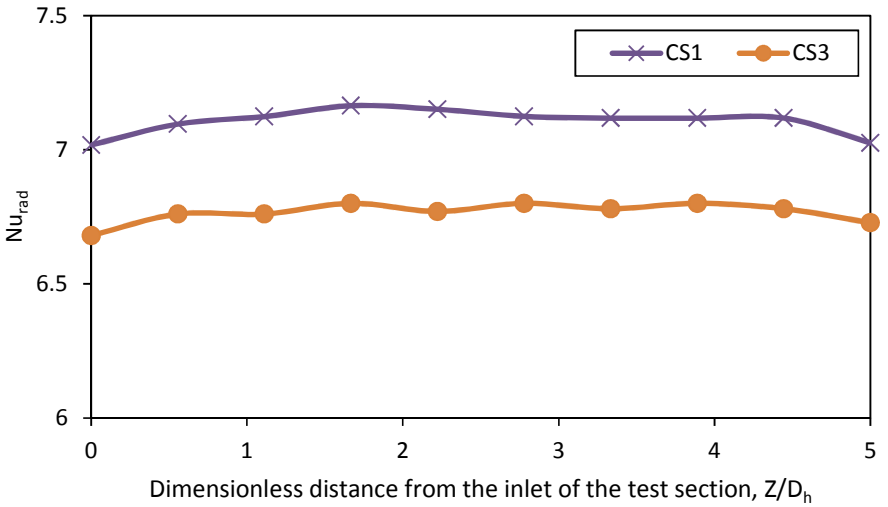

Figure 7.13 Comparison of average radiative Nusselt number at the heated wall between CS1 and CS3 (q = 728 W/m², AR = 1, ε = 0.85).

Figures 7.12 and 7.13 show the average radiative Nusselt number for polished and black surfaces. The average radiative Nusselt number for polished surface was found to be 1.8 and 1.7 for the case of CS1 and CS3 configurations respectively. The average radiative Nusselt number differed by about 4.8 %. Similarly the average radiative Nusselt number for black surface was found to be 7.1 and 6.7 for the case of CS1 and CS3 configuration respectively. The average radiative Nusselt number differed by about 4.6 %. The above comparison showed that the average radiative Nusselt number percentage is higher for CS1 compared to CS3. In this vertical orientation (CS3), the airflow and fluid with higher temperature moves upward direction, both conditions helps to improve the forced convection domination on the heat transfer process with less effect of buoyancy force. Since the forced convection effects are dominant, the wall surface temperatures are lower, and as a consequence, radiative wall to wall energy interactions are smaller. This is why radiative Nusselt number percentage is lower for CS3 compared to CS1.

7.3.3 Mixed Convection Flow Visualization

Figures 7.14 and 7.15 show the mixed convection flow structure for thermally developing flow in horizontal and vertical ducts respectively. In both cases, the flow is induced by buoyancy and the heated flow moves in the upward direction. This was explained earlier in Chapter 4 and 6.

Due to the effect of the buoyancy force, it can be seen that for the vertical duct case (CS3), the heated airflow moves upward from the inlet of the test section to the exit. In this case the buoyant flow and the airflow move together in vertical direction from the inlet of the test section to the exit. For the horizontal duct (CS1) the heated airflow moves upward and accumulates near the top wall adjacent to the hot wall of the duct, and being circulated to the cold wall on the opposite side, the accumulated flow circulates slowly and moves in the horizontal direction from the inlet of the test section to the exit. In this case, the buoyant flow is much smaller than the airflow.

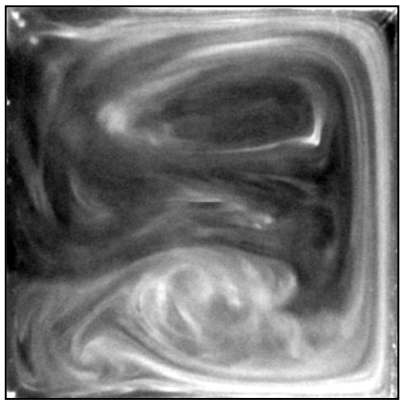

Figure 7.14 Mixed convection flow structure for thermally developing flow in horizontal squareducts (CS1).

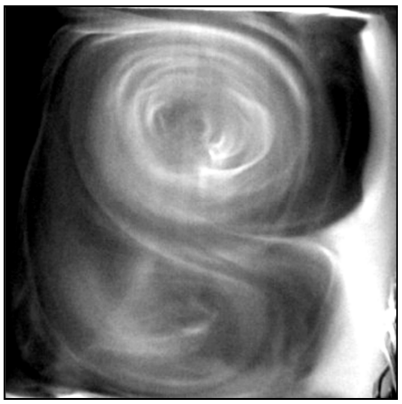

Figure 7.15 Mixed convection flow structure for thermally developing flow in verticalsquare ducts (CS3).

Table 7.1: Nusselt number comparison of CS1 and CS2 for Re = 1788

Description	Polished Surface (q = 862 W/m²)			Black Surface (q = 728 W/m²)		
	CS1	% Difference	CS2	CS1	% Difference	CS2
Convective Nusselt Number	27.3	8.8 %	24.9	21.5	8.8 %	19.6
Radiative Nusselt Number	1.8	3.6 %	1.9	7.1	3.8 %	7.3

Table 7.2: Nusselt number comparison of CS1 and CS3 for Re = 1788

Description	Polished Surface (q = 862 W/m²)			Black Surface (q = 728 W/m²)		
	CS1	% Difference	CS3	CS1	% Difference	CS3
Convective Nusselt Number	27.3	5.2 %	28.8	21.5	2.3 %	22
Radiative Nusselt Number	1.8	4.8 %	1.8	7.1	4.6 %	6.8

7.4 Summary

The results of the comparison of thermally developing flow in horizontal ducts (CS1), hydrodynamically developed thermally developing flow in horizontal ducts (CS2) and thermally developing flow in vertical ducts (CS3) were presented. Table 7.1 presents the Nusselt Number comparison of CS1 and CS2 for the Reynolds number of 1788. It can be concluded that the thermally developing flow condition helps to improve convection heat transfer rate; it also reduces the effects of surface radiation. Table 7.2 presents the Nusselt number comparison of CS1 and CS3 for the Reynolds number of 1788. The results show that the vertical orientation of the duct helps to improve convection heat transfer rate and also helps to reduce the radiation effect. The next chapter provides the conclusions obtained from the investigations conducted on all cases considered in this research.

CHAPTER 8

CONCLUSIONS

8.1 Introduction

A detailed analysis of three case studies were presented in Chapters 4, 5 and 6 and the results of the three case studies CS1, CS2, and CS3 compared and discussed in Chapter 7. The emphasis was on the effect of surface radiation and the aspect ratio on the heat transfer characteristics of steady thermally developing flow through a uniformly heated horizontal and vertical duct. This experimental investigation covered a range of Reynolds numbers from 800 to 2900, the heat flux from 250 W/m^2 to 870 W/m^2, 2 aspect ratios and the emissivity of internal walls 0.05 and 0.85. Overall the variation of surface temperature of the duct walls and local average Nusselt number were presented. The Nusselt number distributions were presented for different Reynolds numbers, different heat fluxes, wall emissivity and aspect ratios. The present investigation has provided results that are useful for the design of industrial equipment used for heat transfer applications. The flow visualization studies clearly showed the flow structure for various cases considered in this research work. Therefore, the research work presented in this thesis is a significant contribution in the study of mixed convection heat transfer in ducts with surface radiation effects.

8.2 Conclusions from the Present Work

The results obtained from the present experimental study have provided a better understanding on the effect of mixed convection heat transfer in duct flows in the presence of surface radiation. It can be observed that the effect of free convection heat transfer in the presence of mixed convection helps to promote and improve the overall heat transfer enhancement irrespective of having strong or weak radiation effects due to the surface emissivities of the walls of the duct.

The variation of surface temperature along the duct is affected by many variables such as heat flux, emissivity of walls, Reynolds number, the entrance length and the length of the test section. It can be observed that for the same heat flux, the surface temperature is higher for low Reynolds number flow. Conversely, convective heat transfer rate is higher for higher Reynolds number flow than low Reynolds number flow due to the dominant forced convection effect. Radiative heat transfer rate is found to be higher for low Reynolds number flow, because of the free convection domination.

The effect of surface radiation along the inside surfaces of the walls is brought in through the wall emissivity. Due to the emissivity of the walls, surface radiation from the walls of the duct affects the overall heat transfer rate. It is observed that, radiation has a multiple effect of contributing to the overall heat transfer enhancement as well as decreasing the convective component.

The duct aspect ratio affects the heat transfer rates on the heated wall. In this study, the heated wall surface area is fixed for all the cases of the experiment. The volume of the duct flow passage increases with aspect ratio, which results in a higher heat transfer rate, due to an increase in the mass flow rate.

It was found that the effect of entry flow conditions and orientation of the duct in the mixed convection region helps to improve the overall heat transfer enhancement. Heat transfer occurs irrespective of whether the flow is developing or fully developed. However the amount of heat transfer rate is higher for developing flow than for the developed flow due to the immediate effect of airflow movement and the shorter length of test section. In addition fully developed airflow helps to extract the heat uniformly from the heated wall, due to that the rate of heat transfer is more uniform than for the cases of the developing flow condition. It is observed that for the same heat flux and same Reynolds number, the rate of heat transfer rate increases as the test section orientation changes from horizontal to vertical, due to forced

convection domination. Also the accumulating buoyancy force and airflow moves together in the upward direction to give significant heat transfer rate enhancement in the vertical orientation of the duct.

8.3 Suggestions for Future Work

The present study considered a thermally developing flow in horizontal and vertical ducts with radiation effects. Future studies may be aimed at conducting a study of thermally developed flow in ducts, hydrodynamically developed thermally developed flow in ducts and hydrodynamically developed thermally developing flow in vertical ducts with a radiatively participating medium. There is also a need to consider more geometries to account for different cross sections of the duct. This will help to extend the knowledge base of the effect of surface radiation on mixed convection heat transfer rates.

REFERENCES

Every reasonable effort has been made to acknowledge the owners of copyright material. I would be pleased to hear from any copyright owner who has been omitted or incorrectly acknowledged.

[1] D G Osborne and F P Incropera. Laminar mixed convection heat transfer for flow between horizontal parallel plates with asymmetric heating. International Journal of Heat and Mass Transfer, 28(1):207-217, 1985.

[2] J R Maughan and F P Incropera. Experiments on mixed convection heat transfer for airflow in a horizontal and inclined channel. International Journal of Heat and Mass Transfer, 30(7):1307-1318, 1987.

[3] J R Maughan and F P Incropera. Regions of heat transfer enhancement for laminar mixed convection in a parallel plate channel. International Journal of Heat and Mass Transfer, 33(3):555-570, 1990.

[4] J M Huang, J D Lin and F C Chou. Combined radiation and laminar mixed convection in the thermal entrance region of horizontal isothermal rectangular channels. Numerical Heat Transfer, Part A, 18:113-125, 1990.

[5] R Smyth and Y K Salman. Combined free and forced convection heat transfer in a rectangular duct. International Communications in Heat and Mass Transfer, 18:669-680, 1991.

[6] C Balaji and S P Venkateshan. Interaction of surface radiation with free convection in a square cavity. International Journal of Heat and Fluid Flow, 14(3):260-267, 1993.

[7] C C Huang and T F Lin. Buoyancy induced flow transition in mixed convective flow of air through a bottom heated horizontal rectangular duct. Internal Journal of Heat transfer and Mass transfer, 37:1235-1255, 1994.

[8] D B Ingham, P Waston and P J Heggs. Recirculating laminar mixed convection in a horizontal parallel plate duct. International Journal of Heat and Fluid Flow, 16:202-210, 1995.

[9] W L Lin and T F Lin. Experimental study of unstable mixed convection of air in a bottom heated horizontal rectangular duct. International Journal of Heat and Mass Transfer, 39:1649-1663, 1996.

[10] W M Yan. Combined buoyancy effects of thermal and mass diffusion on laminar forced convection in horizontal rectangular ducts. International Journal of Heat and Mass Transfer, 39(7):1479-1488, 1996.

[11] J J M Silekens, C C M Rindt and A A V Steenhoven. Development of laminar mixed convection in a horizontal square channel with heated side walls. International Journal of Heat and Fluid Flow, 19:270-281, 1998.

[12] K T Lee and W M Yan. Mixed convection heat transfer in horizontal rectangular ducts with wall transpiration effects. International Journal of Heat and Mass Transfer, 41(2):411-423, 1998.

[13] W M Yan, H Y Li and D Lin. Mixed convection heat transfer in a radially rotating square duct with radiation effects. International Journal of Heat and Mass Transfer, 42:35-47, 1999.

[14] C Gau, Y C Jeng and C G Liu. An experimental study on mixed convection in a horizontal rectangular channel heated from a side. Transactions of the ASME Journal of Heat Transfer, 122:701-707, 2000.

[15] N Ramesh and W Merzkirch. Combined convective and radiative heat transfer in side vented open cavities. International Journal of Heat and Fluid Flow, 22: 180-187, 2000.

[16] N Ramesh and S P Venkateshan. Experimental study of natural convection in a square enclosure using differential interferometer. International Journal of Heat and Mass Transfer, 44:1107-1117, 2001.

[17] J C Leong, N M Brown and F C Lai. Mixed convection from open cavity in a horizontal channel. International Communication in Heat and Mass Transfer, 32:583-592, 2005.

[18] B Premachandran and C Balaji. Conjugate mixed convection with surface radiation from a horizontal channel with protruding heat sources. International Journal of Heat and Mass Transfer, 49:3568-3582, 2006.

[19] H C Chiu, J H Jang, and W M Yan. Mixed convection heat transfer in horizontal rectangular ducts with radiation effects. International Journal of Heat and Mass Transfer, 50:2874-2882, 2007.

[20] C S Yang, C G Liu, and C Gau. Study of channel divergence on the flow and heat transfer in horizontal ducts heated from a side. International Journal of Thermal Sciences, 48:105-113, 2009.

[21] F P Incropera, J S Kerby, D F Moffat and S Ramadhyani. Convection heat transfer from discrete heat sources in a rectangular channel. International Journal of Heat and Mass Transfer, 29(7):1051-1058, 1986.

[22] K C Chiu and F Rosenberger. Mixed convection between horizontal plates-I. Entrance effects. International Journal of Heat and Mass Transfer, 30(8):1645-1654, 1987.

[23] K C Chiu, J Ouazzani and F Rosenberger. Mixed convection between horizontal plates-II. Fully developed flow. International Journal of Heat and Mass Transfer, 30:1655-1662, 1987.

[24] Q M Lei and A C Trupp. Experimental study of laminar mixed convection in the entrance region of a horizontal semicircular duct. International Journal of Heat and Mass Transfer, 34(9):2361-2372, 1991.

[25] T A Nyce, J Ouazzani, A D Daubin and F Rosenberger. Mixed convection in a horizontal rectangular channel-experimental and numerical velocity distributions. International Journal of Heat and Mass Transfer, 35(6):1481-1494, 1992.

[26] W L Lin, Y T Ker and T F Lin. Experimental observation and conjugated heat transfer analyses of vortex flow development in mixed convection of air in a horizontal rectangular duct. International Journal of Heat and Mass Transfer, 17:3667-3683, 1996.

[27] M Y Chang and T F Lin. Experimental study of aspect ratio effects on longitudinal vortex flow in mixed convection of air in a horizontal rectangular duct. International Journal of Heat and Mass Transfer, 41(4):719-733, 1998.

[28] A Barletta and E Zanchini. On the choice of the reference temperature for fully developed mixed convection in vertical channel. International Journal of Heat and Mass Transfer, 42:3169-3181, 1999.

[29] A Dogan, M Sivrioglu and S Baskaya. Experimental investigation of mixed convection heat transfer in a rectangular channel with discrete heat sources at the top and at the bottom. International Communications in Heat and Mass Transfer, 32:1244-1252, 2005.

[30] C R Iskra and C J Simonson. Convective heat transfer coefficient for a hydrodynamically developed airflow in a short rectangular duct. International Journal of Heat and Mass Transfer, 50:2376-2393, 2007.

[31] H A Mohammed and Y K Salman. Experimental investigation of mixed convection heat transfer for thermally developing flow in a horizontal circular cylinder. Applied Thermal Engineering, 27:1522-1533, 2007.

[32] H A Mohammed and Y K Salman. The effects of different entrance sections lengths and heating on free and forced convective heat transfer inside a horizontal circular tube. International Communications in Heat and Mass transfer, 34:769-784, 2007.

[33] H A Mohammed. The effect of different inlet geometries on laminar flow combined convection heat transfer inside a horizontal circular pipe. Applied Thermal Engineering, 29:581-590, 2009.

[34] M Dogan and M Sivrioglu. Experimental investigation of mixed convection heat transfer from longitudinal fins in a horizontal rectangular channel. International Journal of Heat and Mass Transfer, 53:2149-2158, 2010.

[35] T T Chandratilleke, N Ramesh, and P Wangdhamkoom. Convective heat transfer in airflow through a duct with thermal radiation. IOP Conference Series, Materials Science and Engineering, 10:012026, 2010.

[36] T Pirasaci and M Sivrioglu. Experimental investigation of laminar mixed convection heat transfer from arrays of protruded heat sources. International Journal of Energy Conversion and Management, 52:2056-2063, 2011.

[37] J D Jackson, M A Cotton and B P Axcell. Studies of mixed convection in vertical tubes. International Journal of Heat and Fluid Flow, 10(1):1-15, 1989.

[38] T M Huang, C Gau and W Aung. Mixed convection flow and heat transfer in a heated vertical convergent channel. International Journal of Heat and Mass Transfer, 38(13):2445-2456, 1995.

[39] K T Lee, H L Tsai and W M Yan. Mixed convection heat and mass transfer in vertical rectangular ducts. International Journal of Heat and Mass Transfer, 40(7):1621-1631, 1997.

[40] W L Pu, P Cheng and T S Zhao. An experimental study of mixed convection heat transfer in vertical packed channels. AIAA Journal of Thermophysics and Heat Transfer, 13(4):517-521, 1999.

[41] W M Yan and H Y Li. Radiation effects on mixed convection heat transfer in a vertical square duct. International Journal of Heat and Mass Transfer, 44:1401-1410, 2001.

[42] C G Rao, C Balaji and S P Venkateshan. Effect of surface radiation on conjugate mixed convection in a vertical channel with discrete heat source in each wall. International Journal of Heat and Mass Transfer, 45:3331-3347, 2002.

[43] A Barletta, E R D Schio and E Zanchini. Combined forced and free flow in a vertical rectangular duct with prescribed wall heat flux. International Journal of Heat and fluid flow, 24:874-887, 2003.

[44] A S Krishnan, C Balaji and S P Venkateshan. An experimental correlation for combined convection and radiation between parallel vertical plates. ASME Journal of Heat Transfer, 126:849-851, 2004.

[45] A S Krishnan, B Premachandran, C Balaji and S P Venkateshan. Combined experimental and numerical approaches to multimode heat transfer between vertical parallel plates. Experimental Thermal and Fluid Science, 29:75-86, 2004.

[46] C C Huang, W M Yan and J H Jang. Laminar mixed convection heat and transfer in vertical rectangular ducts with film evaporation and condensation. International Journal of Heat and Mass Transfer, 48:1772-1784, 2005.

[47] A Barletta, E Magyari and B Keller. Dual mixed convection flows in a vertical channel. International Journal of Heat and Mass Transfer, 48:4835-4845, 2005.

[48] T Grosan and I Pop. Thermal radiation effect on fully developed mixed convection flow in a vertical channel. TechnischeMechanik, 27:37-47, 2006.

[49] M M Molla and M A Hossain. Radiation effect on mixed convection laminar flow along a vertical wavy surface. International Journal of Thermal Sciences, 46:926-935, 2007.

[50] G M Rao and G S V L Narasimham. Laminar conjugate mixed convection in a vertical channel with heat generating components. International Journal of Heat and Mass Transfer, 50:3561-3574, 2007.

[51] H A Mohammed and Y K Salman. Combined natural and forced convection heat transfer for assisting thermally developing flow in a uniformly heated vertical circular cylinder. International Communications in of Heat and Mass Transfer, 34:474-491, 2007.

[52] C Balaji, M Holling and H Herwig. A temperature wall functions for turbulent mixed convection from vertical, parallel plate channels. International Journal of Thermal Sciences, 47(6):723-729, 2008.

[53] FLUENT 6.1 User's Guide, Fluent Inc., NH, USA, 2004.

[54] GAMBIT 2.2 User's Guide, Fluent Inc., NH, USA, 2004.

[55] S M Marco and L S Han. A note on limiting laminar Nusselt number in ducts with constant temperature gradient by analogy to thin-plate theory. ASME Journal of Heat Transfer, 77:625-630, 1995.

[56] H L Langhaar. Steady flow in the transition length of a straight tube. Journal of Applied Mechanics, 64: A-55, 1942.

[57] H W Coleman and J W G Steele. Experimentation and Uncertainty Analysis for Engineers. John Wiley and Sons, New York 1989.

APPENDIX A1

CALIBRATION OF TYPE K THERMOCOUPLE

The following procedure was adopted in order to calibrate the thermocouples. The thermocouples were made from wires by forming a bead. To prepare the thermocouple wire for beads, about 10 mm of the insulation around the wires were removed and twisted together, then the twisted wire was used for making a small bead. For accurate temperature measurement, the bead sizes were maintained the same for all thermocouples. The thermocouples were made in batches of approximately 10 numbers, as and when required. One or two thermocouples chosen at random from every batch of thermocouples were used for calibration purpose. The thermocouples were carefully positioned in a thermostat with fuzzy control system (WiseCircu Fuzzy Control System, accuracy; ± 0.05 ^{0}C, flow rate: 6 liter/min) containing distilled water. The thermostat was set to a pre-desired temperature and allowed to run uninterrupted for at least one hour. The calibration was carried out with no forced circulation of air, in a room devoid of equipment such as fans, motors or engines. Ice-water mixture contained in a flask was used for zero point reference. Once steady-state conditions were attained (by observing the millivolt reading of the digital voltmeter over a period of time), the digital volt meter reading was recorded and the difference of this reading from the standard absolute thermoemf values for Type K thermocouple for the particular set point was obtained. This was repeated for at least 6 to 8 points that sufficiently covered the required range of measurement encountered in the actual experiment. Figure A 1.1 shows the difference curve obtained for a type K thermocouple used in the present study, by using the above recorded data. An equation to the difference curve in terms of the observed thermoemf ($E_{obs)}$ and the difference between the observed and the standard thermoemf (E_{ref}– E_{obs}) is then obtained.

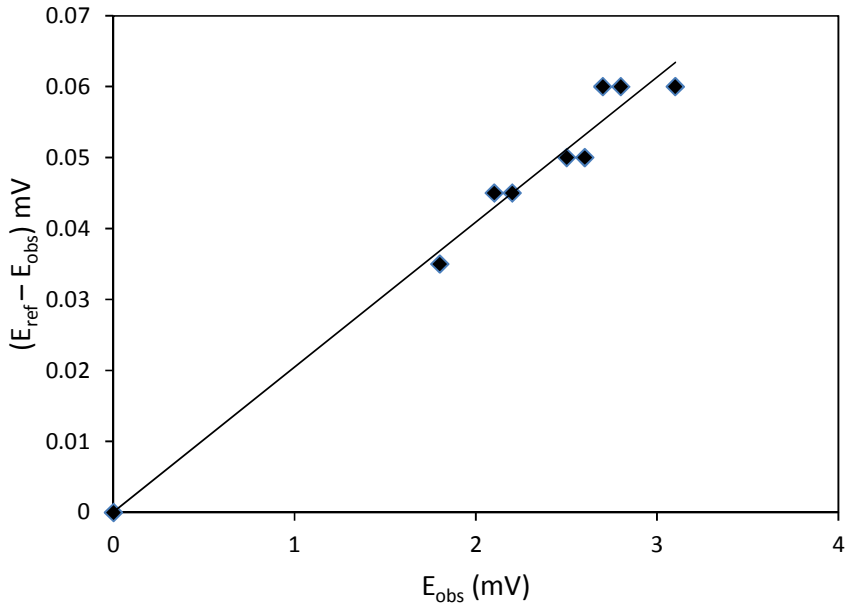

Figure A 1.1 Difference curve for Type K thermocouple.

During the actual experiment on square or rectangular ducts, this equation was made use of in order to obtain the deviation of the observed themoemf from the standard value. The correction for systematic error at any measurement of temperature was thus always accounted for. The corrected value of the observed thermoemf was used in the thermoemf temperature conversion formula, in order to obtain the value of temperature. However, the temperature obtained using the above procedure will carry the random part of the error, which is taken care of in the uncertainty calculations.

APPENDIX A2

UNCERTAINTY ANALYSIS

A sample calculation procedure for the estimation of uncertainty associated with the convective and radiative Nusselt numbers that are evaluated using measured quantities is presented below, for a particular case of the maximum value of the uncertainty, which occurs for a maximum value of ΔT and a maximum value of the surface emissivity ε.

Data: T_h = 361.9 K; T_{in} = 299.2 K; T_{out} = 306.2; T_m = 302; q_c = 806.6 W/m^2; q_r = 55.6 W/m^2; D_h = 54 mm; K_m = 0.026 W/m-K.

If we define a mean temperature of air $T_{m,}$ such that $T_m = \frac{T_{in} + T_{out}}{2}$, and obtain the partial derivations, we get

$$\frac{\partial T_m}{\partial T_{in}} = 0.5$$

$$\frac{\partial T_m}{\partial T_{out}} = 0.5$$

The uncertainty is the measured value of mean temperature of air is given by

$$U_{T_m} = \sqrt{\left(\frac{\partial T_m}{\partial T_{in}} U_{T_{in}}\right)^2 + \left(\frac{\partial T_m}{\partial T_{out}} U_{T_{out}}\right)^2}$$

$$U_{T_m} = \sqrt{(0.5X\,0.04)^2 + (0.5X\,0.04)^2}$$

$$= \pm\, 0.0282\ ^0\text{C}$$

The convective Nusselt number at the hot wall is given as

$$Nu_{conv} = \frac{q_{con} D_h}{(T_h - T_m) k_m}$$

The uncertainty involved in the convective Nusselt number is estimated using the

following partial derivatives that are found out as shown below.

$$\frac{\partial Nu_c}{\partial T_h} = \frac{-q_{con} D_h}{k_m (T_h - T_m)^2}$$

$$\frac{\partial Nu_c}{\partial T_m} = \frac{q_{con} D_h}{k_m (T_h - T_m)^2}$$

$$U_{Nu_c} = \sqrt{\left(\frac{\partial Nu_c}{\partial T_h} U_{T_h}\right)^2 + \left(\frac{\partial Nu_c}{\partial T_m} U_{T_m}\right)^2}$$

$$U_{Nu_c} = \sqrt{(0.479\,X\,0.04)^2 + (0.479\,X\,0.0282)^2}$$

$$= \pm 0.0234$$

The radiative Nusselt number at the hot wall is given as

$$Nu_{rad} = \frac{q_{rad} D_h}{(T_h - T_m) k_m}$$

The uncertainty involved in the radiative Nusselt number is estimated using the following partial derivatives that are found out as shown below.

$$\frac{\partial Nu_r}{\partial T_h} = \frac{-q_{rad} D_h}{k_m (T_h - T_m)^2}$$

$$\frac{\partial Nu_r}{\partial T_m} = \frac{q_{rad} D_h}{k_m (T_h - T_m)^2}$$

$$U_{Nu_r} = \sqrt{\left(\frac{\partial Nu_r}{\partial T_h} U_{T_h}\right)^2 + \left(\frac{\partial Nu_r}{\partial T_m} U_{T_m}\right)^2}$$

$$= \pm 0.016$$

The uncertainty of the total Nusselt number is therefore.

$$U_{Nu_t} = \sqrt{(U_{Nu_c})^2 + (U_{Nu_r})^2}$$

$$= \pm 0.0283$$

The absolute uncertainty for the total Nusselt number was thus found to be ± 0.0283. The overall uncertainty in the estimated Nusselt number from the hot vertical wall of the test section was found to be less than ± 3 % for all the cases considered in this study.

APPENDIX A3

COMPOSITION, STABILITY AND ACTIVITY OF THE BLACKBOARD PAINT

Composition of BlackBoard Paint	
Name	Content
Naptha (Petroleum) Hydro-treated Heavy	10 – 30 %
Carbon Black	1 – 5 %
Cobalt Carboxylate	< 1 %
X ylene	< 1 %
Iso-butane	< 1 %
Ethyl Methyl Ketoxime	< 1 %

Stability:

No particular stability concerns.

Conditions to Avoid:

Avoid heat, flames and other sources of ignition.

Avoid contact with strong oxidizers.

APPENDIX A4

HAND-HELD EMISSOMETER

The ET10 measures emissivity values in two of the most commonly used spectral regions, 3 to 5 and 8 to 12 microns. Its main application is to produce emissivity values for the infrared cameras. The advanced infrared cameras require the input of an emissivity value for accurate temperature calculations. The emissivity values obtained from tables can be far from real, leading to large temperature uncertainties. The ET10 can measure emissivity of any surface in just a few seconds.

APPENDIX A5

THERMAL ANEMOMETER

The Testo 425 thermal anemometer is a compact, easy to use anemometer with attached thermal probe on a telescopic handle. The anemometer measures air velocity and temperatures. Volume flow can also be measured by simply entering the duct measurements into the Testo 425 thermal anemometer. The anemometer displays reading on a large, clear display. Switching between flow and temperature readings is easy. The Testo 425 thermal anemometer includes timed and multi-point mean flow calculations which allow for easy flow analysis, volume accumulation estimates, and temperature variation monitoring. Min-Max values are one button simple, while the "Hold" function freezes the current readings in the display for easy data recording.